NPS ARCHIVE
1966
HART, D.

AN EXPERIMENTAL STUDY OF TONKS - DATTNER RESONANCES IN RARE GAS PLASMA

DAVID AUSTIN HART

LIBRARY
NAVAL POSTGRADUATE SCHOOL
MONTEREY, CALIF. 93940

DUDLEY KNOX LIBRARY
NAVAL POSTGRADUATE SCHOOL
MONTEREY CA 93943-5101

This document has been approved for public
release and sale; its distribution is unlimited.

AN EXPERIMENTAL STUDY OF

TONKS-DATTNER RESONANCES IN RARE GAS PLASMAS

by

David Austin Hart
Lieutenant, United States Navy
B. S., Tulane University, 1958

[redacted]

Submitted in partial fulfillment
for the degree of

DOCTOR OF PHILOSOPHY

from the

UNITED STATES NAVAL POSTGRADUATE SCHOOL
December 1966

1966
Hart, D.

ABSTRACT

A quantitative experimental study of the dipole Tonks-Dattner resonance oscillations of a cylindrical plasma column has been made for neon, argon and xenon plasma columns. Discharges were operated in the range of a few mTorr and resonances have been observed in the UHF and microwave frequency range. The resonances have been studied using strip-line and waveguide techniques and diagnostic studies have been made employing Langmuir probes and microwave cavity methods. For xenon, good agreement has been found with the theory of Parker, Nickel and Gould but for neon and argon definite discrepancies exist. This departure has been attributed to ion mean free paths which are not long compared to the tube radius. The effect of ion collisions seems to be to raise the electron density near the wall of the tube causing the resonances to occur at higher frequencies than are predicted by theory for the case of long ion mean free paths. The appearance of fewer and broader resonances than are observed in mercury columns is attributed primarily to the occurrence of moving striations which produce variations of electron density of about $\pm$ 50% of the average.

LIBRARY
NAVAL POSTGRADUATE SCHOOL
MONTEREY, CALIF. 93940

TABLE OF CONTENTS

Section		Page
I.	INTRODUCTION	13
II.	REVIEW OF PREVIOUS WORK	15
	1. Early Work	15
	2. The Theory of Parker, Nickel, and Gould	22
	(1) The Potential Equation	23
	(2) The Resonance Condition	25
	(3) The Electron Density Profile	28
	3. Other Experiments and Theories	33
III.	APPARATUS	38
	1. Vacuum Systems and Pressure Measuring Equipment	38
	2. Discharge Tubes	42
	3. Discharge Tube Circuits	47
	4. Radio Frequency Circuits	51
	5. Diagnostic Equipment	56
	(1) Langmuir Probe Circuits	56
	(2) Microwave Cavity Circuits	62
	6. Equipment for the Study of Moving Striations	65
IV.	EXPERIMENTAL PROCEDURE FOR THE RESONANCE STUDIES	68
V.	DIAGNOSTIC STUDIES	76
	1. Langmuir Probe Studies	76
	2. Cavity Diagnostics	99
VI.	RESONANCE STUDY RESULTS	113
VII.	SUMMARY AND CONCLUSIONS	137
VIII.	RECOMMENDATIONS FOR FUTURE WORK	146

TABLE OF CONTENTS
(continued)

Section		Page
APPENDIX A.	MOVING STRIATION STUDIES	147
APPENDIX B.	RESONANCE PROBE EXPERIMENTS	172
APPENDIX C.	ELECTRONEGATIVE PLASMA STUDIES	180
BIBLIOGRAPHY		185

LIST OF ILLUSTRATIONS

Figure		Page
1.	The resonance curve of the transmitted power P_{tr} versus the normalized discharge current. (Ref. 5)	17
2.	Propagating and cut-off regions of first T-D mode (Ref. 11)	21
3.	Split cylinder electrode configuration	26
4.	Radial electron density profile - argon	30
5.	Logarithmic derivative of dipole potential - $r_w^2/\bar{\lambda}_D^2 = 72$	31
6.	Theoretical dipole resonance conditions, $K_{eff} = 3.74$	32
7.	Calibration curves for Westinghouse 7903 ion gauge; neon, argon and xenon	41
8.	Experimental discharge tube, 3.5 cm OD	43
9.	Experimental discharge tube, 1.0 cm OD	44
10.	Orientation of probes in smaller (1.0 cm OD) discharge tube	45
11.	Construction of probes in larger (3.5 cm OD) discharge tube	46
12.	Circuit for discharge tube, manually varied current	49
13.	Pulsing circuit for discharge tube current variation	50
14.	Radio frequency circuit, pulsed discharge operation	52
15.	Radio frequency circuit, manual discharge tube operation, transmitted signal measurement	53
16.	Radio frequency circuit, manual discharge tube operation, reflected signal measurement	55
17.	Photographs of strip-lines (dipole devices)	57
18.	Circuit for display of Langmuir probe characteristics on an x-y recorder	59
19.	Circuit for display of Langmuir probe characteristics on an oscilloscope	60
20.	a). Ion current-voltage characteristic of Langmuir probe showing current modulation by moving striation density variation	63

LIST OF ILLUSTRATIONS
(continued)

Figure		Page
20.	b). Time sampled current-voltage characteristic of Langmuir probe at a point 60° before minimum light intensity	63
21.	Microwave cavity construction	64
22.	Circuit arrangement for cavity diagnostics	66
23.	Resonance presentation, pulsed discharge	71
24.	Experimental arrangement for observation of resonances in the presence of moving striations	73
25.	Power in rf field of strip-line as detected on a small dipole antenna	75
26.	Typical current-voltage characteristic of a Langmuir probe	77
27.	Semi-log plot of typical Langmuir probe characteristic	81
28.	Results of analyses of ion characteristics of a Langmuir probe in a xenon plasma column, compared with microwave cavity measurement of electron density	85
29.	Analyses of electron current characteristics of a Langmuir probe in a xenon plasma column, compared with $\beta = 0$ calculations from Chen (Ref. 53)	87
30.	Densities calculated by several methods from probe characteristics in 3.5 cm OD tube, xenon plasma	89
31.	Electron density at center of 3.5 cm OD tube versus discharge tube current, xenon	93
32.	Electron density at center of 3.5 cm OD tube versus discharge tube current, neon	94
33.	Electron density at center of 3.5 cm OD tube versus discharge tube current, argon	95
34.	Electron temperature versus pressure, neon, 3.5 cm OD tube	96
35.	Electron temperature versus pressure, xenon, 3.5 cm OD tube	97
36.	Electron temperature versus pressure, argon, 3.5 cm OD tube	98

LIST OF ILLUSTRATIONS
(continued)

Figure		Page
37.	Normalized radial profile of electron density, xenon, $r_w^2/\lambda_{DO}^2 \simeq 2\times10^4$	100
38.	Normalized radial profile of electron density, xenon, $r_w^2/\lambda_{DO}^2 \simeq 4\times10^3$	101
39.	Normalized radial profile of electron density, neon, $r_w^2/\lambda_{DO}^2 \simeq 9\times10^3$	102
40.	Axial variation of electric field of microwave cavity, cavity diameter 8.3 cm, end hole diameter 3.6 cm	107
41.	Radial variation of electric field of microwave cavity, cavity diameter 8.3 cm, end hole diameter 3.6 cm	108
42.	Axial variation of electric field of microwave cavity, cavity diameter 8.3 cm, end hole diameter 1.0 cm	109
43.	Resonances in neon, K_{eff} = 1.82, relative transmitted rf voltage versus discharge tube current	114
44.	Resonances in argon, K_{eff} = 1.82, relative transmitted rf voltage versus discharge tube current	115
45.	Resonance in xenon, K_{eff} = 3.74, relative transmitted rf voltage versus discharge tube current	116
46.	Comparison of resonance measurements on reflected and transmitted signals, xenon	117
47.	Resonances in xenon determined by maximum in reflected signal from a microwave horn, reflection coefficient versus discharge tube current	118
48.	Current for resonance versus resonant frequency, argon, K_{eff} = 3.74, 2.2 mTorr	120
49.	Current for resonance versus resonant frequency, argon, K_{eff} = 1.82, 3.8 mTorr	121
50.	Current for resonance versus resonant frequency, neon, K_{eff} = 1.82, 21 mTorr	122
51.	Current for resonance versus resonant frequency, neon, K_{eff} = 1.82, 43 mTorr	123

LIST OF ILLUSTRATIONS
(continued)

Figure		Page
52.	Current for resonance versus resonant frequency, neon, K_{eff} = 1.82, 70 mTorr	124
53.	Current for resonance versus resonant frequency, xenon, K_{eff} = 3.74, 1.2 mTorr	125
54.	Current for resonance versus resonant frequency, xenon, K_{eff} = 1.82, 2.2 mTorr	126
55.	Current for resonance versus resonant frequency, xenon, K_{eff} = 2.1 (waveguide horn), 3.9 mTorr	127
56.	Dipole resonance spectrum, neon, K_{eff} = 1.82	129
57.	Dipole resonance spectrum, argon, K_{eff} = 3.74	130
58.	Dipole resonance spectrum, argon, K_{eff} = 1.82	131
59.	Dipole resonance spectrum, xenon, K_{eff} = 3.74	131a
60.	Dipole resonance spectrum, xenon, K_{eff} = 1.82	132
61.	Dipole resonance spectrum, xenon, K_{eff} = 2.1	133
62.	Resonance spectrum, xenon 4.3 mTorr, moving striations present and transmitted signal measurements made in synchronization to moving striation phase	135
63.	Resonance spectrum, neon, 27 mTorr, moving striations present and transmitted signal measurements synchronized to moving striation phase	136
64.	Ratio of actual resonant frequency squared to predicted resonant frequency squared versus ratio of tube radius to ion mean free path	141
A.1	Moving striation velocity in neon as a function of pressure, 3.5 cm OD tube	148
A.2	Moving striation velocity in argon as a function of pressure, 3.5 cm OD tube	149
A.3	Moving striation velocity in xenon as a function of pressure, 3.5 cm OD tube	150
A.4	Moving striation velocity in xenon as a function of pressure, 1.0 cm OD tube	155

LIST OF ILLUSTRATIONS
(continued)

Figure		Page
A.5	Moving striation velocities versus ionic mass	157
A.6	Variation of plasma parameters through moving striations in neon, 15 mTorr, 235 ma discharge current	162
A.7	Radial profile of ion density at crest and trough of moving striations in xenon	163
A.8	Oscillogram of video output of microwave receiver with input from a Langmuir probe in a neon plasma	166
A.9	Variation of microwave noise with an applied axial magnetic field	168
B.1	Schematic of resonance probe circuit	173
B.2	Ideal resonance probe characteristic	174
B.3	Incremental dc increase of probe current for resonance probe in xenon, 8 mTorr, discharge current 20 ma, plasma frequency 1.07 gHz	177
B.4	Resonant frequency of cylindrical resonance probe versus plasma frequency for xenon plasma, 8 mTorr	178
C.1	Plasma discharge tube designed for use with iodine vapor	181

LIST OF SYMBOLS

a	Microwave cavity radius
A	Area
b	Outside radius of discharge tube
c	Radius of strip-line (dipole device)
e	Electron charge
E	Electric field intensity
E_i	Ion energy
f	Distribution function
f_o	Microwave cavity resonant frequency
g	Function of discharge tube radius and strip-line radius
i_s	Probe current
i	Subscript denoting ions
I	Current
j	Current density
J_o	Zeroth order Bessel function
$k(r)$	Wave number
k	Boltzmann constant
K	Relative dielectric constant of glass
K_{eff}	Constant dependent on strip-line configuration
m_e	Electron mass
m_i	Ion mass
n	Order of multipole, $n = 1$ for dipole
n_e	Electron number density
n_{eo}	Electron density at center of discharge tube
p	Pressure
Q	Quality factor of resonance

LIST OF SYMBOLS
(continued)

r	Position vector
r_w	Radius of plasma, inside radius of discharge tube
r_p	Langmuir probe radius
s	Number of ions created per unit volume per unit time
t	Time
T_+	Ion temperature
T_e	Electron temperature
$\mathcal{V}$	Volume
v	Velocity
V	Voltage
z	Normalized radial position, r/r_w
α	Proportionality constant for rate of ion production
β	Ratio of ion energy to electron energy = T_+/T_e
β_{01}	First root of $J_0(x)$
γ	Constant dependent on type of compression
ϵ	Permittivity
ϵ_0	Permittivity of free space
λ_i	Ion mean free path
λ_D	Debye length
λ_{D0}	Debye length at center of discharge tube
$\overline{\lambda_D^2}$	Debye length squared defined in terms of average electron density
ϕ	Electric potential
ω	Angular frequency
ω_p	Electron plasma frequency
ω_{p0}	Electron plasma frequency at center of discharge tube
$\overline{\omega_p^2}$	Electron plasma frequency squared defined in terms of average electron density

ACKNOWLEDGEMENTS

I wish to express my sincere gratitude to my advisor, Professor Norman L. Oleson, for his encouragement and interest in this work. He has provided many valuable suggestions in the course of this work and in reviewing the results reported in this thesis. Thanks are also due to Professor A. W. Cooper for helpful discussions of the work. I am indebted to Mr. H. M. Herreman who has been of great assistance in the design of the vacuum systems and who has provided many useful suggestions in the course of the experiments. I also thank Mr. J. van Gastel for his skillful construction of the glassware and Mr. Peter Wisler for construction of the machined items. Thanks are extended to the Office of Naval Research for the sponsorship of my program of study and for support of the research.

I. INTRODUCTION

When an electromagnetic wave is incident upon the positive column of a low pressure gas discharge in such a way that the direction of propagation and the electric field are both perpendicular to the column axis and the free space wavelength is large compared to the column diameter, a series of resonances is observed in the reflected and transmitted waves as the current of the discharge is varied. The usual method whereby the resonances are observed is to place the column across a waveguide and to detect the resonances as minima in the signal transmitted past the column. They may also be detected on a two-strip transmission line split in such a manner as to pass around the plasma column. Resonances are detected in the radio frequency power transmitted past the column. A strong resonance is observed for a given current and weaker resonances are detected as the current and hence the electron density is lowered. These resonances were first reported by Tonk in 1931. Much later extensive experimental studies of these resonances were made by Dattner on the positive columns of mercury discharge tubes. Although a great deal of experimental and theoretical work has been done on these resonances by other workers, the resonances are commonly referred to as Tonks-Dattner resonances.

The present study is concerned with observations of the Tonks-Dattner resonances in positive columns of rare gas discharges. This work has been undertaken because most previous experimental studies have been made using only mercury discharges. An attempt has been made to observe how the resonances in rare gases differ from those in mercury.

Section II gives an extensive review of previous experimental and theoretical work. This includes a theoretical treatment of the problem

by Parker, Nickel and Gould which has given the most successful quantitative prediction of the experimentally observed resonance conditions of any theoretical description to date.

Section III is concerned with the experimental apparatus used in the present study and Section IV with the experimental procedure. Section V is concerned with diagnostic studies of the plasmas with both Langmuir probe techniques and with microwave cavities.

In the course of studying the resonances in the rare gases, it was noted that the discharges contained low frequency oscillations which affected the observations of resonances and could not be eliminated. These oscillations were identified as moving striations. A study of some of the properties of the moving striations was made in order to determine their velocities and the electron density variations which they produce since these variations affect the resonance conditions. The results of the study of the moving striation characteristics is reported in Appendix A.

Section VI contains the results of the resonance study in the rare gases both for the case in which electron density variations produced by the striations are small as well as the case where the striations produce significant density variations. These results are discussed in Section VII.

II. REVIEW OF PREVIOUS WORK

1. Early Work

The first experimental study of the resonance behavior of a cylindrical plasma column was reported by Tonks [1,2] in 1931. A large resonance was observed for a given discharge tube current together with a resonance of somewhat smaller amplitude at a lower current when a constant frequency signal was applied to plates of either side of the discharge tube. The plasma was regarded as a dielectric with a frequency dependent permittivity

$$\epsilon = \epsilon_0 \left(1 - \omega_p^2/\omega^2\right) \tag{1}$$

where $\omega_p^2 = ne^2/m\epsilon_0$ is the electron plasma frequency squared and ω is the applied frequency. Here n is the electron density, e is the electron charge, m is the electron mass, and ϵ_0 is the permittivity of free space. It was shown by Tonks' work that the resonance of the stronger sort occurred for frequencies approximately proportional to ω_p.

In a paper on plasma resonance in the ionized trails of meteors, Herlofson [3] revived the subject of resonances of a cylindrical ionized column in 1951. Following this theoretical paper of Herlofson's, Romell [4] measured the reflection of 30 cm waves from a cylindrical mercury discharge. Multiple resonances were detected when the incident wave was polarized with the electric vector perpendicular to the column whereas Herlofson had predicted only a single dipole resonance. When the plane of polarization was rotated parallel to the column axis, the reflected wave became unobservable.

A very extensive experimental study of the resonances was performed

by Dattner in 1957. [5] A discharge tube was inserted across a waveguide with the electric field perpendicular to the column axis. Resonances were observed in the radio frequency (rf) power transmitted past the section of waveguide in which the column was placed. Up to six resonances were observed as the discharge current was varied. A typical resonance spectrum as observed by Dattner is shown in Figure 1. Subsequent to Dattner's original work, Boley [6] demonstrated that the three largest resonances were dipolar in nature, that is, the angular variation in the electromagnetic radiation scattered by the positive column corresponds to a radiating dipole.

Herlofson had predicted that higher multipole resonances, if they occurred, would be found at frequencies higher than for the larger dipole resonance. It is evident then that the secondary resonances cannot be due to higher order modes of oscillations.

The experiments of Dattner have been repeated by a number of workers. Agdur, Kerzar, and Sellberg [7] measured both scattered radiation and noise radiation at microwave frequencies and at different values of gas pressure. While it was expected that the ratio between emissivity and absorptivity would be constant, large variations were observed. (More recent data [8] shows less discrepancy in this respect.) Messiaen and Vandenplas [9] determined resonant frequencies and amplitudes both with and without an axially applied magnetic field. They also established experimentally that the discharge currents for resonance and the relative amplitudes of resonances were independent of waveguide antenna-plasma distance, that is, the secondary peaks are not due to plasma-antenna interaction but are characteristic of the plasma itself. Willis and Petroff [10] showed that the resonances could also be seen when the un-

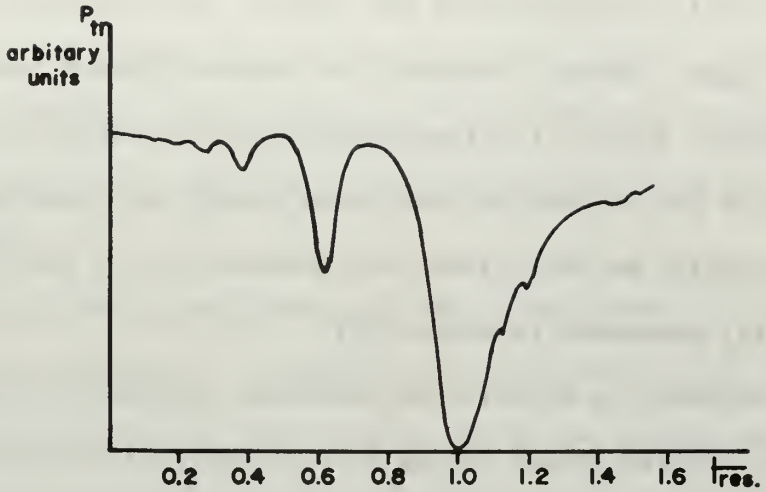

The resonance curve of the transmitted power P_{tr} versus the normalized discharge current (Ref. 5)

Figure 1

perturbed electric field in a waveguide through which a discharge tube was pladed was parallel to the column. The main resonance was shifted to a higher current; however, the secondary resonances were nearly unaffected. This is in disagreement with the earlier experiment of Romell, probably due to the fact that even though the unperturbed electric field was parallel to the column, the introduction of the discharge tube caused a radial component to exist. [11]

Attempts to explain the secondary resonances theoretically were first centered around taking into consideration the fact that the electron density in a positive column is non-uniform. The work of Kaiser and Closs [12] and of Makinson and Slade [13] attempted to account for multiple resonances by approximating a cold non-uniform plasma by a series of uniform annular dielectric shells. One additional resonance was predicted for each discontinuity in the density. It was claimed that some of these resonant modes would be observable when the steps became infinitely small and in the limit the stepped distribution approaches a smooth distribution. However, this claim was not substantiated by a later work by Keitel [14] who calculated the scattering from a Gaussian radial distribution of electron density. No resonance of appreciable amplitude was predicted; rather some scattering was predicted at all frequencies.

These results seemed to show the inadequacy of a dielectric description of the plasma to explain multiple resonances. A factor of importance which had been neglected up to this point was that the electrons in a glow discharge are in random thermal motion. The first description of the effect of electron temperature on the plasma's response as a wave propagation medium was given by Gould. [15]

A property of a plasma which is not present in the dielectric model

is the ability of the plasma to propagate longitudinal plasma waves. In a treatment by Gould of a spatially uniform plasma with appropriate boundary conditions, the plasma is found to exhibit an infinite number of resonances. The spacing of the resonances is in very poor agreement with experiment in that it is about an order of magnitude below that observed experimentally.

The assumption of finite temperature allows plasma waves of the type described by Bohm and Gross to propagate in the plasma. [16] These waves result from oscillations of electrons in which the average motion of the electrons and the electric field which causes that motion are parallel. If the electrons have no random thermal motion they merely oscillate about their equilibrium positions and the oscillations do not propagate; however, thermal motion of the electrons will cause the oscillations to propagate. The dispersion relation for these waves can be written approximately as:

$$k^2(r) = \left[\omega^2 - \omega_p^2(r)\right] / \frac{3kT_e}{m} \tag{2}$$

where k(r) is the wave vector, r is the position, k is Boltzmann's constant, and T_e is the electron temperature. Gould assumed that the waves could be reflected back and forth across the plasma giving rise to resonances for

$$\omega_m^2 = \omega_p^2 + \frac{3kT_e}{m} k_m^2 \tag{3}$$

where k_m is a wave vector dependent upon the size of the plasma. Here k_m is perpendicular to the plasma boundary.

If one now considers the non-uniformity of the plasma, the dispersion depends upon position. In those regions where the density is low

enough, the waves propagate and where the density is high $[\omega_p(r) > \omega]$, the plasma waves are evanescent, i.e., the wave vector becomes imaginary and the waves cut off. Since in a cylindrical discharge the electron density falls monotonically from the center to the wall, for a frequency somewhat below the plasma frequency at the center, propagation may be expected from the wall to the point on the radial profile where where it would be reflected. The longitudinal wave does not propagate to the center. One might expect the resonance condition to be approximated by

$$\int_{r_m}^{r_w} k(r)\,dr = m\pi \quad \text{or} \quad (2m+1)\frac{\pi}{2} \tag{4}$$

where we take a phase integral from r_m, the radius at which the applied frequency equals the local plasma frequency, to r_w the wall radius; m is an integer. The basic mechanism proposed here can be seen by reference to Fig. 2 (reproduced from Crawford [11]). The resonance condition is such that for a given frequency ω' the total phase shift when the wave returns to the wall is 2π, that is, there is a standing wave between the wall and the cut off region. Successively higher frequencies lead to further resonances.

Crawford [11] has attempted to determine the resonance spectrum from this approach. The result was in qualitative agreement with experiment in that wider separation in the resonances was predicted due to the smaller region over which the longitudinal waves propagate compared to the the uniform plasma case. The phase integral approach gives a qualitative understanding of how the additional resonances arise and of the importance of both finite temperature and radial electron density profile. However, this approach is not rigorously applicable due to the

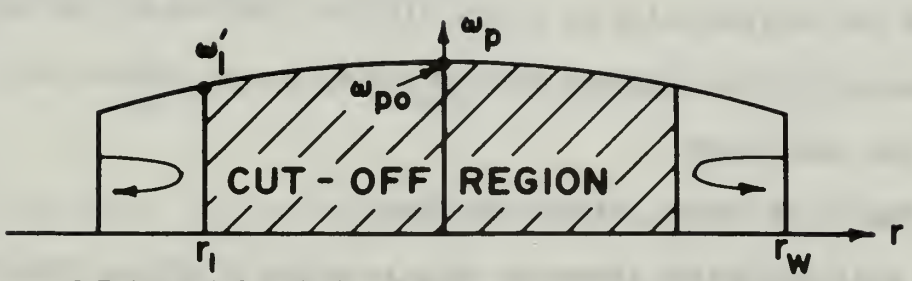

PROPAGATING AND CUT-OFF REGIONS OF FIRST T.-D. MODE (REF. 11)

Figure 2

fact that the dispersion relation, Eq. (2), is not strictly applicable except to cases where ω is near ω_p. Since it is possible that at the wall the plasma frequency may be much lower than the frequency which defines the first resonance, the use of Eq. (2) may not be justified. Furthermore, it is not certain which of the resonance conditions given in Eq. (4) is applicable.

Recently the problem has been attacked by a return to the basic equations of a collisionless, non-uniform electron gas with finite temperature. Moments of the Boltzmann equation have been employed. Several authors have used this method. Vandenplas and Gould [17] formulated a theory assuming a tensor electron pressure and a parabolic electron density profile for the distribution of electrons in a cylindrical plasma. In order to obtain numerical solutions, however, it was necessary to assume a scalar pressure. [18]

Theoretical treatments using moments of the Boltzmann equation were reported by Hoh [19] and by Weissglas. [20] While quantitative predictions which could be compared exactly to experiments were lacking from these theories because of the many assumptions required, they served to show that the consideration of finite electron temperature and spatial non-uniformity of the electron density could account for the main properties of the resonances.

2. The Theory of Parker, Nickel and Gould

The most successful theory to date in terms of giving good quantitative agreement with the observed conditions for the resonances has been put forth by Parker, Nickel and Gould. [21] The basic equations for a collisionless, non-uniform, electron gas at non-zero temperature are employed. Solution of the resulting equations is accomplished by

numerical methods.

(1) The potential equation

The basic equations used in the theory are

$$\frac{\partial f}{\partial t} + \vec{u} \cdot \frac{\partial f}{\partial \vec{r}} - \frac{e}{m} \vec{E} \cdot \frac{\partial f}{\partial \vec{u}} = 0 \tag{5}$$

$$\vec{E} = -\nabla \phi \tag{6}$$

$$\nabla^2 \phi = -\frac{\rho}{\epsilon} \tag{7}$$

where $f(\vec{r}, \vec{u})$ is the electron distribution function. $\vec{u}$ and $\vec{r}$ are velocity and position respectively. Solution is effected by taking moments of the collisionless Boltzmann equation, Eq. (5), and terminating the chain of moments after including the second moment. A further simplifying assumption is the replacement of the pressure tensor arising from the second moment with a scalar pressure proportional to density.

The moment equations are the equation of continuity:

$$\frac{\partial n_e}{\partial t} + \nabla \cdot (n_e \vec{v}) = 0 \tag{8}$$

and the momentum transport equation:

$$\frac{\partial \vec{v}}{\partial t} + (\vec{v} \cdot \nabla) \vec{v} = \frac{1}{m n_e} \left\{ -n_e |e| \vec{E} - \nabla p \right\} \tag{9}$$

If all quantities are represented as sums of steady state terms (subscript zero) and small perturbations (subscript 1), we have:

$$n_e = n_{eo} f(r) + n_1(\vec{r}) e^{-i\omega t} \tag{10}$$

$$p = p_o(\vec{r}) + p_1(\vec{r}) e^{-i\omega t} \tag{11}$$

$$\vec{E} = \vec{E}_o + \vec{E}_1 \tag{12}$$

$$\vec{v} = \vec{v}_1(\vec{r})\, e^{-i\omega t} \tag{13}$$

Here f(r) is a dimensionless function which describes the non-uniformity of the electron density. The ions are assumed to be stationary.

Substituting these expressions into equations (8) and (9) and neglecting drift motions, since time and spatial variations of the steady state drift velocity are assumed to be small

$$i\omega n_{eo} m_e f(r) \vec{v}_1 = n_{eo} f(r) |e| \vec{E}_1 + n_1 |e| \vec{E}_o + \gamma K T_e \nabla n_1 \tag{14}$$

and

$$-i\omega n_1 = \nabla \cdot (n_{eo} f(r) \vec{v}_1) \tag{15}$$

where γ is a constant dependent upon the type of compression. Since the plasma electrons undergo one-dimensional adiabatic compression in the absence of collisions, γ is taken to be 3. It has been assumed here that

$$p_o = n_{eo} f(r) K T_e \tag{16}$$

and

$$p_1 = \gamma K T_e n_1 \tag{17}$$

Assuming that Boltzmann's law applies to the steady state part of the electron distribution:

$$n_{eo} = n_o e^{-e\phi_o/KT_e} \tag{18}$$

Then

$$\nabla \phi_o = -\vec{E}_o = \left(\frac{KT_e}{|e|}\right)\left(\frac{\nabla n_{eo}}{n_{eo}}\right) \tag{19}$$

Poisson's equation, Eq. (7), must be satisfied.

$$\nabla \cdot \vec{E}_1 = \frac{-n_1 |e|}{\epsilon_o} \tag{20}$$

Combining (14), (15), (19) and (20) we get for the potential since $\vec{E}_1 = -\nabla \phi_1$:

$$\nabla^2 \nabla^2 \phi_1 - \frac{1}{\gamma}\left(\frac{\nabla f}{f} \cdot \nabla\right) \nabla^2 \phi_1 + \left[\frac{1}{\gamma \lambda_{DO}^2}\left(\frac{\omega^2}{\omega_{po}^2} - f\right)\right.$$

$$\left. - \frac{1}{\gamma} \nabla \cdot \left(\frac{\nabla f}{f}\right)\right] \nabla^2 \phi_1 - \frac{1}{\gamma} \nabla f \cdot \nabla \phi_1 = 0 \tag{21}$$

This is a fourth order differential equation in ϕ_1 the electrical perturbational potential. The substitution

$$\phi_1(r, \theta) = \Phi_n(r) e^{in\theta} \tag{22}$$

produces a fourth order ordinary differential equation where the angular dependence has been separated out. The equation was put into dimensionless form introducing $z = \frac{r}{r_w}$ for numerical solution by Parker, [22] et. al., and was then found to depend only on the dimensionless variables $\left(\frac{r_w^2}{\lambda_{DO}^2}\right)$ and $\left(\frac{\omega^2}{\omega_{po}^2}\right)$ where λ_{DO} and ω_{po} are Debye length and plasma frequency respectively at the center of the column, r_w is the radius of the wall of the discharge column. λ_{DO} is defined as $\left(\frac{\epsilon_o K T_e}{n_o e^2}\right)$.

(2) The Resonance Condition

J.C. Nickel [23] has derived the resonance conditions for an electrode configuration designed to excite a dipolar mode of oscillation in the plasma column. A split cylinder of the type used in the experiments described in this thesis gives the configuration shown in Fig. 3.

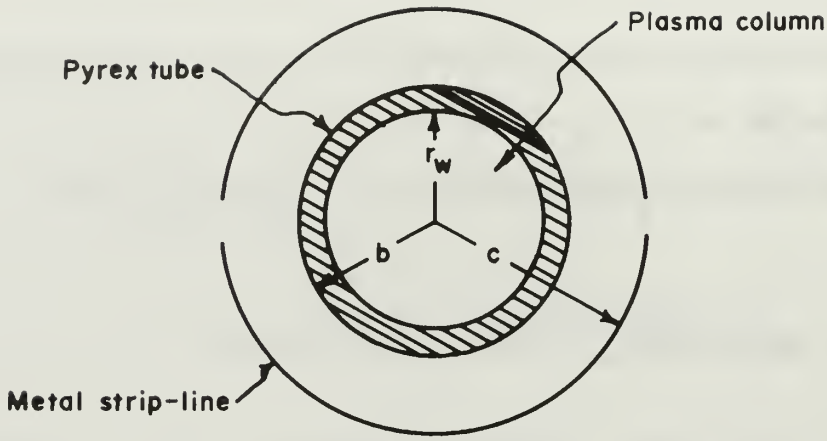

(a) Construction

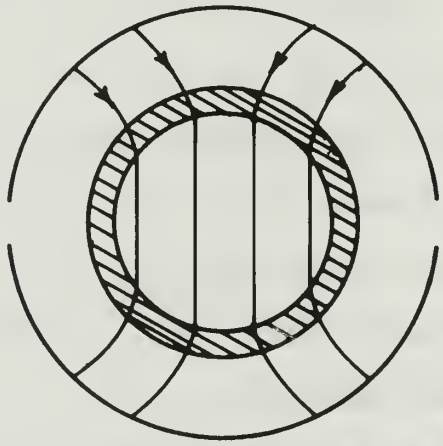

(b) Field Distribution

Split cylinder electrode configuration

Figure 3

A resonance is considered to arise when the applied field becomes zero while the scattered field remains finite, i.e., for poles of the scattering amplitude. The effects of the glass tube and the space between the dipole device and the tube wall are to modify the effective dielectric constant of the medium surrounding the plasma. The resonance condition is seen to depend on the experimental apparatus as well as the perturbed electric potential of the plasma and is given by:

$$L_n = -n K_{eff} \tag{23}$$

where L_n is the logarithmic derivative of electrical potential and is defined by:

$$L_n = \left[\frac{r}{\Phi_n} \frac{d\phi_n}{dr} \right]_{r=r_w} = \frac{\Phi_n'(z=1)}{\Phi_n(z=1)} \tag{24}$$

where $z = \frac{r}{r_w}$. K_{eff} is the effective dielectric constant of the medium surrounding the plasma and is given by:

$$K_{eff} = K \frac{\left(\frac{b}{r_w}\right)^n (K+g) - \left(\frac{r_w}{b}\right)^n (K-g)}{\left(\frac{b}{r_w}\right)^n (K+g) - \left(\frac{r_w}{b}\right)^n (K-g)} \tag{25}$$

where K is the relative dielectric constant of the glass and

$$g = \frac{(1 + b/c)^{2n}}{(1 - b/c)^{2n}} \tag{26}$$

For the case of dipole resonances, which should be the mode primarily excited by the split cylinder, n = 1. When interpreting waveguide data it is assumed that the field is the same as if applied from a split cylinder (strip-line) of infinite radius, i.e., $K_{eff} \doteq K_{eff}(K, r_w, b, c = \infty)$.

(3) The electron density profile

The electron density profile has been calculated theoretically by Parker. [22] The model used is that of a slightly ionized plasma with a neutral gas assumed to be at room temperature. It is assumed that ions are created at a rate proportional to the local electron density and that ions are created with zero velocity. When created, an ion moves radially without colliding with neutrals until it reaches the wall. It is also assumed that the electron distribution is Maxwellian. The assumptions here are those of the Langmuir "free fall theory"; however, the solution by Langmuir [24] involves the additional assumption that $r_w \gg \lambda_D$.

From the assumptions an integro-differential equation is obtained in the following dimensionless variables:

$$\eta(r) = -\frac{e\phi(r)}{KT_e} \tag{27}$$

$$s = \alpha r \Big/ \sqrt{2KT_e/m_i} \tag{28}$$

$$\beta^2 = 2n_{eo}e^2/\epsilon_o m_i \alpha^2 \tag{29}$$

In these equations, α is the proportionality constant for the rate of ion production. The number of ions created per unit volume s(r) is proportional to the local electron density, i.e., $s(r) = \alpha n_e$. The mathematical expression for the electron density variation is then:

$$s\frac{d^2\eta}{ds^2} + \frac{d\eta}{ds} = \beta^2\left[\int_0^s \frac{e^{-\eta(\sigma)}\sigma\, d\sigma}{\sqrt{\eta(s)-\eta(\sigma)}} - se^{-\eta(s)}\right] \tag{30}$$

Parker solved this equation numerically with the boundary condition that the net current at the wall is zero:

$$e^{\eta(S_w)} \int_0^{S_w} e^{-\eta(\sigma)} \frac{\sigma}{S_w} d\sigma = \sqrt{\frac{m_i}{4\pi m_e}} \tag{31}$$

where

$$S_w = S(r_w) \tag{32}$$

It can be shown that:

$$\beta^2 = \frac{n_{eo} e^2}{m_i \epsilon_o} \frac{m_i}{kT_e} \left(\frac{r_w}{S_w}\right)^2 = \frac{1}{S_w^2} \left(\frac{r_w^2}{\lambda_{DO}^2}\right) \tag{33}$$

The solution of the above equation for the radial electron density function is plotted in Fig. 4 for the gas argon. In the plot z is the dimensionless parameter $\frac{r}{r_w}$. Crawford [11] has compared electron density profiles taken with Langmuir probes with the theoretical curves of Parker for mercury. Some discrepancy was noted and was attributed to ions making some collisions before reaching the wall.

(4) The theoretical resonance curves

Numerical integration of Eq. (21) has been performed by Parker using the theoretical electron density profile for mercury. The boundary condition here is that the electron current to the wall vanishes. The results of this treatment are plots of Φ'/Φ versus $\frac{\omega^2}{\overline{\omega_p^2}}$ where $\overline{\omega_p^2}$ is the average electron plasma frequency. A typical curve of the sort obtained is shown in Fig. 5. The dashed line at Φ'/Φ = -3.74 represents the dipole resonance condition, Eq. (23), for K_{eff} = 3.74. Other curves are given by Parker [22] for various values of $r_w^2/\overline{\lambda_D^2}$ between 72 and 4530. for dipole and quadripole resonances. From these curves can be obtained the theoretical conditions for dipole resonances. Fig. 6 shows the conditions for main and first and second Tonks-Dattner dipole

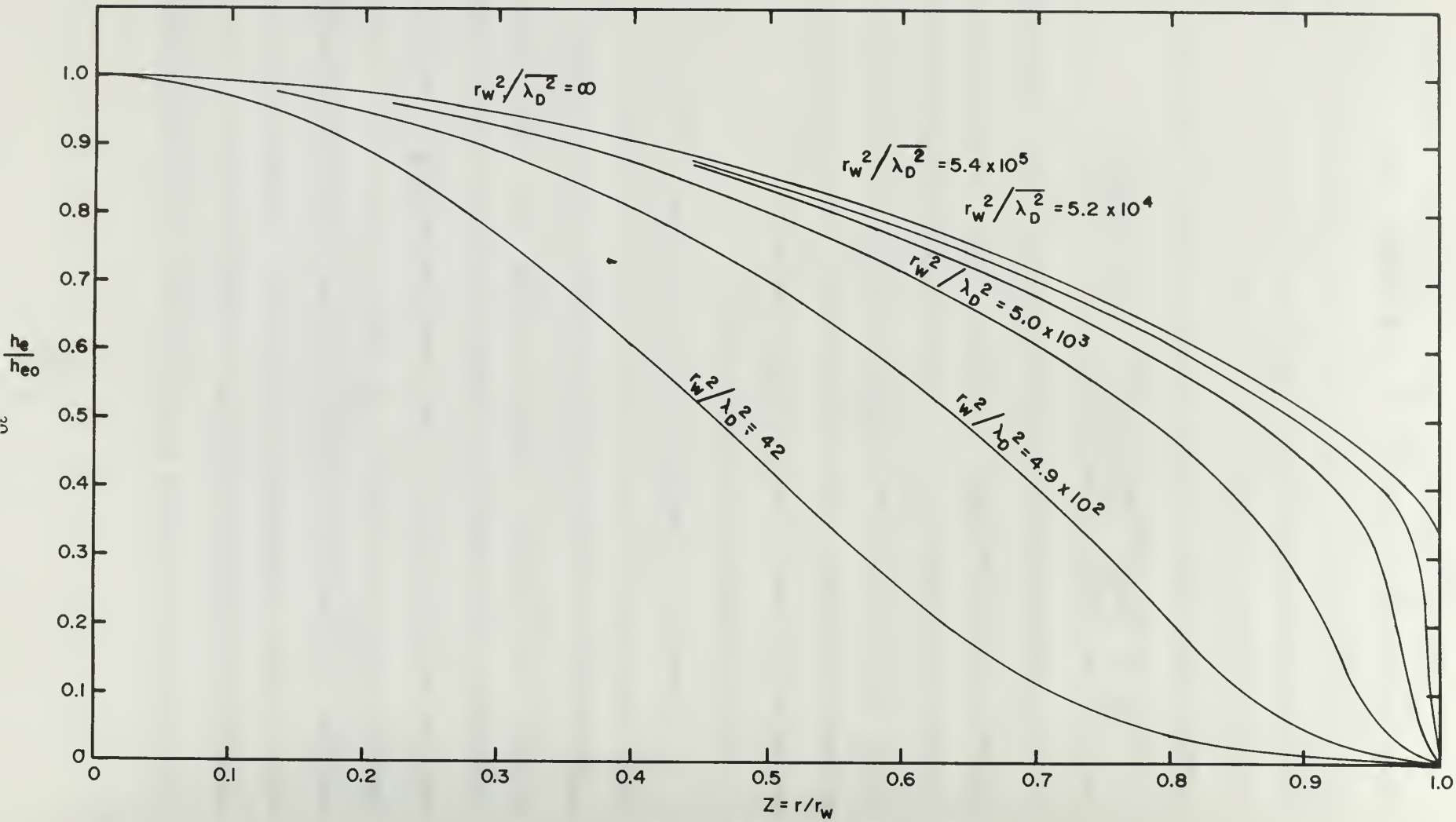

Radical electron density profile – Argon

Figure 4

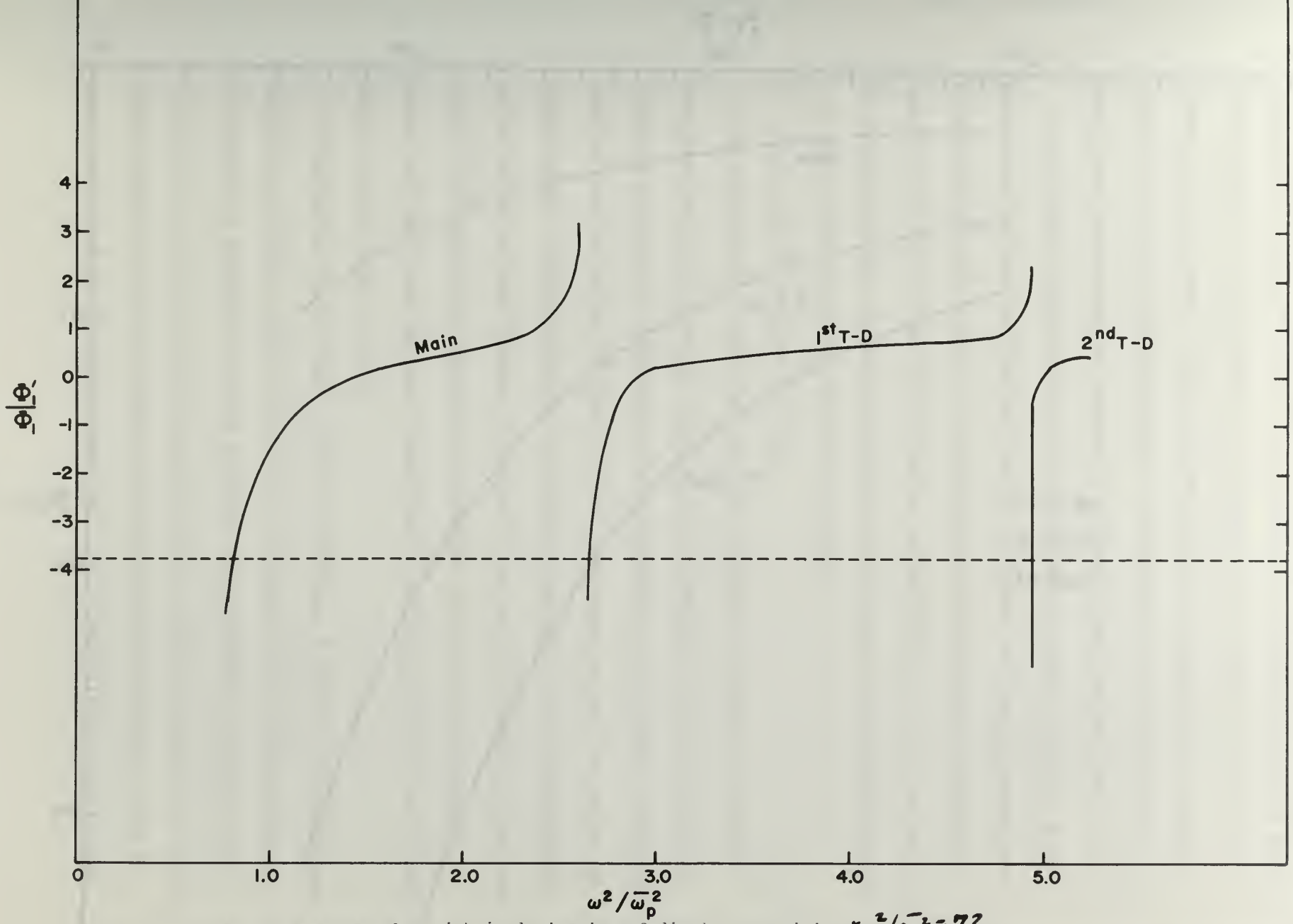

Logarithmic derivative of dipole potential $- r\omega^2/\bar{\lambda}_D^2 = 72$

Figure 5

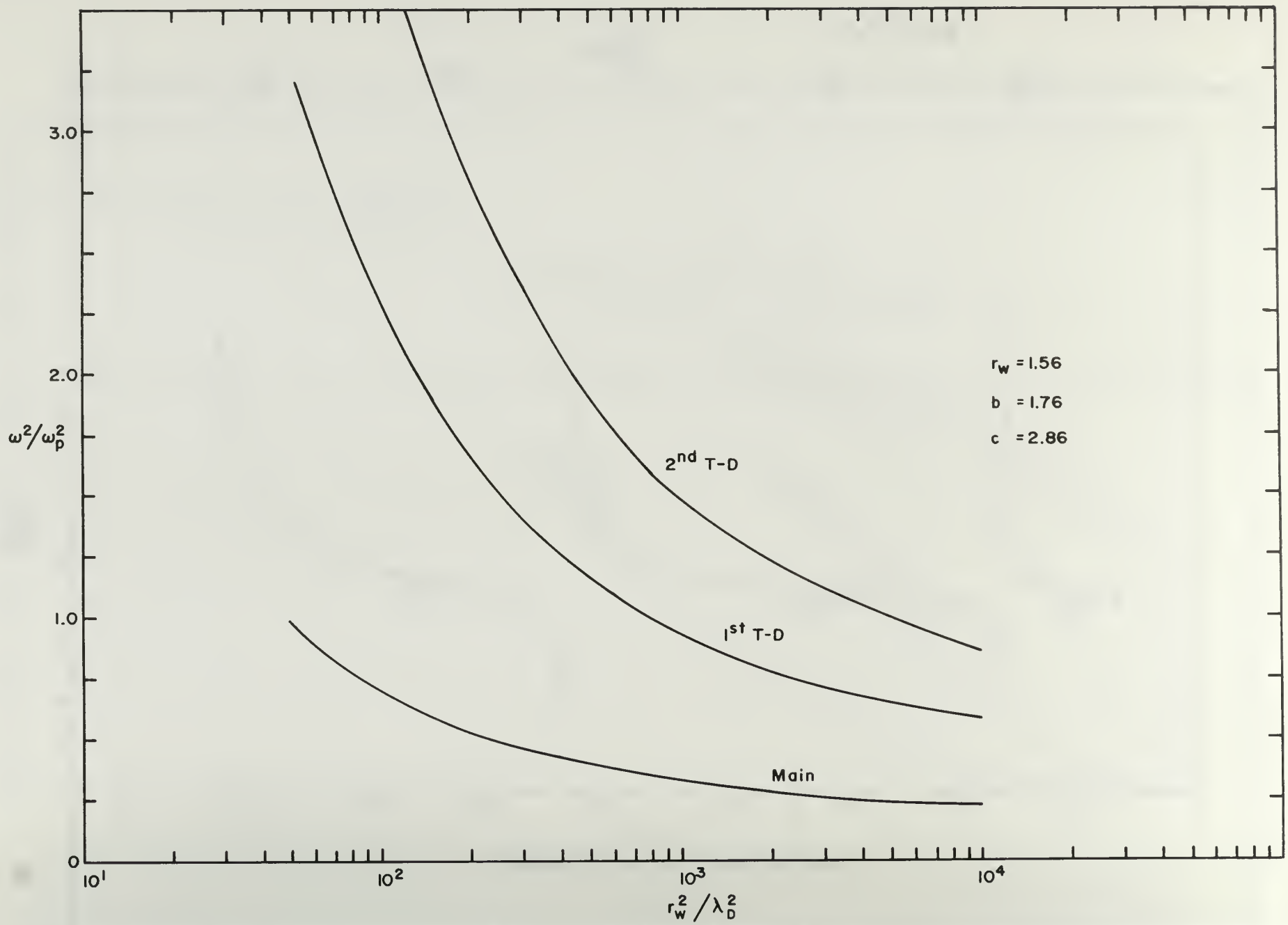

Theoretical dipole resonance conditions, $K_{eff} = 3.74$

Figure 6

resonances for $K_{eff} = 3.74$. This was among the values calculated for the diameters of strip-lines and discharge tubes used in the work reported in this thesis. Here we have adopted the nomenclature used by Parker, et.al., for the resonances. The largest is called the main; subsidiary resonances are numbered in order, first, second, etc.

Quadrupole resonances have been observed by Nickel [23] for a mercury column using a cylindrical device with four sections of equal arcs insulated from one another. The alternate sections were driven with opposite polarity to excite resonances corresponding to n = 2 in Eq. (23). No attempt was made to excite quadrupole resonances in the present work; only the dipole resonances have been studied.

3. Other Experiments and Theories

Crawford, Kino, Self, and Spalter [25] have developed a method of observing the resonances by replacing the waveguide with an easily constructed strip-line. The device is constructed of two copper electrodes bent to circular shape so that an electrode passes around the column on either side. The device gives essentially the same field configuration as the split cylinder device discussed in the work of Parker, Nickel and Gould. [21] Recently, Crawford has reported on the theory of Parker, Nickel and Gould and has made comparison of Dattner's and his own experimental results with it. [26]

Vandenplas and Messiaen [18] have developed a theory using the same approach as Parker, Nickel and Gould. They also used a scalar pressure but assumed a parabolic density profile. The resonance positions are not given as well as by the theory of Parker, Nickel and Gould but their calculations have the advantage of showing that the resonance peaks become less important as the electron density decreases for a fixed fre-

quency as is experimentally observed.

A recent theory has been proposed by Leavens [27] in which he attributes the resonance to oscillations entirely within the sheath which is formed on the inner wall of the column. He abandons the fluid approach and solves the Vlasov equation by the conductivity kernel method. No quantitative data are available from this theory as the solutin requires knowledge of the static fields of the sheath which have not been experimentally determined for a cylindrical case. In principle this should be a more accurate theory. A conclusion of the theory is that the total oscillating field does not penetrate to the inner boundary of the sheath, that is, oscillating fields are confined to within a few Debye lengths of the wall.

A very interesting experimental study has been performed by Bryant and Franklin. [28] An attempt was made to establish experimentally the location of charge separation and to deduce the boundary conditions associated with the resonant scattering. A narrow strip of conducting coating was applied to the inner wall of the tube parallel to the tube axis. Resonance spectra were taken with the plane of the strip parallel and perpendicular to the applied field. The main resonance with the plane of the strip perpendicular to the field was reduced compared to the resonance with the strip parallel to the field while the subsidiary resonances were unaffected. Thus it would appear that the charge separation associated with the main resonance occurs at the wall and the origin of the subsidiary resonances must be within the plasma volume. When a wire loop of diameter one half the tube diameter was situated centrally with its plane perpendicular to the tube axis, the main resonance was unaffected while the second and subsidiary resonances were considerably

reduced. Thus it was concluded that "the penetration of the disturbances associated with the higher order subsidiaries becomes increasingly close to the center of the tube as the order increases".

This experimental study gives added confidence to the model proposed by Nickel, Parker and Gould as they have shown that the electron density variation associated with the resonances penetrates farther into the plasma as the order of the resonances increases. For example, for a value of $r_w^2/\bar{\lambda}_D^2 = 72$ the variations of electron density associated with the first Tonks-Dattner resonance extend more than half way into the center of the column.

Moore [29] has shown fairly good agreement between experimental resonant frequency ratios and those determined from a theory for standing radial electron sound waves in a cylindrical column in which the number density is assumed to vary in a Gaussian manner with radius. The good fit of experimental frequency ratios is secured by adjusting the parameters of the assumed Gaussian profile.

In a recent paper by Wolschke [30], the resonances are considered as arising in a cold plasma due to non-uniform radial distribution of electron density. A non-vanishing electron-neutral collision frequency is also considered. Only two resonances are predicted and the prediction of these requires a rather unusual shape for the radial profile in order to give separation of resonances of the order of those experimentally observed. However, some similarity is found for the damping of the resonances as predicted by the theory and that experimentally determined by Franklin. [31] The electron temperature has been neglected in this treatment and the profile models are somewhat unrealistic.

Several workers have successfully used the Tonks-Dattner resonances as a diagnostic method. Nygaard [32] has demonstrated the existence of

radial standing neutral gas sound waves in a 10 Torr neon afterglow by observing the perturbations the waves produce on the Tonks-Dattner resonances. The electron temperature in the afterglow is much lower than in current maintained discharges, thus electrons make few collisions even though the pressure is relatively high and the resonances are not severely damped as might be expected due to electron-neutral collisions. Schmitt 33 has employed the resonances to determine the electron density decay rate and the ambipolar diffusion coefficient in an afterglow plasma.

Stern and Tzoar [34] have employed the Tonks-Dattner resonances to demonstrate scattering from plasma oscillations. Resonant plasma oscillations were excited at the Tonks-Dattner resonant frequencies and a much higher frequency signal was beamed at the plasma simultaneously. The scattering of the high frequency signal from the plasma oscillations led to the appearance of a scattered signal at the difference frequency when resonance occurred for the lower frequency.

Very little experimental work on the Tonks-Dattner resonances has been done in plasmas other than mercury. Messiaen [35] has reported observing the resonances in cesium, argon, neon, helium, nitrogen and hydrogen. No electron density measurements were undertaken and only a single frequency was employed. Resonances were obtained over a wide range of pressures (2-250 mTorr). The secondary resonances were of lower amplitude than for mercury in the case of all gases studied.

Stern [36] has studied the resonances in helium for frequencies between 2 and 4 gHz. Fewer and broader resonances were found than are reported in mercury plasmas. In later experiments, Stern [37] has reported cross-modulation of microwave signals chosen so as to excite different Tonks-Dattner resonances; harmonic generation and frequency

mixing have also been shown to occur for frequencies exciting the resonances. [38]

In the course of studying the splitting of standing surface wave resonances, Kojima, Hagiwara and Ogihara [39] have observed that fewer resonances are found in neon at pressures between 0.13 and 0.73 Torr, using 4 gHz microwaves, than in mercury.

G. F. Haggquist [40] made a study of the main dipole resonances in argon and neon; however, measurements of electron density and temperature were not made.

It was suggested in 1964 by N. L. Oleson that the Tonks-Dattner resonances be studied experimentally in the rare gases since there has been on complete quantitative data on these gases. The results described in this thesis have followed from this suggestion.

III. APPARATUS

This section describes the equipment and circuits used in the present study of the Tonks-Dattner resonances in rare gas plasmas. The essential parts of a system designed to excite the Tonks-Dattner resonances are a discharge tube and a waveguide or transmission line system with its signal generators and detectors. In addition to these, a vacuum system and gas filling system are required. Langmuir probe circuits and microwave cavity resonator systems are required for diagnostic studies. The apparatus is described in detail in the following paragraphs while the procedures and details on applications are given in Sections IV and V.

1. Vacuum Systems and Pressure Measuring Equipment

The discharge tubes used in this study were operated in direct connection with the evacuating and filling system to allow rapid and convenient variation of filling gas and pressure. Two vacuum systems were used. The first (Vacuum System 1) was of small bore glass tubing evacuated with a Consolidated Electrodynamics Corporation, three stage, glass, oil diffusion pump (speed 25 l/sec) trapped with a liquid nitrogen trap. Two one liter flasks of the filling gas (Airco neon, Linde argon or xenon) were isolated from the pumping train with glass vacuum stopcocks. Discharge tubes were isolated from the filling system with a one-half inch Granville-Phillips bakeable valve. The ultimate pressures ($\simeq 10^{-7}$ Torr) obtained after baking the discharge tubes and system lines with heating tapes were monitored with a Veeco RG-75P ionization gauge.

A second vacuum system (Vacuum System 2) was constructed in order to obtain improvements over the pumping speed and cleanliness of Vacuum System 1. This system was evacuated with a Veeco EP2-1, two inch metal diffusion pump (speed 80 l/sec) trapped with an AeroVac Model AT2F

liquid mitrogen trap. Connection to the remainder of the system which was of glass was through a General Electric 1½ inch bakeable valve. The discharge tube and one inch diameter lines connecting the filling system were mounted above a Transite table top to allow lowering of an oven over the table top for baking. Granville-Phillips one half inch valves were used throughout. Only one flask of filling gas was connected to the system. After baking, ultimate pressures of 10^{-8} Torr and below were obtained on Vacuum System 2 as measured with an NRC type 563-P ionization gauge. The pumping speed of this system was considerably improved over that of Vacuum System 1, largely due to the use of shorter sections of larger tubing in connection of the components.

On both vacuum systems, pressures in the operating range (10^{-3} to 10^{-1} Torr) were measured with a Westinghouse type 7903 ionization gauge, calibrated by use of an oil filled manometer. Manometers were closed off from the systems after calibration of the gauge which was accomplished as follows:

Define the volume of the system including the discharge tube as V_s and the volume of the manometer with the oil level at zero pressure as V_m. V_m includes the volume of glass tubing between the oil surface and the valve separating the manometer from the system. The manometer was filled with gas to a pressure P_{1m} (cm oil) and the manometer valve closed. The system was evacuated to a very low pressure P_{1s} and the line to the pumps was closed. When the manometer contents were released into the system the overall pressure became P_2 (cm oil). Then assuming constant temperature

$$P_{1s} V_s + P_{1m}(V_m + \Delta_1) = P_2 (V_s + V_m + \Delta_2) \qquad (34)$$

where $\Delta_{1,2}$ are the volumes of manometer tubing increase due to oil displaced by P_{1m} and P_2 respectively. In general, Δ_2 is negligible compared to $V_m + V_s$ and P_{1s} is negligible compared to P_{1m}. By measuring the lengths of glass tubing it was found that

$$\frac{\Delta_1}{V_m} \simeq 0.005\, P_{1m} \tag{35}$$

Therefore, the ratio $V_r = \frac{V_s}{V_m}$ can be calculated from the formula

$$V_r = \frac{P_{1m}(1 + 0.005\, P_{1m})}{P_2} - 1 \tag{36}$$

By repeating this procedure several times using large values of P_{1m} so that P_2 could be read accurately, the value of V_r could be determined accurately and then subsequent pressures (in Torr) P_2' could be calculated from

$$P_2' = \frac{(1 + 0.005\, P_{1m})\, P_{1m}}{V_r + 1} \left(0.672\, \frac{\text{Torr}}{\text{cm oil}}\right) \tag{37}$$

In this manner pressures as low as 10^{-3} Torr could be accurately determined. V_r was found to be 53.3 ± 1.1 for Vacuum System 1, therefore, a P_1 of 10 cm oil corresponded to a P_2' of 1.30×10^{-1} Torr.

Numerous fillings of the manometer allowed calibration of the 7903 ion gauge. The manometer was read by a cathetometer at a distance of about 10 feet.

Having calibrated the ion gauge by this method, pressures could be read directly by the gauge. Calibration curves for the gauge tube on Vacuum System 1 are shown in Fig. 7 for argon, neon, and xenon. It is estimated that by this procedure pressures in the discharge tube could be read to within 5%. The calibration curves show the ratio of ion current I_+, to the electron current I_-, plotted against pressure.

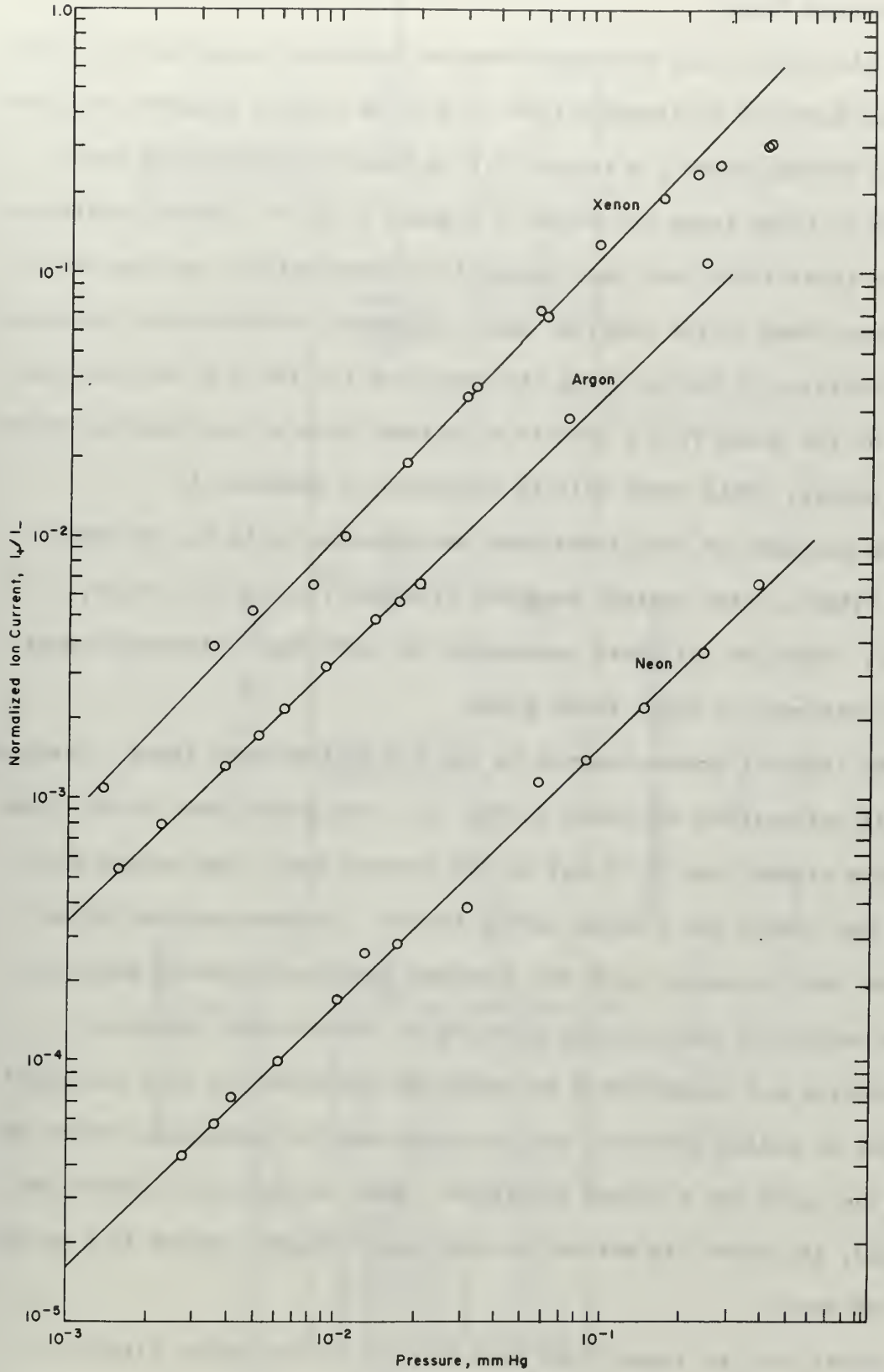

Figure 7. Calibration curves for W[illegible]inghouse 7903 ion gauge; neon, argon and xenon.

2. Discharge Tubes

In this study, two discharge tubes of different diameters were used. On Vacuum System 1 a discharge tube of 3.51 cm outside diameter was used while on Vacuum System 2 a tube of 1.0 cm outside diameter was used. Diagrams of these tubes are shown in Figures 8 and 9. Several modifications to these tubes were made during the investigation, but the basic dimensions shown in the diagrams were unaltered. Modifications consisted in the addition of probes along the tube, and for the 3.51 cm tube, the change of the anode from a disk to a cylinder with a flat tungsten spiral at its center. This anode will be discussed in Appendix A.

The cathodes of both tubes were Westinghouse Style No. 14-39601 coiled ribbon, oxide coated, tungsten filaments, rated at 5 volts, 7.5 amperes. Tantalum cylinders surrounded the cathodes. Discharge tubes were constructed of Pyrex brand glass.

The Langmuir probes mounted in the 1.0 cm tube were fixed. Drawings of their orientation are shown in Fig. 10. The probes were 20 mil tungsten wire etched down to 15 mil in the exposed part. The etched part ended just inside the alumina tubing sleeve. In this way, the probe base was not in contact with the sleeving and thus spattered deposits on the outside of the sleeving were not in contact with the probe.

Etching was accomplished by immersing the probe tip in a saturated solution of sodium hydroxide and passing a small alternating current between the probe and a crabon electrode. When the desired diameter was obtained, the probe tip was cut to the proper length, ground flat on the end, and bent.

Probes for the larger tube were movable in the radial direction. Diagrams of the construction are shown in Figure 11. Probes were made

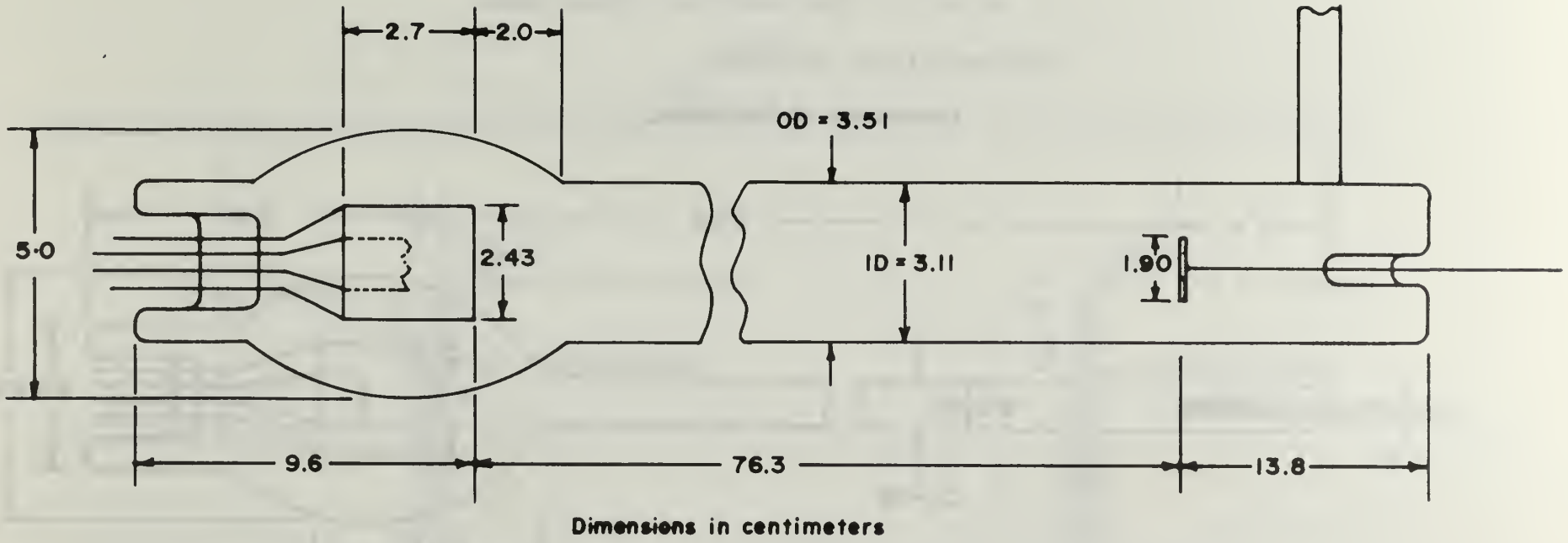

Figure 8

Experimental discharge tube, 3.5 cm OD

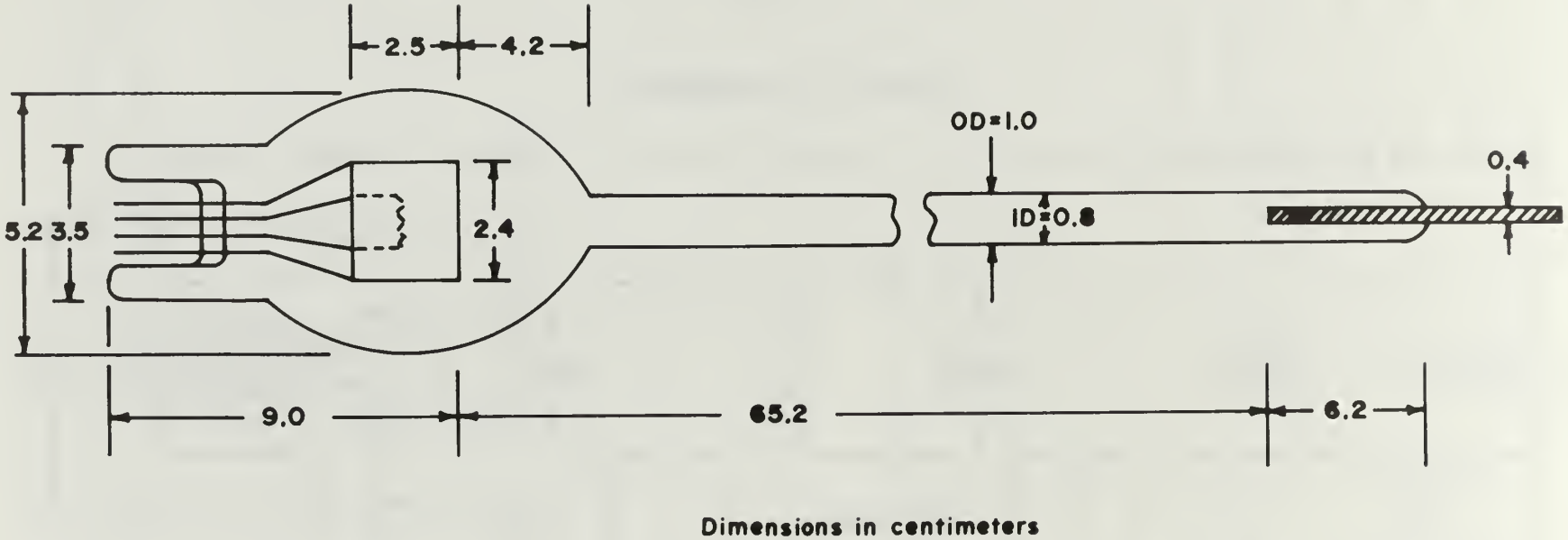

Figure 9

Experimental discharge tube, 1.0 cm OD

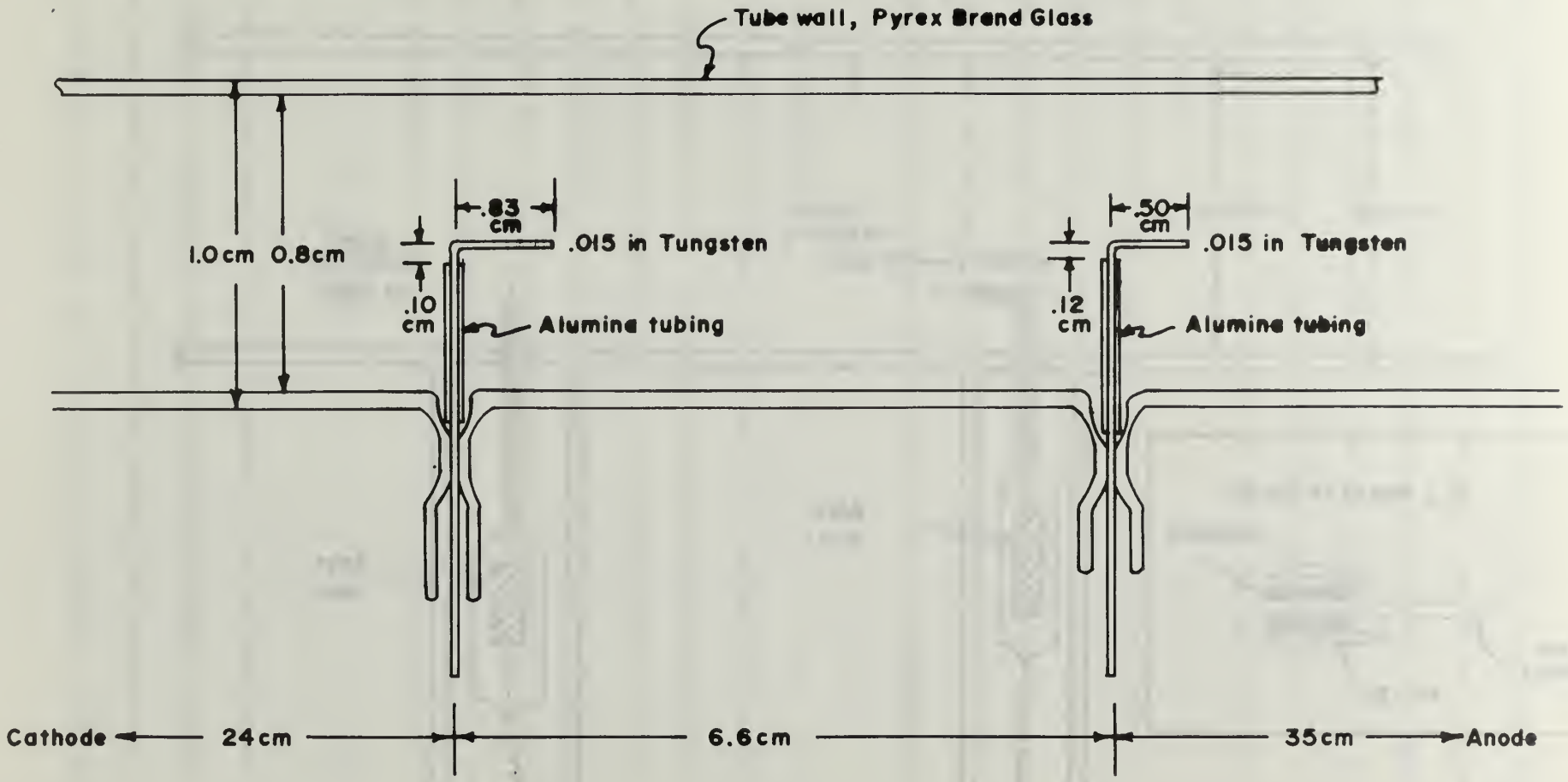

Figure 10

Orientation of probes in smaller (1.0 cm OD) discharge tube

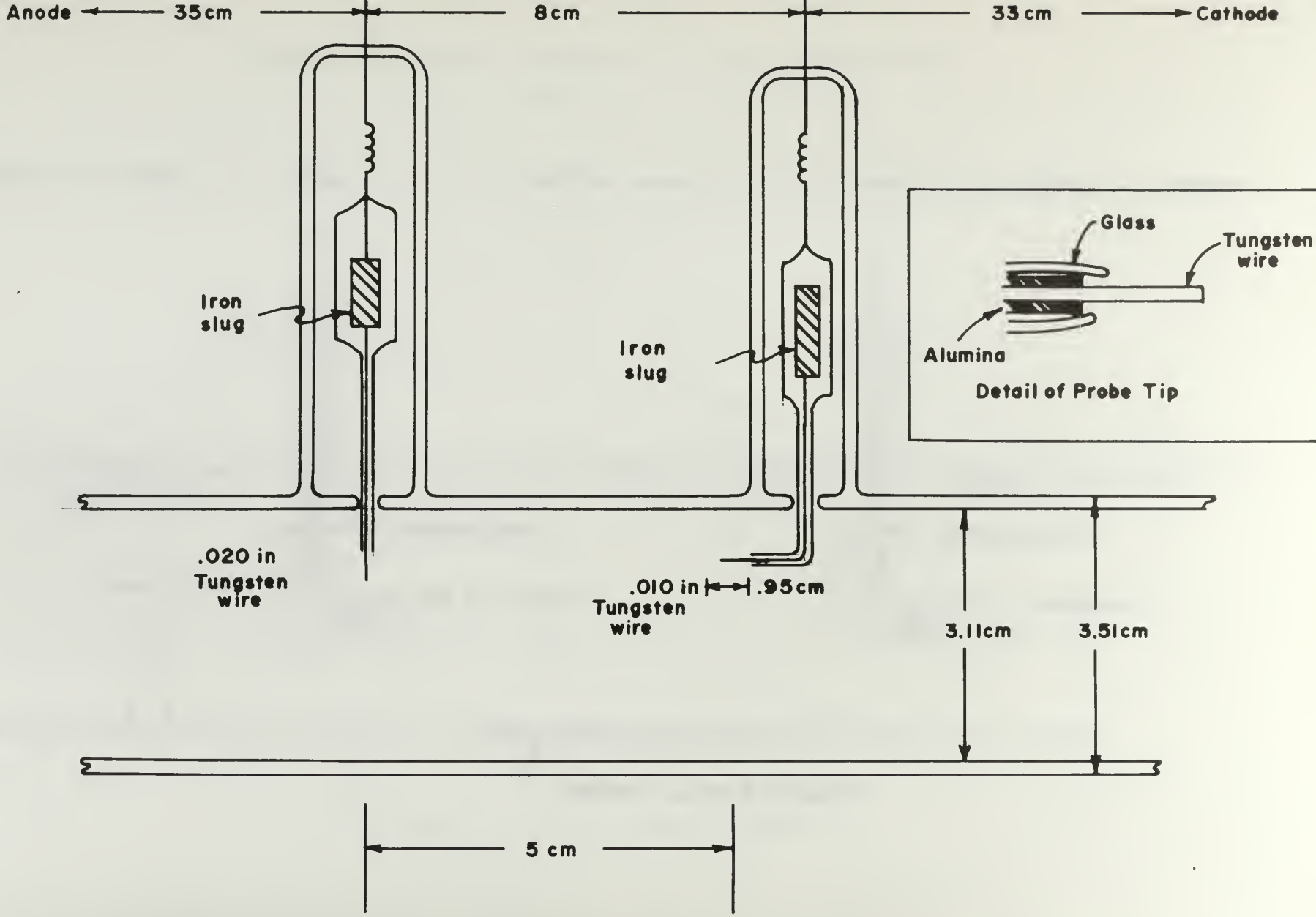

Figure 11

Construction of probes in larger (3.5 cm OD) discharge tube

of tungsten wire. The radially directed probe tips were 20 mil and either 0.34 or 0.68 cm long while the axially directed probe was 10 mil. Glass sleeves which were closed to within 0.2 mm of the wire covered the unexposed wire. A close fitting alumina tube acted as a spacer to hold the probe in the center of the glass opening (see inset of Fig. 11). A steel slug was enclosed in glass for moving the probe in and out with a small permanent magnet.

The probe along the axis of the discharge tube was 10 mil wire and the construction of the tip was similar to the previously described probe. The wall of the carrier tube and the glass around the magnetic slug were flattened on one side to prevent drooping of the probe tip.

Probe positions were determined with a mirror and a cathetometer at a distance of 10 feet.

3. Discharge Tube Circuits

In order to avoid the problems associated with tuning rf circuits for different frequencies, it is desirable to vary the current in the discharge tube when observing resonances. It is characteristic of the discharge in a plasma column at certain pressures that the voltage across the tube is constant for a varying current through the tube. Since the electron drift velocity is much greater than the ion drift velocity the current can be found from

$$I = \bar{n}_e \bar{v}_e e A \tag{38}$$

where $\bar{v}_e$ is the average electron drift velocity, A is the area of the tube, e is the electron charge and $\bar{n}_e$ is the average electron density. Thus it can be seen that the average electron density is proportional to the current, providing the average drift velocity is constant. The drift

velocity will remain constant for a given pressure provided the axial electric field is constant, which is constant provided the voltage drop across the tube does not change.

In most of the experiments described in this work, the discharge current was varied manually. Fig. 12 shows the wiring of the circuit for the discharge tubes.

The discharge tube filament supply for the 3.5 cm tube was provided by a diode rectifier, filtered 9 volt power supply which was controlled by an autotransformer. The ripple on the filament direct current was about 10%, 120 Hz. The filament supply for the 1 cm tube was similar except for somewhat better filtering which reduced ripple to less than 0.1%.

Discharge tube current was controlled by the voltage of the power supply which is connected through the series resistance to the discharge tube. The supply for the 3.5 cm tube was a locally constructed 0 - 5 KV, 0 - 1 ampere, dc, unregulated, filtered supply with output voltage controlled by an autotransformer on the input of the supply. The supply for the 1 cm tube was a Kepco Model 1250B regulated, 0 - 1000 v, 0 - 500 ma dc supply.

In early work on attempting to observe the resonances a pulsing circuit was constructed. The circuit is shown in Fig. 13 and is nearly identical to that used by Nickel. [23] A 0.1 mfd capacitor was charged through a high resistance and was discharged through a thyratron causing a current through the discharge tube which decayed approximately exponentially. The firing pulse for the thyratron was provided by a General Radio Model 1217-B unit pulse generator. The pulse repetition rate was 10 sec^{-1}.

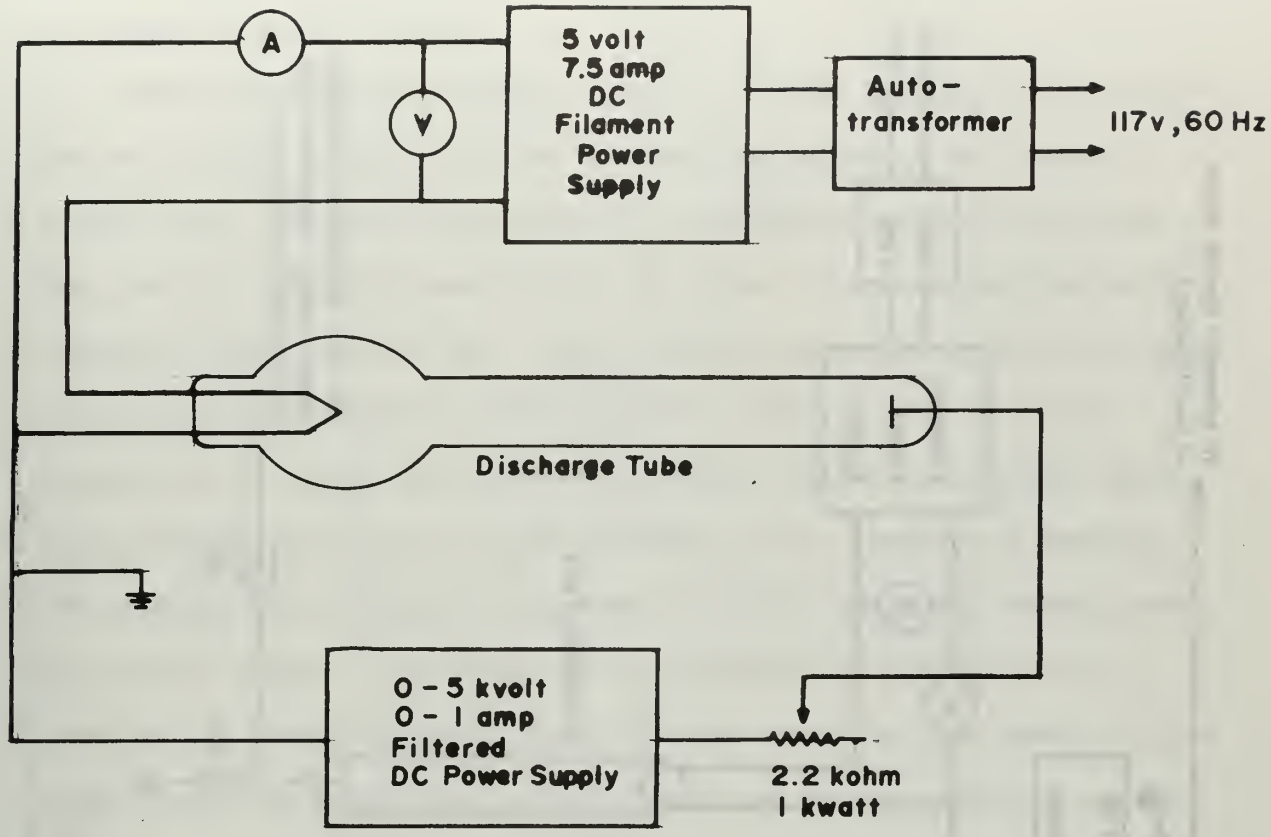

Figure 12

Circuit for discharge tube, manually varied current

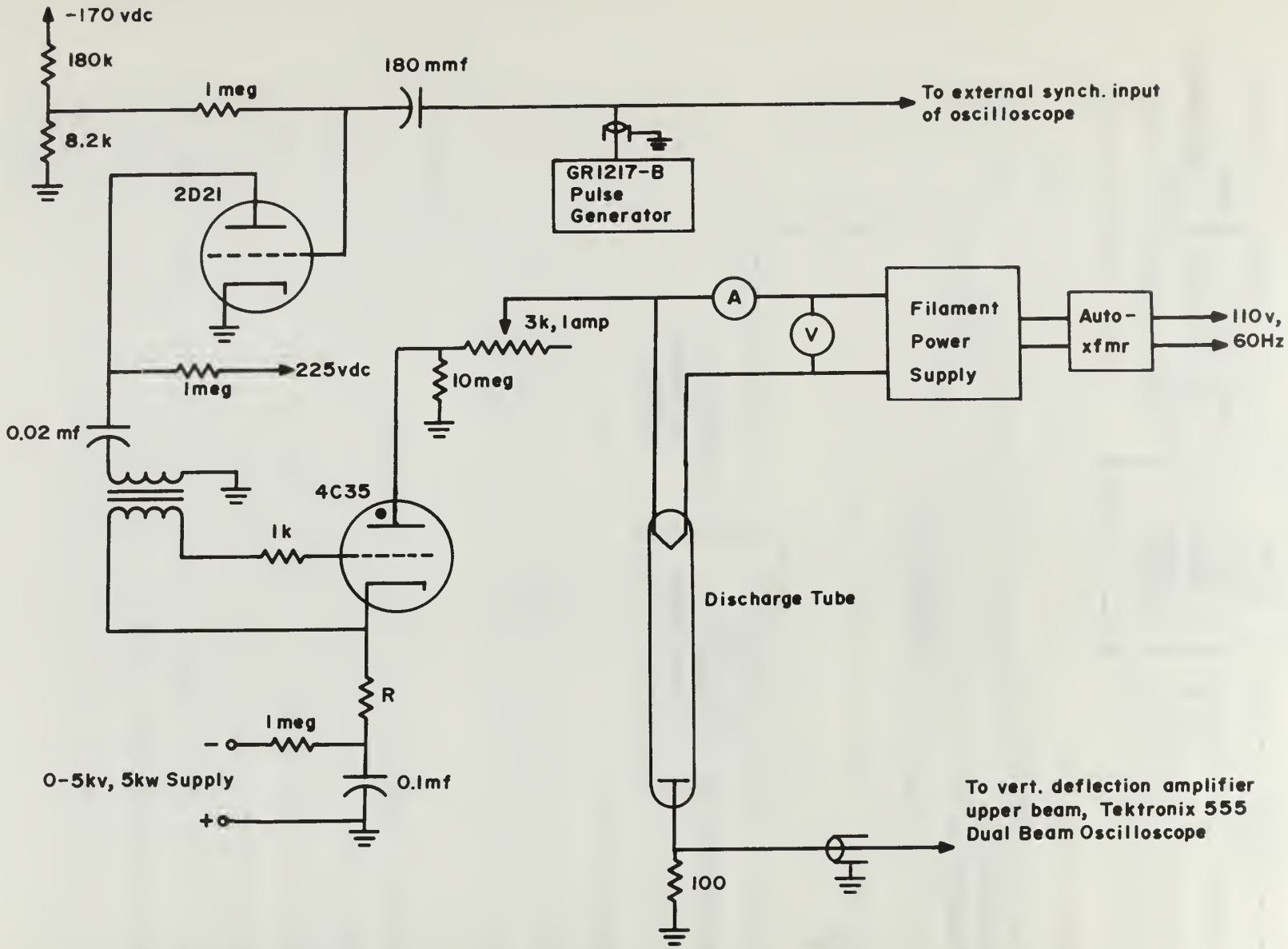

Figure 13

Pulsing circuit for discharge tube current variation

A signal proportional to the instantaneous discharge tube current was available at the 100 ohm resistor connected to the cathode.

4. Radio Frequency Circuits

When operating the discharge tube in a pulsed fashion the rf circuit was as is shown in Fig. 14. The rf signal was provided by a Hewlett Packard 608 C VHF signal generator for frequencies between 100 and 450 MHz, and by a Hewlett Packard 612 A UHF signal generator for frequencies between 450 MHz and 1000 MHz. The signal was connected by coaxial cables to a strip-line concentric with the tube. From the other end of the strip-line the signal was conducted by coaxial cable to a General Radio 50 cm tuneable stub and a 50 ohm adjustable line, thence to a detector. The detector was a Sylvania 1N26 crystal held in a Hewlett Packard Model 420 crystal holder. The output of the detector was connected to the lower beam vertical amplifier of a Tektronix Model 555 dual beam oscilloscope. Both the lower beam and the upper beam on which current was displayed were triggered by a pulse from the pulse generator.

For manual variation of the discharge tube current, two rf circuits were used. One method measured the signal transmitted beyond the strip-line, and the other measured the signal reflected by the strip-line. The method of measuring the transmitted signal is shown in Fig. 15. The circuit is essentially the same as in Fig. 14 except that the signal is detected with the probe input of a Hewlett-Packard Model 411 A rf millivoltmeter. The output of the HP 411 A was conducted to the x-y recorder where it was plotted against the discharge current.

The signal reflected from the strip-line can also be used to indicate the resonances. If the transmission line is matched in such a way that the reflected signal is a maximum in the absence of a plasma in the

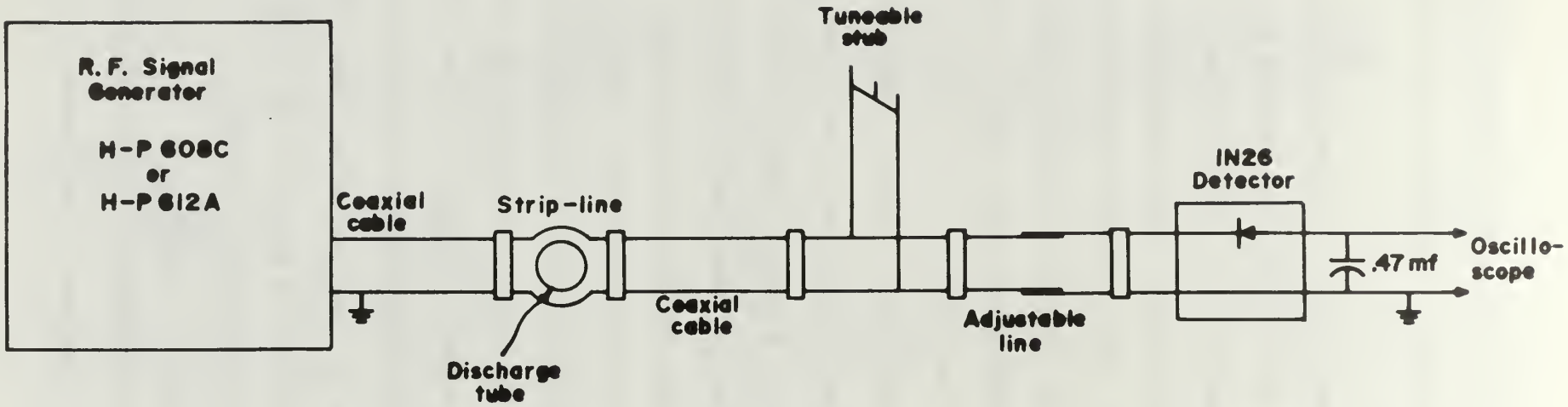

Figure 14

Radio frequency circuit, pulsed discharge operation

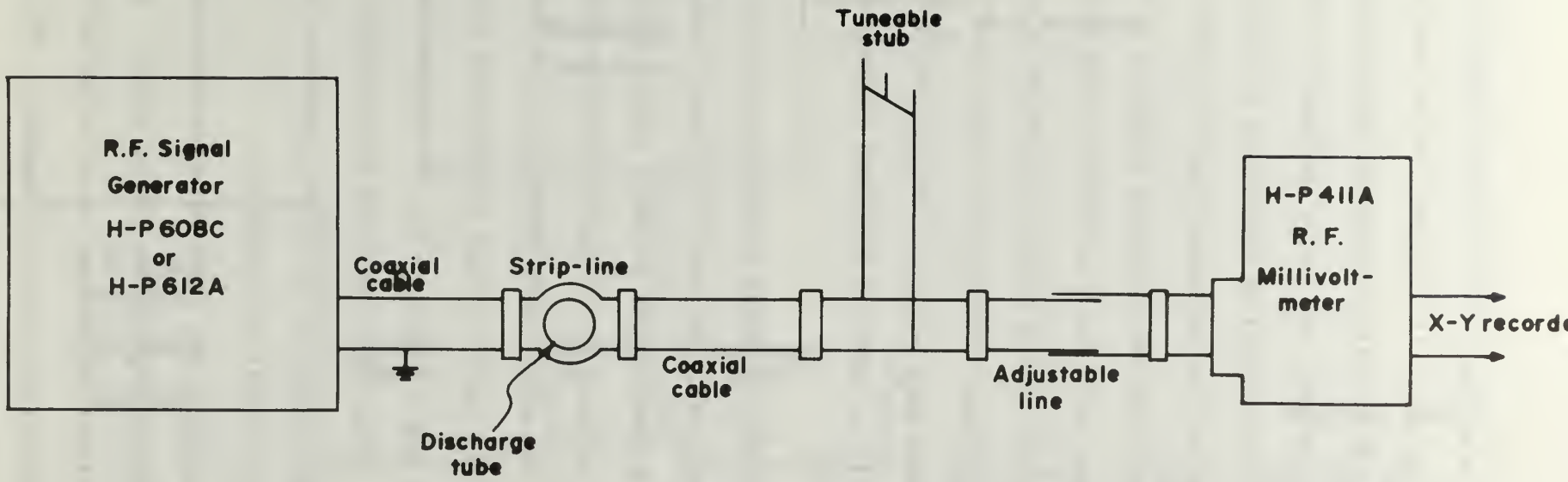

Figure 15

Radio frequency circuit, manual discharge tube operation, transmitted signal measurement

tube, the resonances will show as minima in the reflected signal as the plasma current is varied since the power is scattered out of the forward direction at resonance. This is essentially the method used by Nickel [22] in his measurements with dipole devices. No tuning devices are ordinarily required in this arrangement as the strip-line appears as an approximate open circuit in this arrangement and the reflected signal is large. If the line is matched in such a way that the reflected signal is a minimum without the plasma, the resonances will occur as maxima in the reflected signal. The latter method requires tuning devices before the strip-line to reduce the reflection to zero before igniting the plasma, and is described by Stern. [36] Both methods were employed, once it had been ascertained that the resonance conditions were not dependent on the method of observation.

When taking data on the resonances using a reflected signal, the circuit shown in Fig. 16 was employed. The dual directional couplers, Hewlett-Packard models 765D and 764D sampled incident and reflected signals. These were detected by Sylvania 1N26 crystals in Hewlett Packard Model 420 A crystal holders. The signals were compared in the ratio meter, Hewlett Packard Model 416A and an output voltage proportional to the ratio of reflected to incident power was recorded on the x-y recorder as a function of discharge current. The ratio meter has the advantage of compensating for any changes in the output of the signal generator due to changes in the impedance of the circuit at resonance.

For high frequency measurements, the ratio meter was employed with a TS-403, 2 - 4 gHz, signal generator providing the rf signal. A Hewlett Packard Model 767D dual directional coupler was used. A pyramidal S-band waveguide horn replaced the strip-line in this arrangement. The 1000 Hz

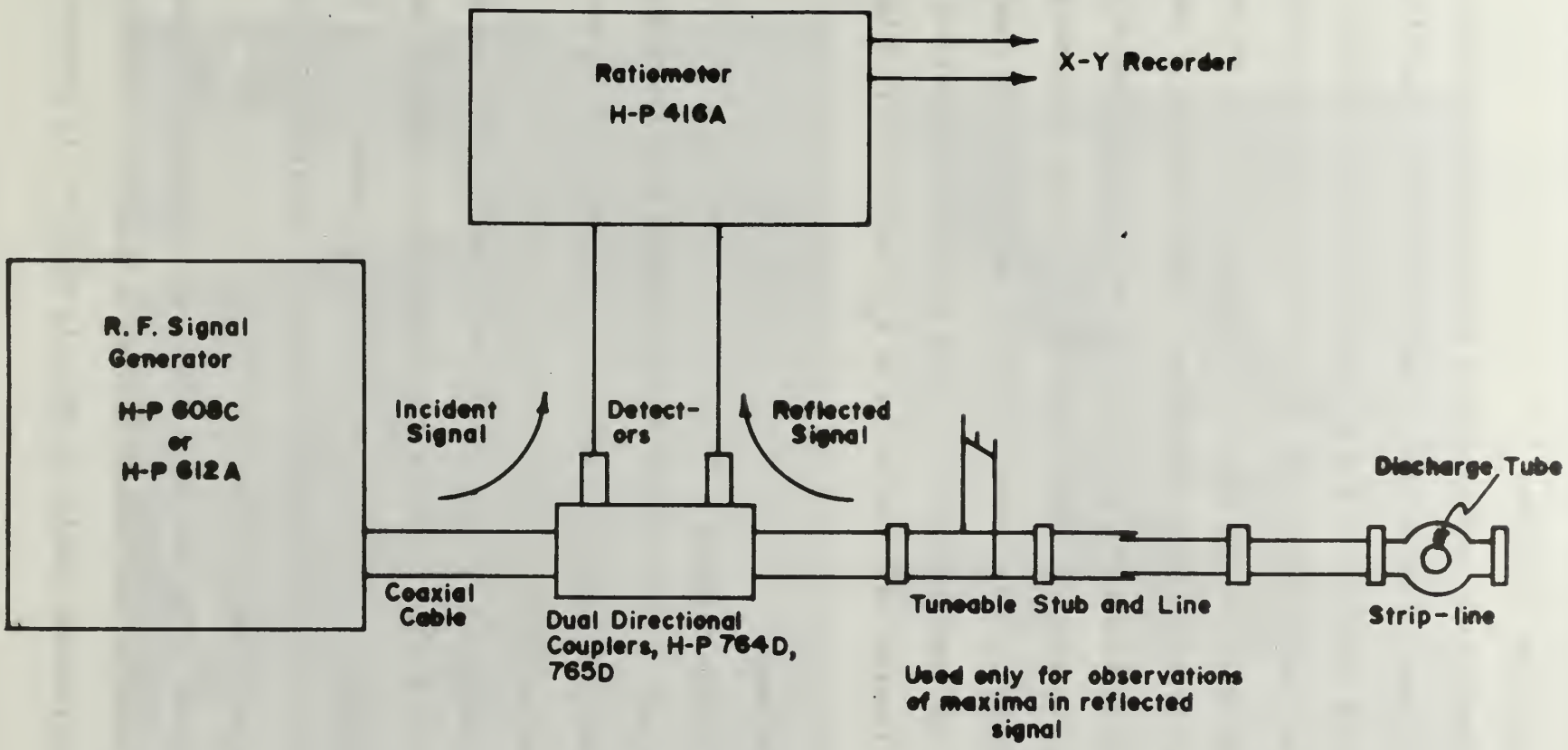

Figure 16

Radio frequency circuit, manual discharge tube operation, reflected signal measurement

modulation required by the ratio meter was provided by modulating the TS-403 with a square wave of 1000 Hz.

The strip-lines for the observations of resonances were locally constructed. They were patterned after lines described by Crawford but have characteristics identical to the dipole devices used by Nickel.

Several sizes of strip-lines were used but the construction in all cases consisted of copper strips bent into semicircles so that one strip passed around each side of the discharge tube. Some extension of the strips was allowed on either end of the device for connection which was made with BNC type connectors. These end extensions were insulated from one another by Plexiglas brand acrylic plastic. Photographs of some of the devices used are shown in Fig. 17. Table 1 gives the dimensions of the devices used together with the values of K_{eff} calculated from Eqs. (25) and (26).

5. Diagnostic Equipment

(1) Langmuir Probe Circuits

A large part of the diagnostic investigation for this work was accomplished by means of Langmuir probes. Actual probe construction has been discussed earlier.

Probe characteristics for the case in which moving striations produced small density changes and potential changes were taken with the help of an x-y recorder. A simple circuit was constructed to vary the bias on the probe and to give outputs proportional to voltage and current. This circuit is shown in Fig. 18.

In order to observe the effect of moving striations on the Langmuir probe characteristics an oscilloscope display is necessary. The circuit most used for oscilloscope display is shown in Fig. 19. It combines

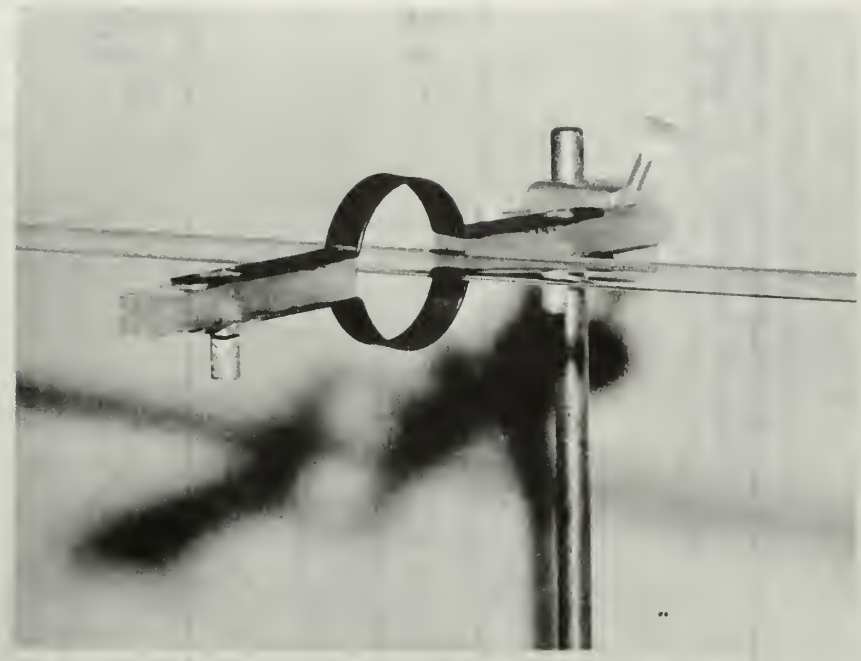

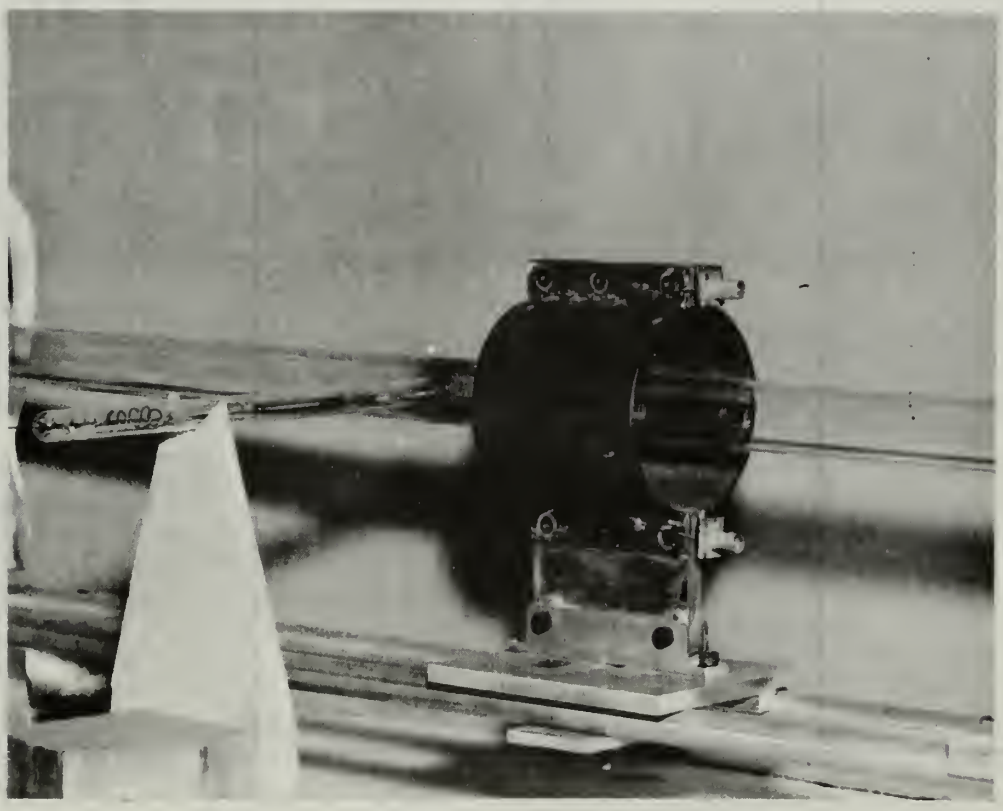

Figure 17

Photographs of strip-lines (dipole devices)

Stripline Radius cm	Stripline Width cm	Tube Inside Radius cm	Tube Outside Radius cm	K_{eff}
2.86	1.60	1.56	1.76	3.74
5.08	3.0	1.56	1.76	1.82
5.06	10.0	1.56	1.76	1.82
2.35	1.6	0.4	0.5	2.1

Table 1

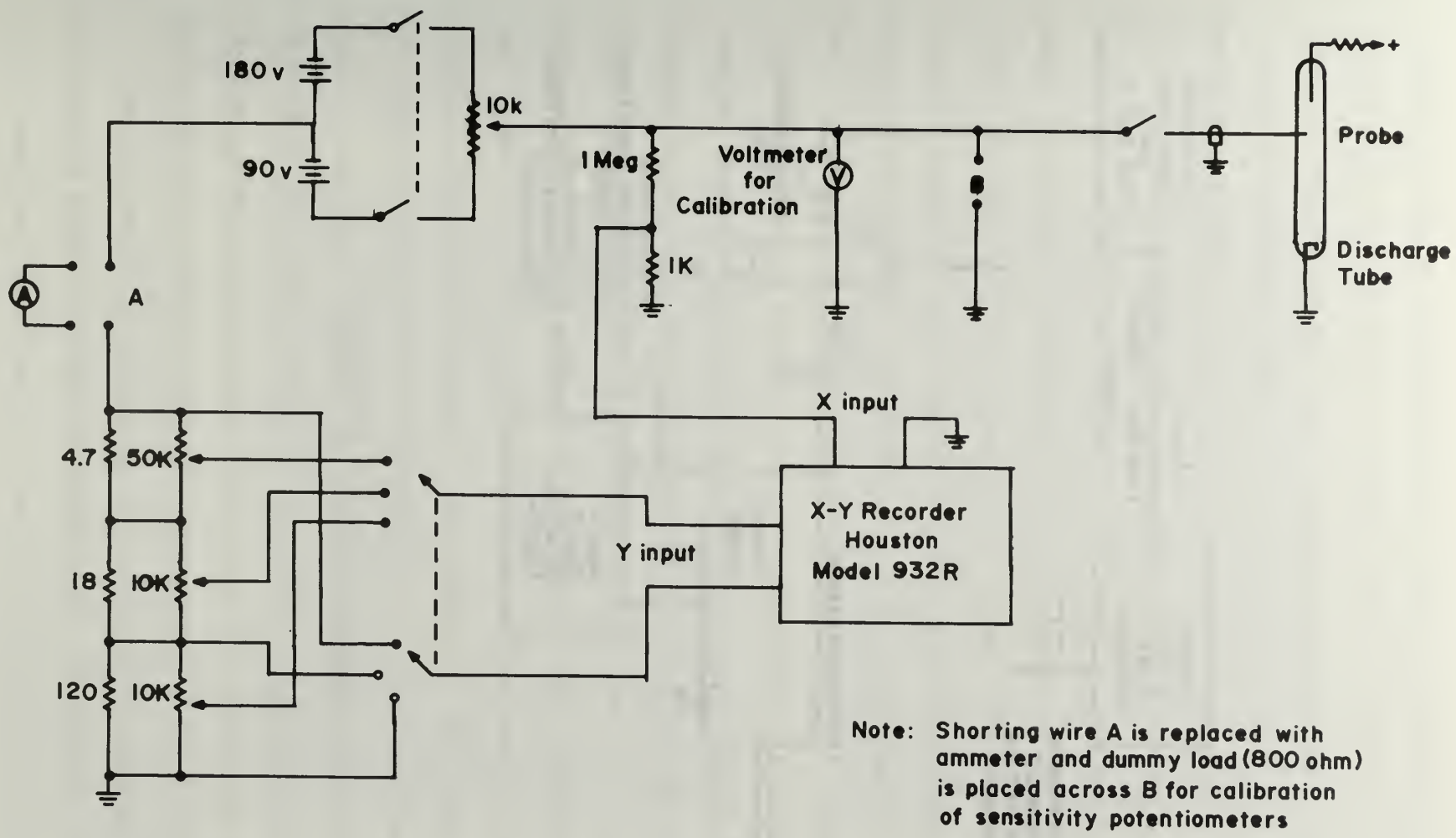

Figure 18

Circuit for display of Langmuir probe characteristics on an x-y recorder

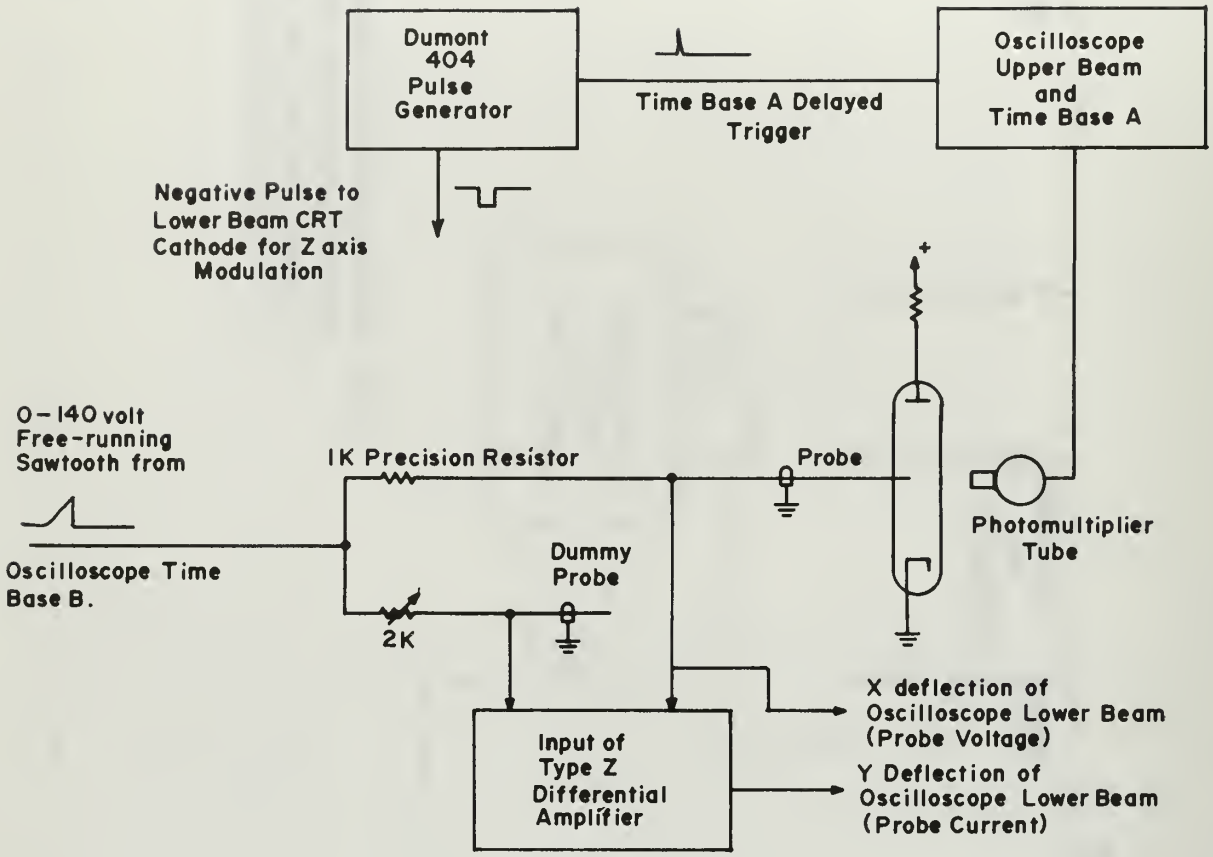

Figure 19

Circuit for display of Langmuir probe characteristics on an oscilloscope

features of several techniques for x-y display of probe characteristics. [41,42,43] It was intended to use the circuit to study the moving striations by sweeping the voltage on the probe in a time short compared to the moving striation period. For this method, a dummy cable was required to buck out the stray capacitance of the line to the probe. However, the distributed capacitances of the lines to the probe and to the dummy cable were so large that the current for charging them was large compared to ion currents collected. The ion characteristics were severely distorted. Since the ion current was of primary interest, the sweep rate was lowered so that a number of moving striations passed the probe during the sweep time. This caused the striations to modulate the current characteristic. If the current characteristic for a given phase of the striation was desired, it could be obtained by intensity modulating the display. The light intensity variations of the striations were observed on the upper beam of a Tektronix 555 dual beam oscilloscope. The sweep for this display was provided by time base A. A trigger pulse was available from the scope at a time which could be variably delayed with respect to the beginning of the sweep of time base A, i.e., with respect to the rise of striation light intensity. This pulse was used to trigger a Dumont Model 404 pulse generator, which provided a negative pulse of sufficient amplitude to intensity modulate the oscilloscope beam on which probe voltage and current were displayed for a time very short compared to the moving striation period. In this manner the probe characteristic could be obtained for any portion of the striation.

Without intensity modulation, the entire probe characteristic could be displayed showing information on all points of the striation in a single sweep (but not allowing connection of points for similar striation

phase). This was of value for extablishing maximum and minimum densities occurring during the striation. Oscillograms of the probe characteristics obtained in this manner are shown in Figures 20a and 20b. Figure 20a shows the ion current-voltage characteristic as modulated by the moving striations, while Fig. 20b shows the time-sampled characteristic for a point about 60° before the minimum light intensity.

The variable resistance in the dummy probe branch of Fig. 19 was necessary because the Type Z input could not be balanced internally on all voltage ranges. The range of voltage sweep about the floating potential of the probe could be altered by adding series resistances between the cathode of the discharge tube and ground.

(2) Microwave Cavity Circuits

A cylindrical microwave cavity was constructed for the purpose of making electron density measurements in the discharge tubes. This method involves placing the plasma column in the cavity and measuring the shift of cavity resonant frequency resulting. The theory of operation is discussed in Section V. The diagnostic system requires a signal generator to excite the cavity at its resonant frequency in a given mode, a detector for indicating resonance and a frequency meter for accurately determining the resonant frequency. The cavity was designed to be resonant in the TM_{010} mode at 2.44 GHz.

The cavity was constructed of copper and is shown in Fig. 21. The ends of the cavity were removable so as to use the same body for insertion of both large and small discharge tubes along the cavity axis. The cavity was excited by a probe parallel to the cavity axis and approximately 1 mm in length. A second probe of identical construction was located on the opposite side of the cavity centerline and this probe

a)

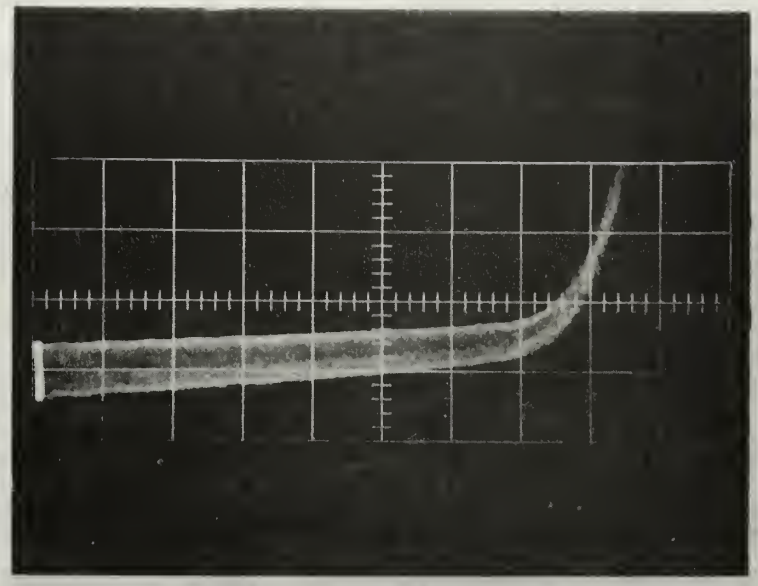

b)

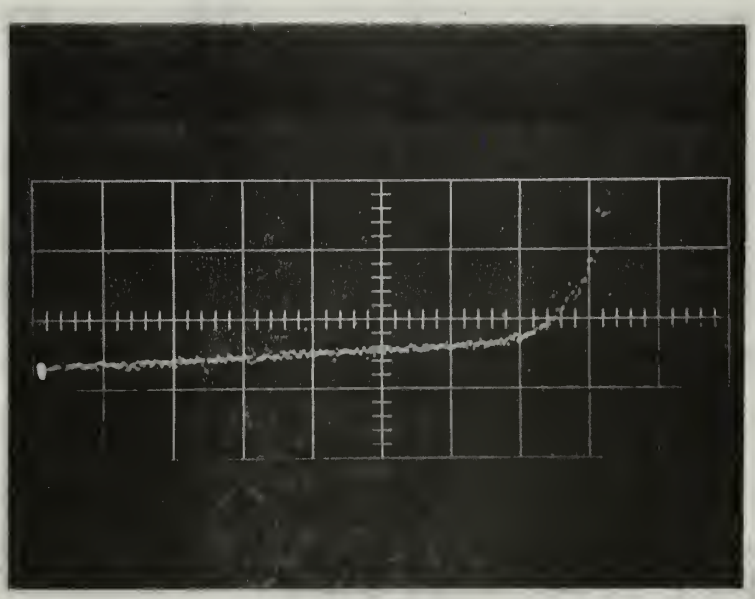

Figure 20

a) Ion current-voltage characteristic of Langmuir probe modulated by moving striation density variation.

b) Time sampled current voltage characteristic of Langmuir probe at a point about 60° before minimum light intensity.

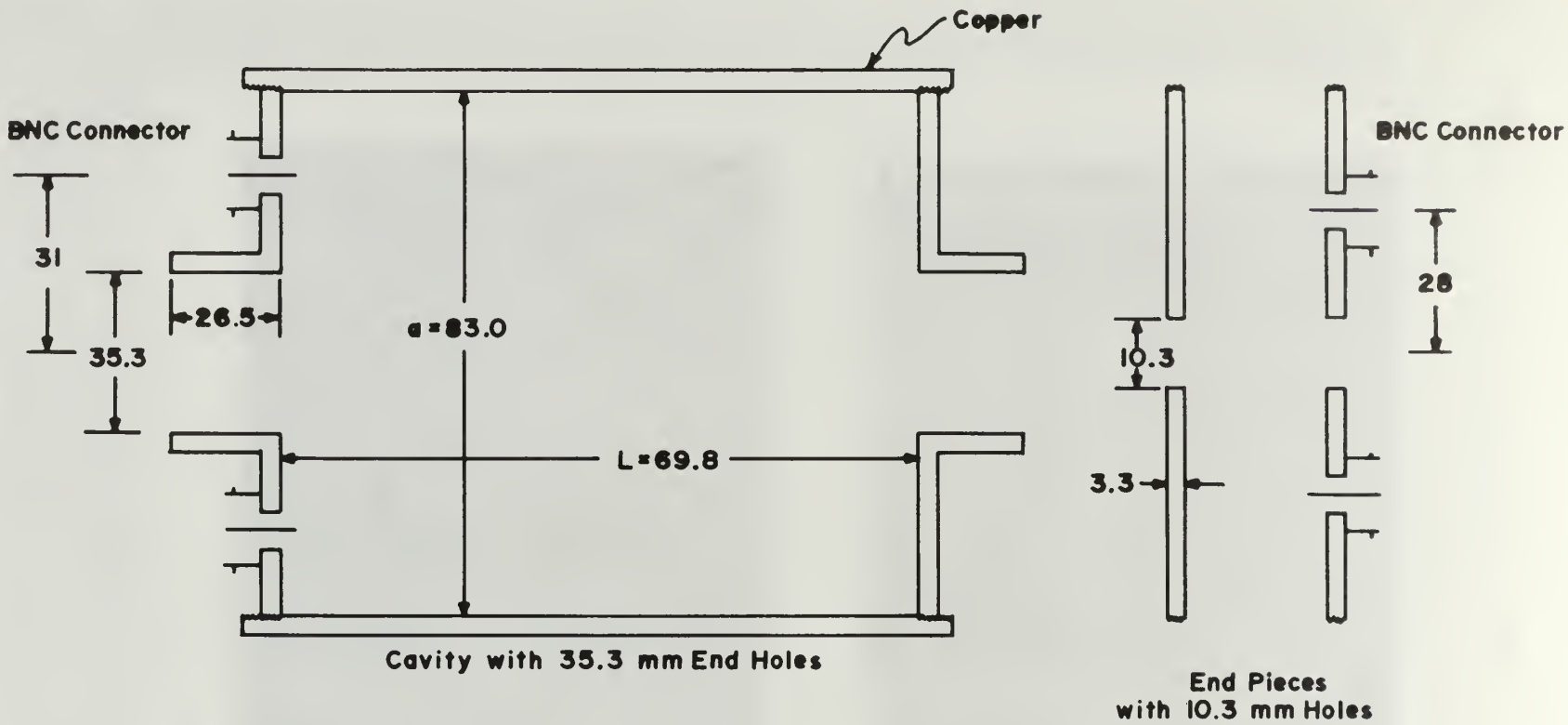

Figure 21

Microwave cavity construction

coupled the cavity signal to a detector. Cavity resonance was indicated by a maximum in the transmitted signal. Probes were used for coupling to prevent coupling to the neaby TE_{111} mode.

The Q of the empty cavity was 2800 but upon insertion of the large glass discharge tube with no plasma the Q was 432. These Q's were determined from the frequencies at which the voltage response dropped to 70.7% of the response at resonance.

$$Q = \frac{\text{resonant frequency}}{\text{difference of 70.7\% response frequencies}} \qquad (39)$$

The end pieces of the cavity with large holes had sections of circular waveguide attached to them for which the frequency of cavity resonance was below cut-off. This was to prevent loss of power by radiation.

The circuit arrangement for cavity diagnostics is shown in Fig. 22.

6. Equipment for the study of Moving Striations

Moving striations in the positive columns of low pressure rare gases could be detected by a variety of means. Probably the simplest is to observe the floating potential variations on a Langmuir probe inserted in the plasma. For the striations present in the gases studied, this signal had an amplitude on the order of 0.5 volt. In order to measure wavelengths of striations, a second independent method of observation was required. This was provided by a photomultiplier tube. A long tube with a vertical slit at its end provided collimation of the light observed by the phototube. The phototube could be moved along the discharge tube parallel to the axis.

For detecting wave propagation at frequencies other than the fundamental striation frequency and measuring velocities of these frequency

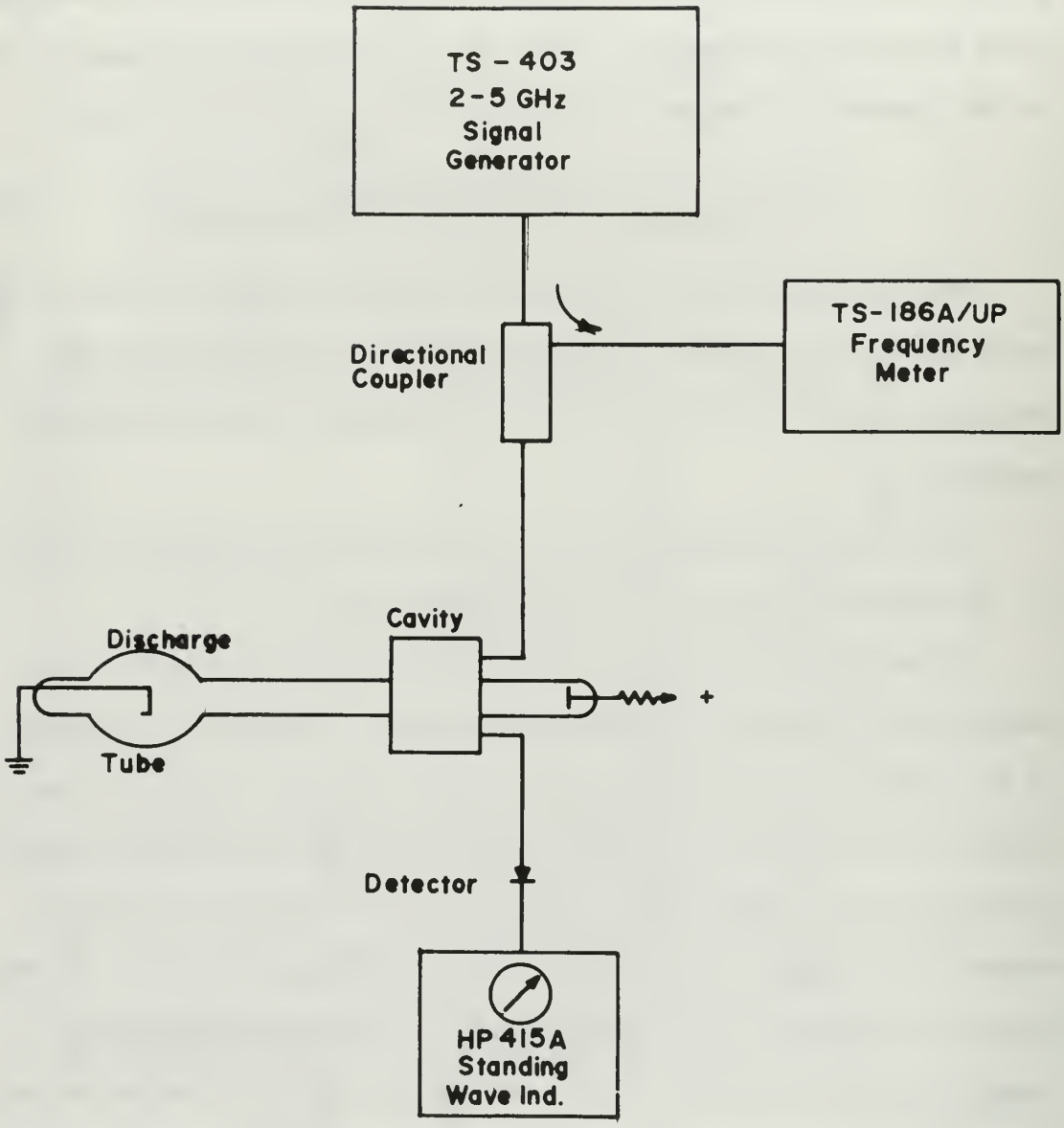

Figure 22

Circuit arrangement for cavity diagnostics

components, a Princeton Applied Research lock-in-amplifier Model JB-5 was used. The light intensity signal was coupled into the amplifier from the phototube. A reference signal was provided from a probe in the discharge tube and the output of the phototube was phase sensitively detected. The purpose of employing a lock-in-amplifier and phase sensitive detection was to select a narrow band of frequencies from the spectrum of frequencies present in the moving striation waveform and to observe the relative phase of the signals from a fixed point and from another point some distance away. The output of the phase sensitive detector gives the cosine of the relative phase of the reference signal (the probe floating potential) and the signal from a detector (the phototube) which is moved along the tube. By observing the change of phase with the distance between these points, the wavelength of a given frequency component can be determined and the velocity can be obtained from these data. The frequencies of interest were the fundamental moving striation frequency and the harmonics of this frequency. Since the harmonic content is rather small the narrow band width of the lock-in-amplifier was required.

The results of studies of moving striation characteristics are given in Appendix A.

IV. EXPERIMENTAL PROCEDURE FOR THE RESONANCE STUDIES

Before making measurements, the tube was evacuated to a very low pressure (on the order of 10^{-7} Torr) and the metal components of the system were degassed. The tube was baked for several hours with heating tapes or oven as appropriate. The tube was filled to a pressure near that at which it was desired to operate. The filament was turned on and cooling air was directed at the cathode bulb. The discharge was turned on and was allowed to operate at a moderate direct current (about 200 ma) for several minutes before taking data. This was done in order to avoid pressure changes due to clean-up effects while taking data on the resonances. The pressure was monitored during operation using the Westinghouse 7903 ion gauge. It was found that fluctuations in pressure were less than $\pm$ 5% about the average pressure for pressures between 1 and 100 mTorr after the tube was operated several minutes. Clean-up was most pronounced after filling a freshly baked tube and somewhat longer operation was necessary before the pressure stabilized. Clean-up effects were more noticeable at lower pressures and were most severe in xenon at pressures around 1 mTorr. It should be pointed out that no data was ever taken on the first filling of the tube with a given gas. The tube was always operated, then pumped out and refilled to purge the tube with the gas being studied.

Lower limits of pressure for operating the tube were determined by the failure of the discharge to remain in a normal glow mode of operation. At pressures around 10 mTorr in neon and 1 mTorr in argon and xenon, the discharge changed to what is termed a "collapsed" discharge. This unstable discharge form has been reported by several other workers. [40,44] In this situation the voltage across the tube no longer remained constant

for changing current but rose with increasing current. This mode is characterized by an increased dark space in front of the cathode and a somewhat fainter glow in the remainder of the column. It is easily recognized when it sets in. The current-voltage characteristic of this mode is not reproducible. Also the discharge may oscillate at random between the normal mode and the collapsed mode. This mode occurred at somewhat higher pressures in a newly installed tube, possibly due to an incompletely activated cathode.

After assuring stable operation of the discharge, the circuit was changed for pulse operation to that shown in Fig. 13. The resistance R was adjusted to give the largest possible change in current through the tube without causing an abnormal discharge form. In order to assure that a normal glow was present in pulsed operation, the voltage across the tube was observed on an oscilloscope. Subsequently, the signal generator was turned on and using the oscilloscope presentation of detector output as a reference, the tuning stub and line were adjusted for a maximum transmitted signal past the strip-line at the desired frequency. When resonances occurred for the applied signal frequency the oscilloscope presentation was photographed. From the photographs the current for resonance could be determined.

The time constant of the current decrease in this mode of operation was about 5 milliseconds. The relaxation time of the electron density distribution is on the order of 20 microseconds, thus the above time constant is large compared to this value and it can be assumed that the electron density distribution is in equilibrium with the current.

The pulsed method was found to be unsatisfactory for obtaining clear resonances other than the main resonance. There seemed to be some evi-

dence that the first Tonks-Dattner resonance was being detected in argon at a pressure of about 10^{-2} Torr. A photograph of a typical presentation is shown in Fig. 23. The main resonance is clearly visible in both photographs and the first T-D resonance seems to be faintly visible as the current decays. The absorption for the first T-D resonance is very small relative to the main resonance on this the most sensitive scale (.005 v/cm) of the oscilloscope vertical amplifier.

In subsequent work it was shown that the failure to observe the resonances with a pulsed discharge was due to the occurrence of moving striations. These striations will be discussed in more detail in Appendix A. The failure to observe the resonances clearly using the pulsed technique caused its abandonment. It was employed only on argon and no quantitative data were obtained.

The most successful method of observing the resonances by varying discharge current was one in which the current was varied manually while simultaneously recoring rf power and discharge current on an x-y recorder. Two rf circuits were employed in this connection as described in Figs. 15 and 16. Traces were made on the x-y recorder starting at high current, slowly decreasing the applied voltage until the discharge extinguished. Traces were started at high current since the discharge would not ignite at low currents but started at some value large compared to the minimum obtainable. Curves were plotted at frequency intervals of about 25 MHz throughout the region where resonances were present.

Absolute values of rf power in the transmitted signal were not measured; the attempt was to make resonances as well defined as possible.

The technique used for reflected signal measurements was similar to that used to make transmitted signal measurements and used the circuits

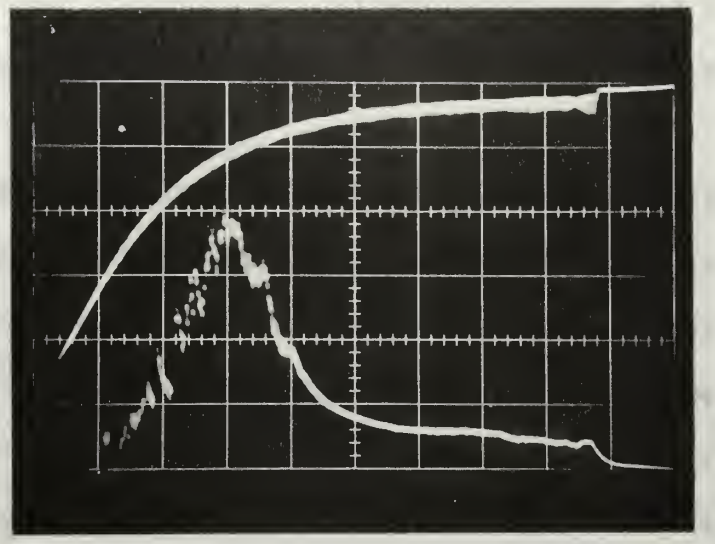

190 MHz

Upper trace: Discharge tube current, 20 ma/cm increasing downward

Lower trace: Transmitted rf power, increasing downward

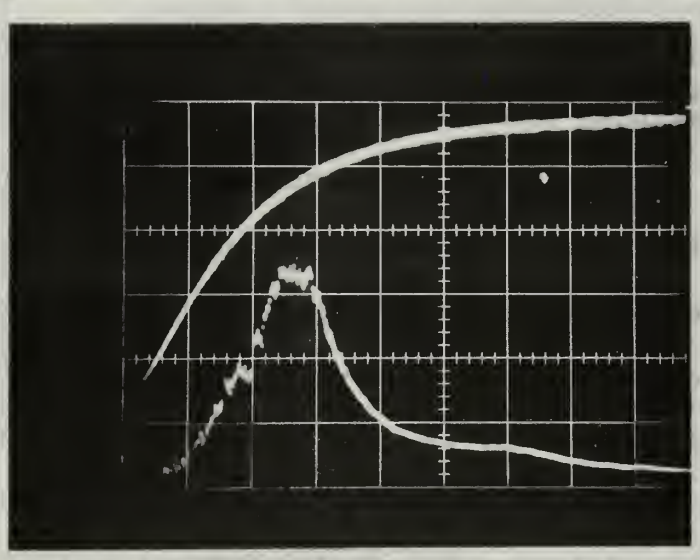

210 MHz

Upper trace: Discharge tube current, 20 ma/cm increasing downward

Lower trace: Transmitted rf power, increasing downward

Figure 23. Resonance presentation, pulsed discharge, argon, 6.5 mTorr

described in section II. While the manufacturer recommends that matched detectors be used for ratio measurements, the detectors used were sufficiently similar in characteristics that this was not considered necessary.

Since moving striations damped resonances observed by the previously described methods, these methods were only applicable in regions where the density variations produced by striations were small. Even in this case it was not possible to observe more than two resonances in neon and argon and three resonances in xenon.

At pressures above 7 mTorr, 70 mTorr and 6 mTorr in argon, neon and xenon respectively, no Tonks-Dattner resonances were observed by any of the above techniques.

When it was discovered that moving striations were present in the columns in which the resonances were being observed it was necessary to devise a technique to examine the resonances taking into account the variations that occurred in electron density. A first requirement of such a technique was that striations be regular in time, a condition which was not fulfilled at all currents and pressures.

To study the resonances in the presence of moving striations the experimental arrangement was as is shown in Fig. 24. The photomultiplier supplied a signal proportional to light intensity and this signal was displayed on the oscilloscope upper beam. A delayed trigger could be provided from the oscilloscope to coincide with any portion of the moving striation waveform. This triggered a pulse generator which provided pulsed operation of the signal generator. The pulse width was chosen to be short compared to the moving striation period. (The only purpose of pulsing was to have a zero power reference available as a means of

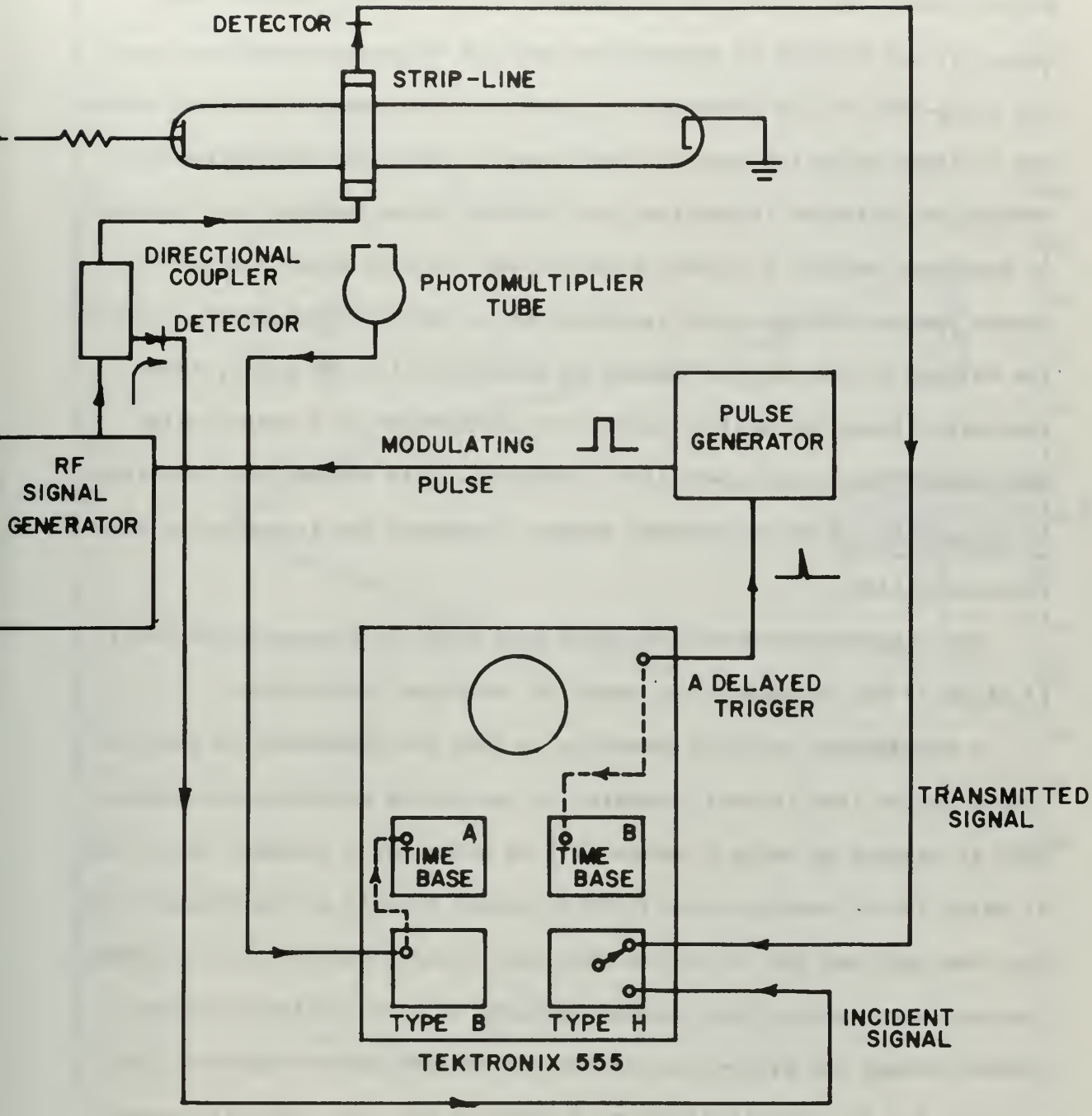

Figure 24

Experimental arrangement for observation of resonances in the presence of moving striations

measuring transmitted power.) The signal generator output was fed to the strip-line through a directional coupler. Both incident and transmitted signals were detected and displayed on the oscilloscope lower beam. It was desired to measure the ratio of rf power transmitted past the strip-line in the presence of a plasma to the power transmitted without a plasma (with the same incident power). This was accomplished by reading the detected transmitted and incident pulse heights as a function of frequency without a plasma; then reading the same heights with a plasma present and the pulse synchronized to the striation phase. Since the voltage of the detector output is proportional to rf power, these readings allowed the desired ratio to be determined in a manner which was insensitive to the power level variations with frequency of the signal generator and to directional coupler, detector and transmission line characteristics.

The measurements described above were taken at frequency intervals of about 25 MHz throughout the range of the signal generators.

A requirement for this technique is that the resonances be observed over a region that is small compared to the moving striation wavelength. This is assured by using a narrow (1.5 cm wide) small diameter strip-line in which the rf energy in the field falls off rapidly in the direction of the tube axis and the strip-line sees only a short section of the column. The half power points were located by means of a small dipole antenna passed through the strip-line and the variation of power coupled to the antenna as a function of distance is shown in Fig. 25. The half power points are about 4 cm apart, thus it can be said that resonance effects are being observed over something on the order of a quarter of the moving striation wavelength.

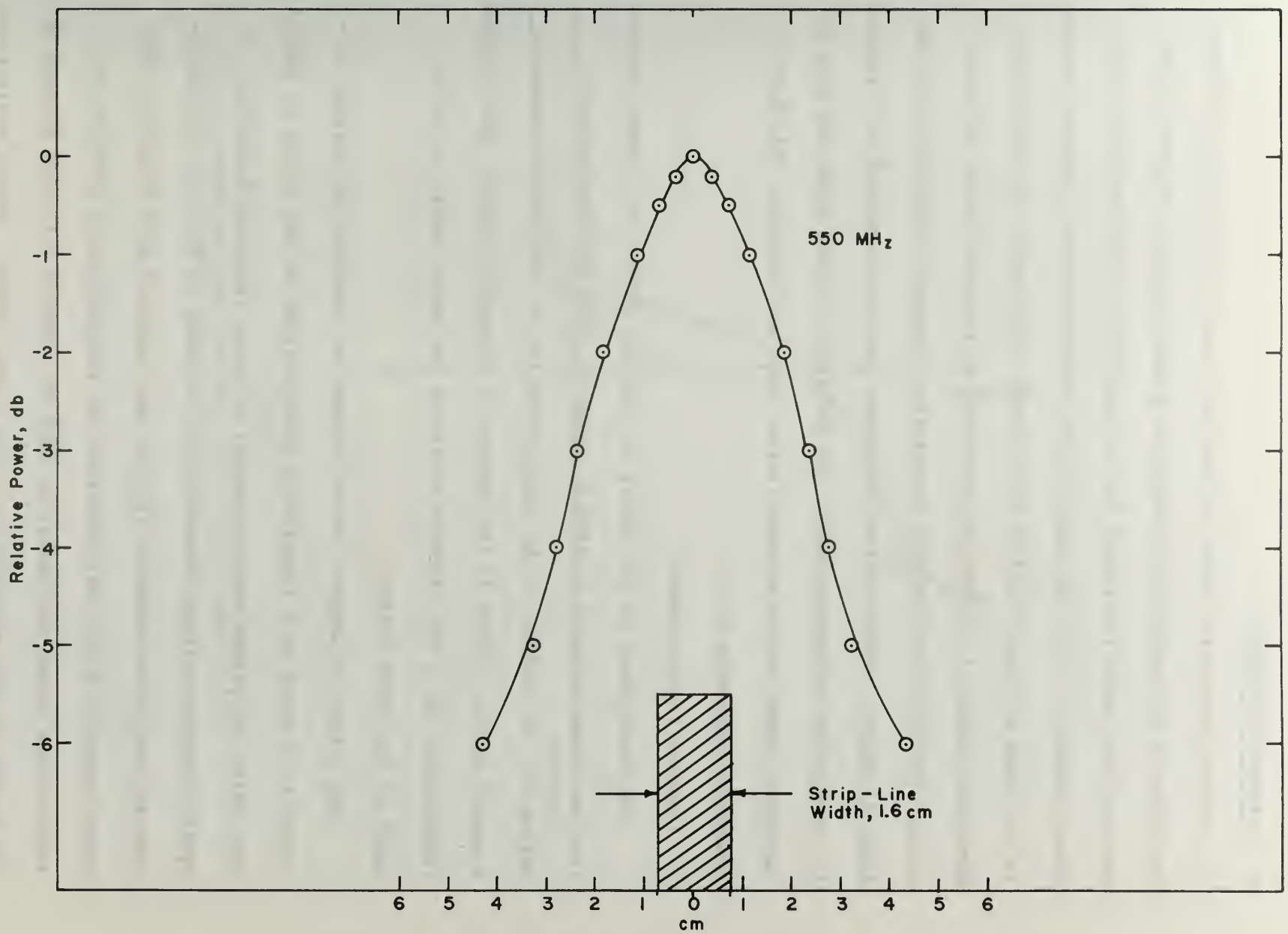

Figure 25. Power in rf field of strip-line as detected on a small dipole antanna

V. DIAGNOSTIC STUDIES

Plasma diagnostics plays an important role in any plasma experiment. The value of any quantitative theory on plasma behavior depends on the accuracy with which the theory can be compared to experimentally determined parameters. For the quantitative determination of electron density in the range of those found in the present experiments, the most highly developed diagnostic techniques are those of Langmuir probes and microwaves. For measuring electron temperature, Langmuir probes provide the simplest means. Both cavities and probes have been employed for diagnostic studies in the present work. In addition, a brief study was made of resonance probes but as no quantitative data was obtained, this work is reported in Appendix B.

1. Langmuir Probe Studies

The development of the theory of electric probes for plasma diagnostics was begun as early as 1924 by Langmuir. [45] The discussion to follow will be limited to the characteristics of cylindrical probes in a weakly ionized plasma in the absence of a magnetic field. The electron temperatures are a few electron volts and the Debye length is on the order of the probe radius.

The method of Langmuir probe diagnostics involves the current collected by a probe as a function of probe voltage as the latter is varied from below the plasma space potential to above the space potential. A typical current-voltage characteristic is shown in Fig. 26. In the region AB, the probe potential (V_p) is very negative with respect to the space potential (V_s). All electrons are repelled and a positive ion sheath forms around the probe, so that the current collected depends on the number of ions entering the space charge sheath. When a cylindrical

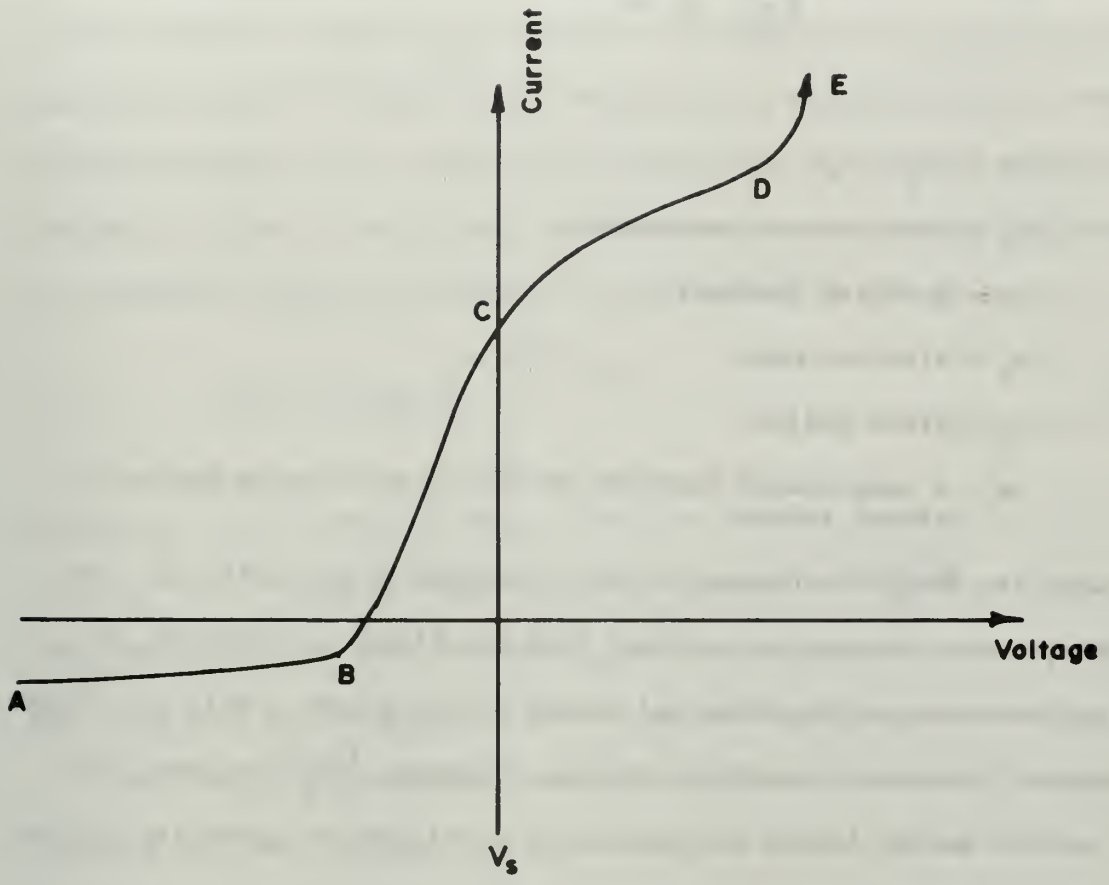

Figure 26

Typical current-voltage characteristic of a Langmuir probe

probe is used under conditions such that the sheath thickness is small compared to the radius of the cylinder, the corrected space charge equation for the current to the probe per unit length is:

$$j = \frac{14.68 \times 10^{-6}\ V^{3/2} \left(1 + 0.0247 \sqrt{\frac{T_+}{V}}\right)}{\sqrt{\frac{m_i}{m_e}}\ r_p\ \beta^2} \quad (p.u.) \tag{40}$$

where

$V = V_p - V_s$

T_+ = positive ion temperature

m_i = positive ion mass

m_e = electron mass

r_p = probe radius

β = a complicated function of the ratio of probe radius to sheath radius

When the sheath thickness is large compared to the radius of the cylinder, a fast moving ion arriving from the plasma may describe an orbital motion about the probe and return to the plasma. This is a case of current limitation by orbital motion. Langmuir [45] has shown that when orbital motion limits the current to a cylindrical probe the current i_s is given by

$$i_s^2 = \frac{4A^2 j_{pi}}{\pi} \left(\frac{Ve}{kT_+} + 1\right) \tag{41}$$

where j_{pi} is the random ion current density at the sheath edge, A is probe area, and k is Boltzmann's constant.

The slope of a plot of i_s^2 versus V is $4A^2 j_{pi}^2\, e / \pi k T_+$ or

$$di_s^2/dV = \frac{-2e^3 n_i^2 A^2}{\pi^2 m_i} \tag{42}$$

n_i being the ion density.

Using this relation the ion density can be calculated from the slope of the i_s^2 versus V plot. Complications arise, however, in the case where the probe is on the order of the sheath thickness.

In the region BC when the probe is less negative with respect to space potential, high energy electrons can penetrate to the probe and the probe current is made up of decreasing ion current and increasing electron current. If a Maxwellian distribution of electron energies is assumed to exist in the plasma, Boltzmann's relation can be applied to this region to give the electron current density to the probe.

$$j_{es} = j_{pe}\, e^{-eV/kT_e} \tag{43}$$

where j_{es} = total current density less ion current density = $j - j_+$ and j_{pc} = random electron current density = $\frac{n_e e \bar{v}_e}{4}$. The absolute temperature of the electrons T_e may be determined from the slope of the logarithm of the electron current plotted against probe voltage.

When the probe potential reaches the plasma potential, the sheath vanishes and the Boltzmann relation breaks down, as can be seen by the fact that the logarithm of the electron current (plotted versus voltage) departs from a straight line. At V_s the probe collects the random electron current. Since the electron temperature has been determined from Eq. (43), the electron density can be found from

$$j_{es}\Big|_{V_s = V_p} = j_{pe} = \frac{n_e \bar{v}_e e}{4} = e\, n_e \sqrt{\frac{kT_e}{2\pi m_e}} \tag{44}$$

where $\bar{v}_e$ is the mean electron velocity.

At more positive probe potentials the electrons are attracted to

the probe and an electron space-charge sheath forms around it. The electron current follows the law previously discussed for the positive ions. This region of increasing electron current corresponds to the region CD in Fig. 26.

If the probe voltage is increased to very positive voltages, electrons acquire sufficient energy to ionize neutral particles in passing through the sheath, and the electrons resulting from these ionizations are collected by the probe while the ions are repelled. There is a sudden increase of the probe current as shown in region DE.

The above discussion summarizes the classical Langmuir theory for electric probes in a plasma.

From the point of view of experimental convenience it is desirable to measure electron temperatures and densities from the electron current to a probe. However, several factors lead to errors in densities measured from the electron saturation current. One of these is the magnitude of the probe current drawn by a probe as compared to the discharge current. If this becomes significant it is apparent that the plasma will be perturbed by use of the probe.

Secondly there is the difficulty of establishing the space potential. In a practical case the transition from electron repulsion to electron saturation is never sharp. This is shown in Fig. 27 where we have plotted the logarithm of electron current versus voltage. It is seen that there is pronounced rounding of the knee of the curve. One cause of this rounding is that the rapid build-up of the electron sheath effectively increases the collection area of the probe, thus instead of the current remaining constant with increasing probe potential, the current continues to rise. Furthermore, probe measurements are generally made

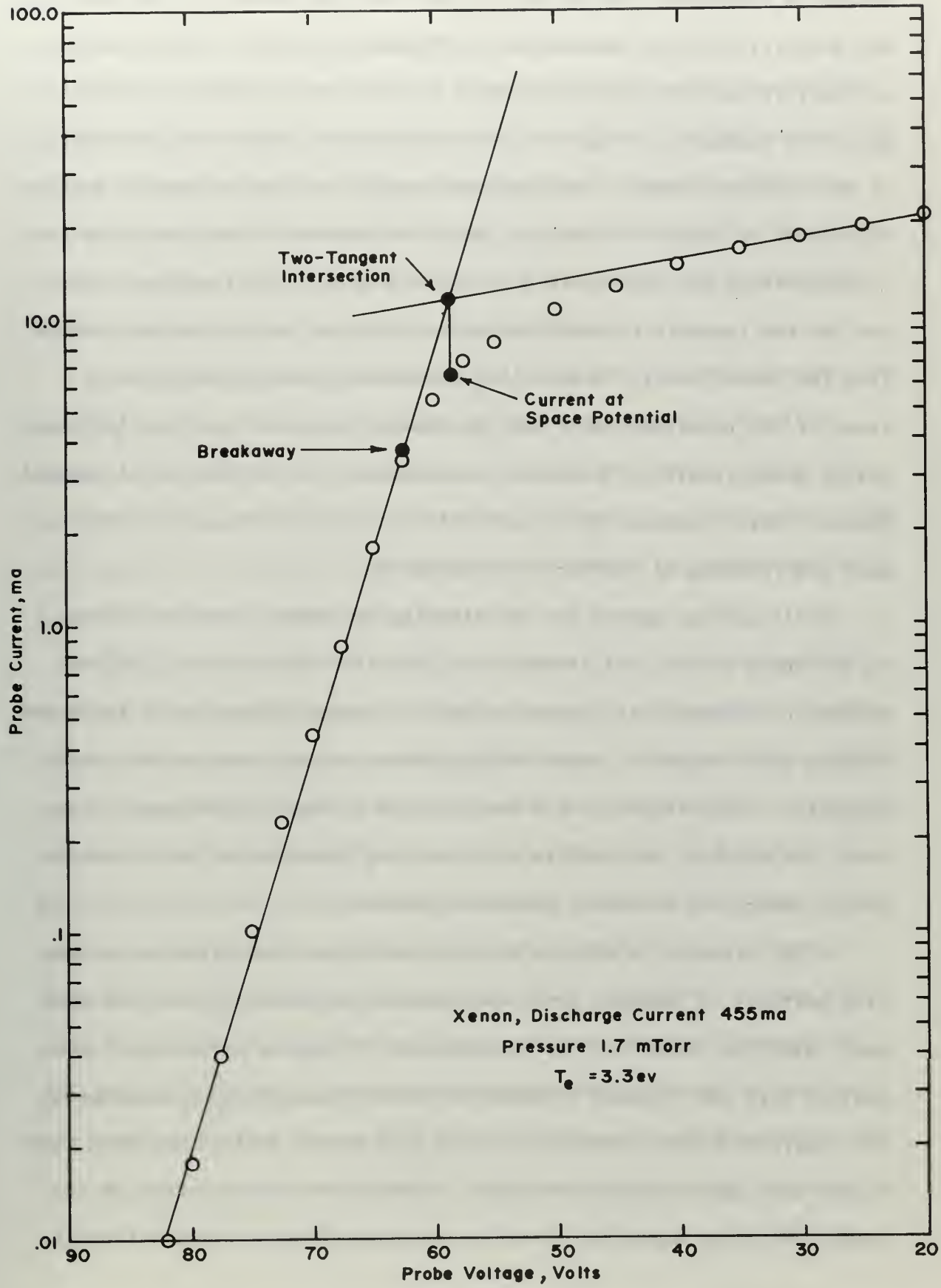

Figure 27. Semi-log plot of typical Langmuir probe characteristic

against a background fluctuation in the discharge parameters such as number density, electron temperature and discharge current. Different investigators have advocated the use of at least three different saturation points as indicated on Fig. 27. One method is to locate the intersection of two tangents drawn to the repulsion portion and the saturation portion. Another is to select the point at which the current breaks away from the linear portion for the electron repulsion region. Still another is to use the two tangents to establish space potential and to use the current from the curve itself. Hoyaux [46] provides convincing arguments in favor of the breakaway point and experiments by Nicoll and Basu [47] comparing probe results to microwave measurements lend weight to this method. However, this breakaway point is difficult to establish, particularly when the rounding of the knee is pronounced.

Still another method for establishing the space potential (which is not shown on Fig. 27) is based on a result of Druyvesteyn, [48] who showed in a theoretical treatment that the second derivative of the probe current with respect to probe voltage passes through zero at the space potential. This technique has been applied by some experimenters; however, the accuracy required is such that the technique is not generally useful except for extremely quiescent plasmas.

First attempts to measure electron densities from electron saturation portions of Langmuir probe characteristics taken in this work were made using the current at the intersection of the two tangents. A comparison with the resonant frequencies for the main dipole resonance and the theory of Parker, Nickel and Gould [21] appear to indicate that these values were approximately 30% high. Although use of the criterion of Hoyaux [46] gave densities in better agreement with the predictions of

the theory (of Parker, et.al.) for resonances, there was some difficulty in accurately establishing the desired point.

The above results point up the disadvantages of using the electron current portion of the Langmuir probe characteristic. Attention was then turned to the ion portion of the characteristics. However, since the densities with which these experiments deal are such that the ion sheath is not very large compared to the probe radius, the use of the Langmuir orbital-limited theory (Eq. (41)) is questionable.

Recently several unified theories for ion probe characteristics have appeared. Allen, Boyd and Reynolds [49] have extended the classical theory of Langmuir to deal with the potential distribution within the positive ion sheath, and the increase in ion current as the probe is made more negative. They have dealt with the case where the ion energy far from the probe is assumed to be zero.

Bernstein and Rabinowitz [50] have given a more or less complete solution which includes cases of finite ion energy. They have, however, used a monoenergetic ion energy distribution far from the probe. Several workers have found objections to this model and have adopted more general methods. Hall and Fries [51] have used the equations of Bernstein and Rabinowitz but have assumed a Maxwellian ion energy distribution to obtain numerical solutions which express the parameters of a plasma in terms of the current-voltage characteristic of the probe. A very complete analysis for a Maxwellian plasma has been presented recently by Laframboise [52] using numerical methods and the equations of Bernstein and Rabinowitz. The theories of Hall and Fries and of Laframboise represent the most complete analyses to date for probes in a collisionless plasma. These theories have, however, the disadvantage of presenting

the results in a form which can be used experimentally only in a trial-and-error fashion. The two theories present their results in different manners and thus direct comparison of the results is difficult.

Chen [53] has given numerical computations for the theories of Allen, et.al. [49] and Bernstein and Rabinowitz, [50] and has presented the results for electron density in a readily applicable form.

The Allen, Boyd and Reynolds equations for a cylindrical probe have been solved by Chen [53] assuming that the distribution of angular momenta at distances far from the probe is a delta function around zero.

It is estimated that in the plasmas encountered in this experimental work, the ions are approximately at room temperature. This means that electrons have about 100 times the energies of the ions or more. The inference from this is that the Allen, Boyd and Reynolds theory is more appropriate even though the influence of ion energy E_i on the Bernstein and Rabinowitz solution is slight. The Allen, Boyd and Reynolds theory is applicable for $\beta = \frac{E_i}{kT_e}$ = normalized ion energy = 0, while the Bernstein and Rabinowitz theory considers the finite β case.

With the objective of determining the validity of the Allen, Boyd and Reynolds theory, for which Chen provides numerical computations, a series of probe measurements was taken in a 0.8 cm inside diameter xenon plasma column at 4.8 mTorr. Cavity measurements of average electron densities were made at the same currents used for the probe measurements. The probe data was analyzed applying several different theories to find ion densities and the results are plotted in Fig. 28.

It should first be pointed out that for the small tube used in this experiment, the cavity perturbation theory (discussed in Section V) is quite reliable. Also, measurements were performed at a pressure low enough that moving striations only slightly perturb the density. The

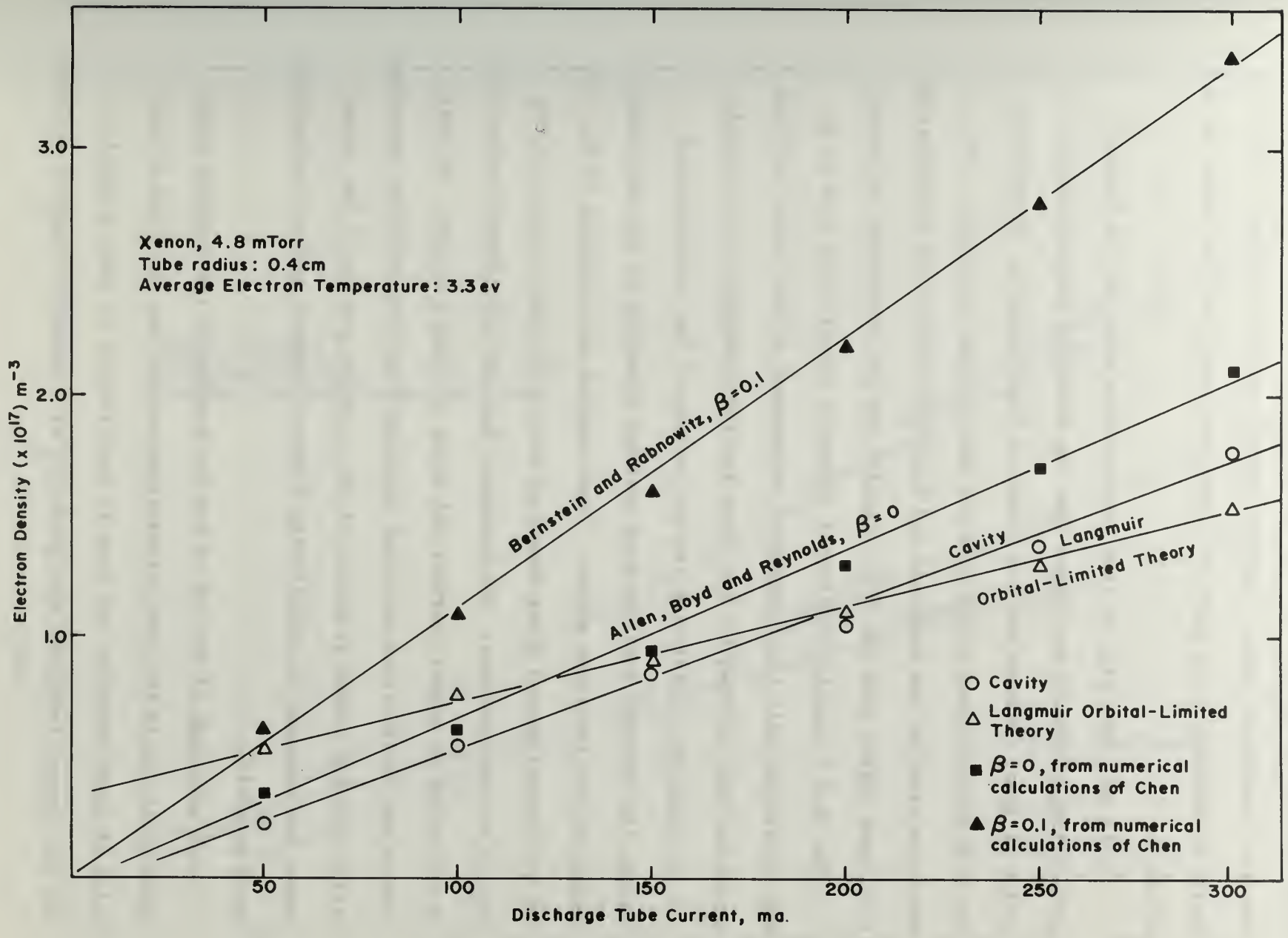

Figure 28

Results of analyses of ion characteristics of a Langmuir probe in a xenon plasma column, compared with microwave cavity measurement of electron density

cavity gives densities that are averages over the tube cross section and from the theoretical radial electron density profile of Parker, [22] this should be expected to be about 0.7 times the density at the center of the column.

It is seen from Fig. 28 that the densities given by the Langmuir orbital-limited theory are higher than the densities measured by the cavity at lower currents and are higher at high currents. Furthermore, the line through these points does not pass through the origin. The densities given by the Bernstein and Rabinowitz theory are approximately 1.66 imes higher than the $\beta = 0$ results and are considered too high.

The $\beta = 0$ results from Chen's numerical calculations seem to be most consistent with the independent measurement by the cavity and this method has been adopted for the probe results presented in this thesis.

In addition to analyzing the ion portion of the aforementioned curves, the electron portions were analyzed according to the two-tangent method and the breakaway method. These results are presented in Fig. 29. The two-tangent method gives densities about 1.41 times those from the Chen $\beta = 0$ calculations. The breakaway data are considerably below the $\beta = 0$ values at higher currents and above at lower currents. In addition to the difficulties mentioned previously with the electron characteristics this has caused rejection of the electron portion of the curves except for purposes of establishing electron temperatures and estimating space potential.

One advantage of the use of the ion portion of the Langmuir probe characteristics is that the calculations are not too sensitive to the value of space potential and thus to oscillations in space potential. The ion current increases more gradually with potential than the electron

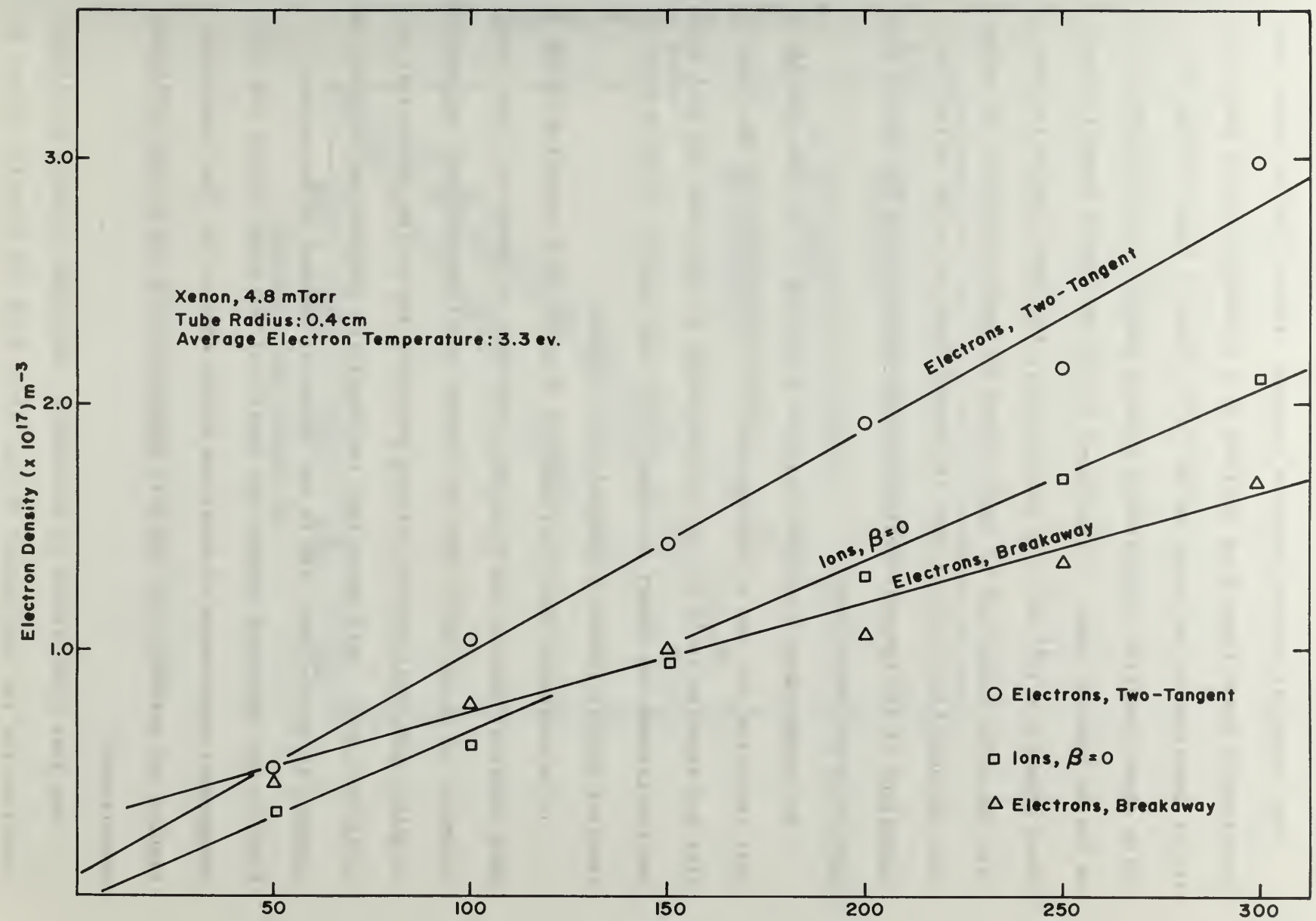

Figure 29

Analyses of electron current characteristics of a Langmuir probe in a xenon plasma column, compared with $\beta = 0$ calculations from Chen (Ref. 53)

current.

The densities derived from the Langmuir orbital-limited theory were consistently above those from the Chen $\beta = 0$ computations in the vicinity of densities on the order of 10^{16} m^{-3}. This is shown in Fig. 30 which shows densities calculated by several methods in the larger 31.2 mm inside diameter tube. A cross-over of the two curves seems to take place around 2×10^{16} m^{-3}. At this density, the Debye length is about half the probe radius and is smaller with increasing density. It seems that the densities are such that the sheath does not quite satisfy the conditions of the Langmuir orbital-limited theory except for points very much below the cross-over.

Two probe curves have been analyzed according to the theories of Hall and Fries [44] and of Laframboise. [45] The results for ion densities are shown in Table 2. It is interesting to note that the Hall theory and the Laframboise theory give nearly the same result. Both of these theories require tedious trial-and-error methods.

It is estimated that the reduction of probe data according to the Chen numerical results can be accomplished with an error of $\pm$ 10%. Furthermore, it is estimated that the current densities measured are accurate to within 10%, this deviation being primarily due to the uncertainty of collection area. This means that the densities obtained can be taken as accurate to within about 15% if the theory is assumed to be correct. Based on the agreement between the results of the probe theory and the independent measurement of densities with a cavity, the Chen numerical results are assumed to be the most appropriate for the plasma conditions encountered.

One last point should be mentioned. According to Chen, a validity condition for the application of the Allen, Boyd and Reynolds theory for

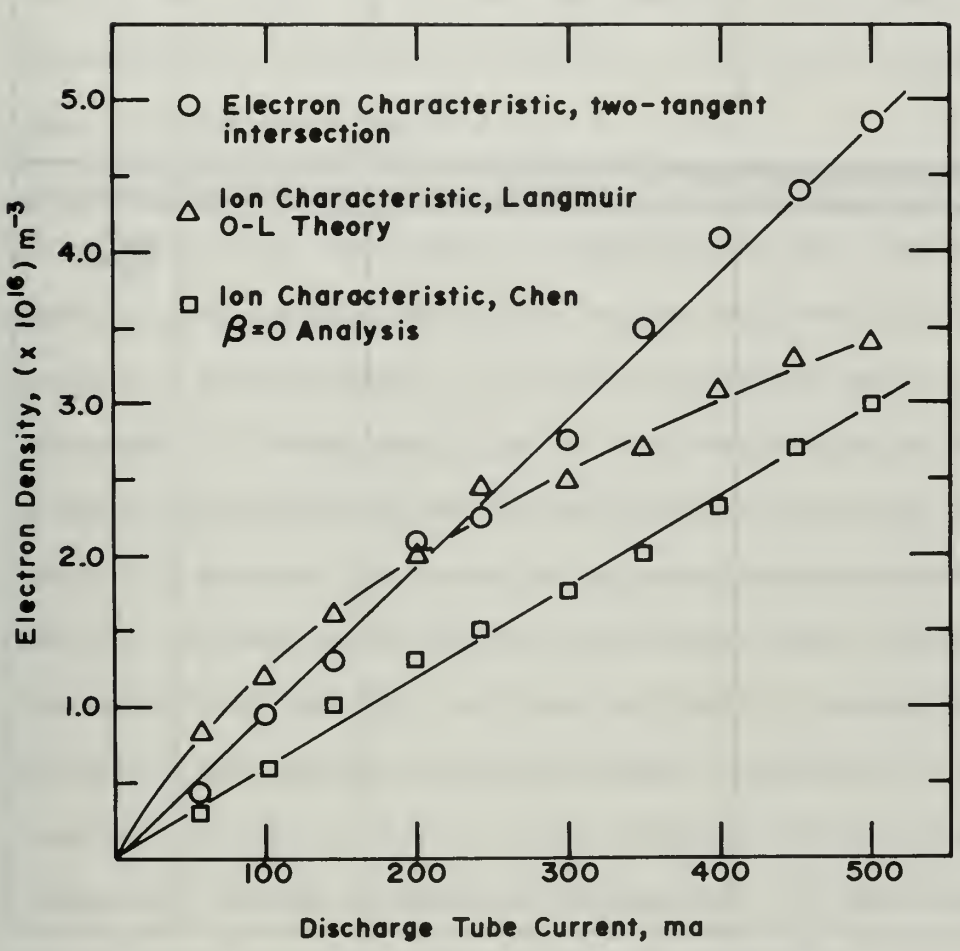

Figure 30

Densities calculated by several methods from probe characteristics in 3.5 cm OD tube, xenon plasma

n_i L-O Theory	n_i Allen, Boyd, Reynolds $\beta=0$	n_i Bernstein & Rabinowitz $\beta=0.1$	n_i Laframboise	
3.6	2.1	2.5	4.8	$\times 10^{16}$
1.5	2.1	3.4	3.05	$\times 10^{17}$
n_i Hall & Fries				
4.0				$\times 10^{16}$
2.4				$\times 10^{17}$

Table 2

a cylindrical probe is that

$$\frac{-E_i}{eV_p} \ll \frac{r_p^2}{\lambda_i^2} \tag{45}$$

where E_i = ion energy

λ_i = ion mean free path

r_p = probe radius

Calculations show that for the range of pressures considered $\frac{-E_i}{eV_p}$ is smaller than $\frac{r_p^2}{\lambda_i^2}$ but not very much smaller. The effect of this can be minimized by weighting the currents at high probe voltage somewhat more in interpreting the data.

An experiment has been performed by Messiaen and Vandenplas [54] using the Chen $\beta = 0$ analysis. Comparison has been made with densities measured from electron saturation currents and from a dipole resonance probe in a mercury plasma. In the case of mercury there is evidence that the break at electron saturation is much sharper than in the rare gas plasmas, allowing better determination of the saturation current. The results of Messiaen and Vandenplas show good agreement between the three methods. Vandenplas and Messiaen were aware of the situation regarding the criterion of Eq. (45), and that the finite β case of Bernstein and Rabinowitz gave densities about 50% higher than the $\beta = 0$ case. However, they feel that the $\beta = 0$ case gives results in better agreement with independent methods of measuring the density. [55] This is the same conclusion that has been reached in this investigation.

In compiling the data required in the present work, probe characteristics were taken at several currents for a given tube pressure. Resulting electron densities were computed and plotted as a function of discharge tube current. The probe was at the center of the column except

in cases where it was desired to determine the radial profile. Results are shown in Figs. 31, 32, and 33 for xenon, neon, and argon respectively. For values of current or pressure not explicitly shown on the graphs, linear interpolation was employed.

Temperature of electrons for neon, xenon, and argon plasmas are shown as a function of pressure in Figs. 34, 35, and 36. Also shown on these plots are the theoretical electron temperatures predicted both from the Langmuir "free-fall theory" [56] and the "diffusion" [57] theory. The assumptions of these theories are quite different. The free-fall theory assumes ions drift to the wall without making collisions whereas the diffusion theory assumes there are many electron collisions along the tube radius and particle loss to the wall is limited by ambipolar diffusion. On the figures the theoretical curves in the region where the assumptions of the theories are not met have been dotted and one would expect a smooth transition in the intermediate region. It is noted that the agreement is quite good for the argon data and the free-fall theory. However, neon shows a lower electron temperature than predicted by this theory. It should be pointed out that in this region of pressures for neon, the ion mean free paths are on the order of one cm which is less than the tube radius and the assumptions of the free-fall theory are definitely not true. Thus it is not too surprising that the electron temperatures are below those predicted. It is possible that there is an additional influence in lowering the observed electron temperatures, viz., two-stage ionization, but it is believed that the primary influence is the one just discussed, namely, ion-neutral collisions. It would not be expected that either theory would give the proper electron temperature in the region of pressures for which neon data in Fig. 34 have been taken. If experimental

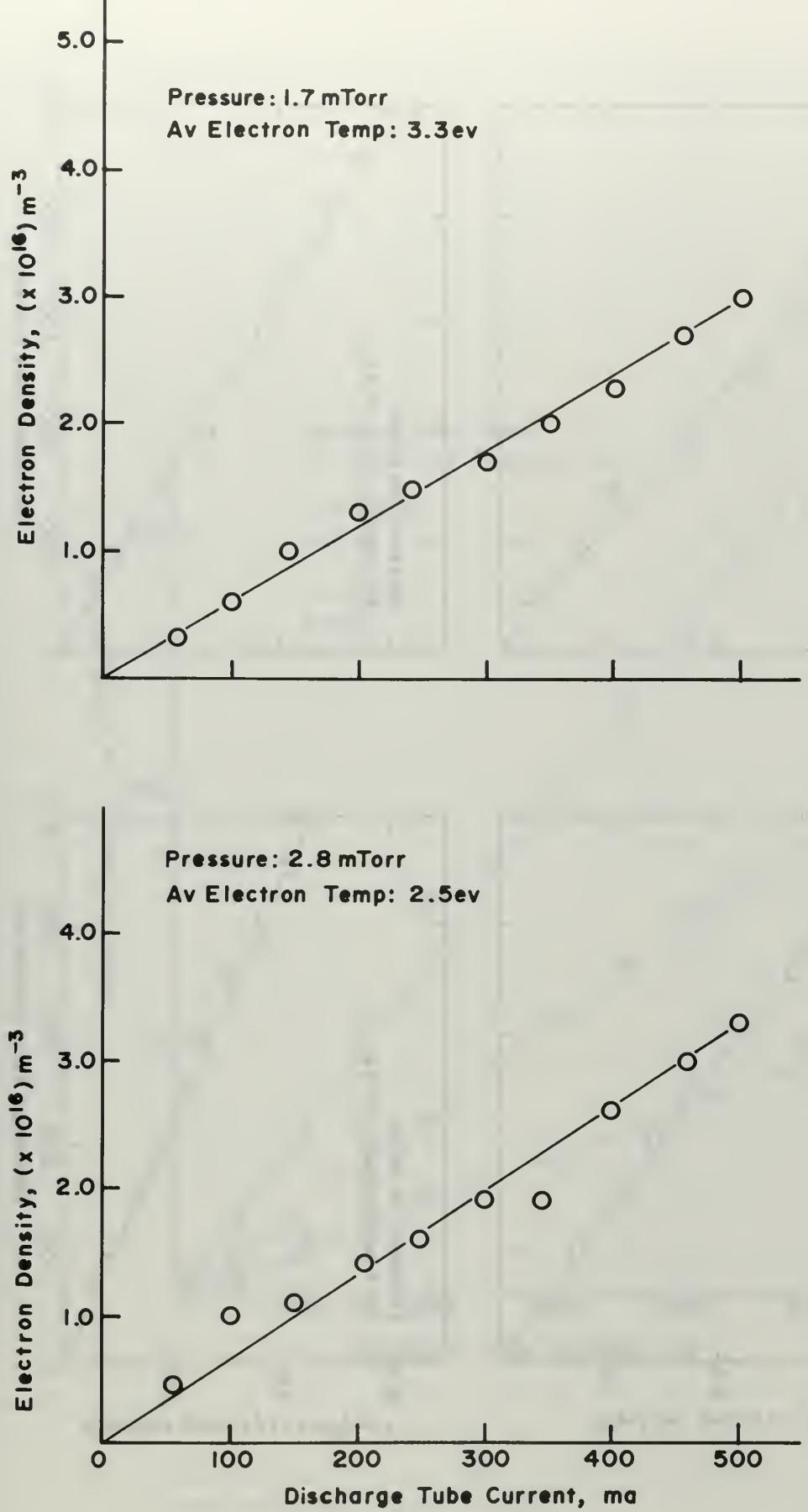

Figure 31

Electron density at center of 3.5 cm OD tube versus discharge tube current, xenon

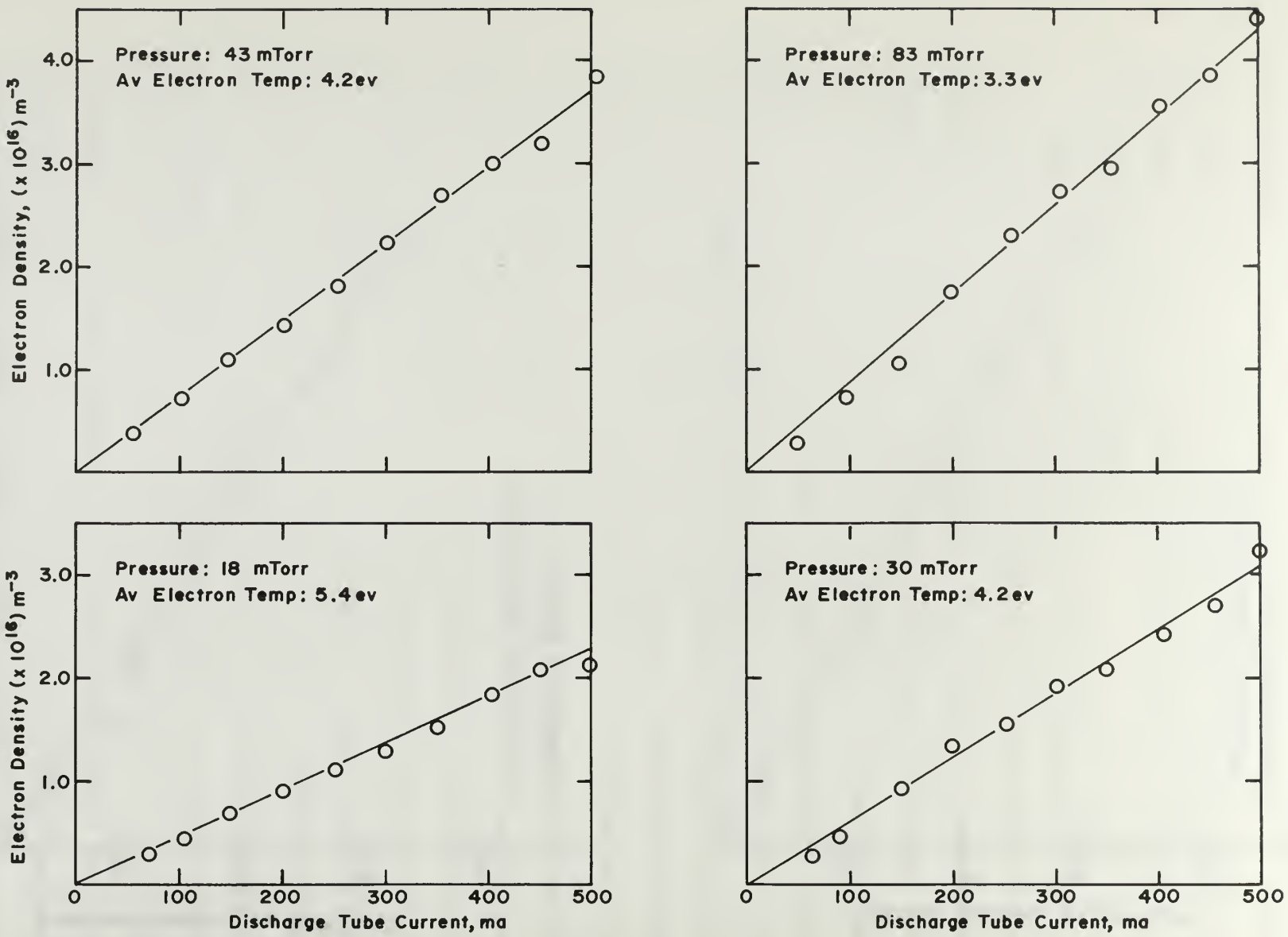

Figure 32

Electron density at center of 3.5 cm OD tube versus discharge tube current. neon

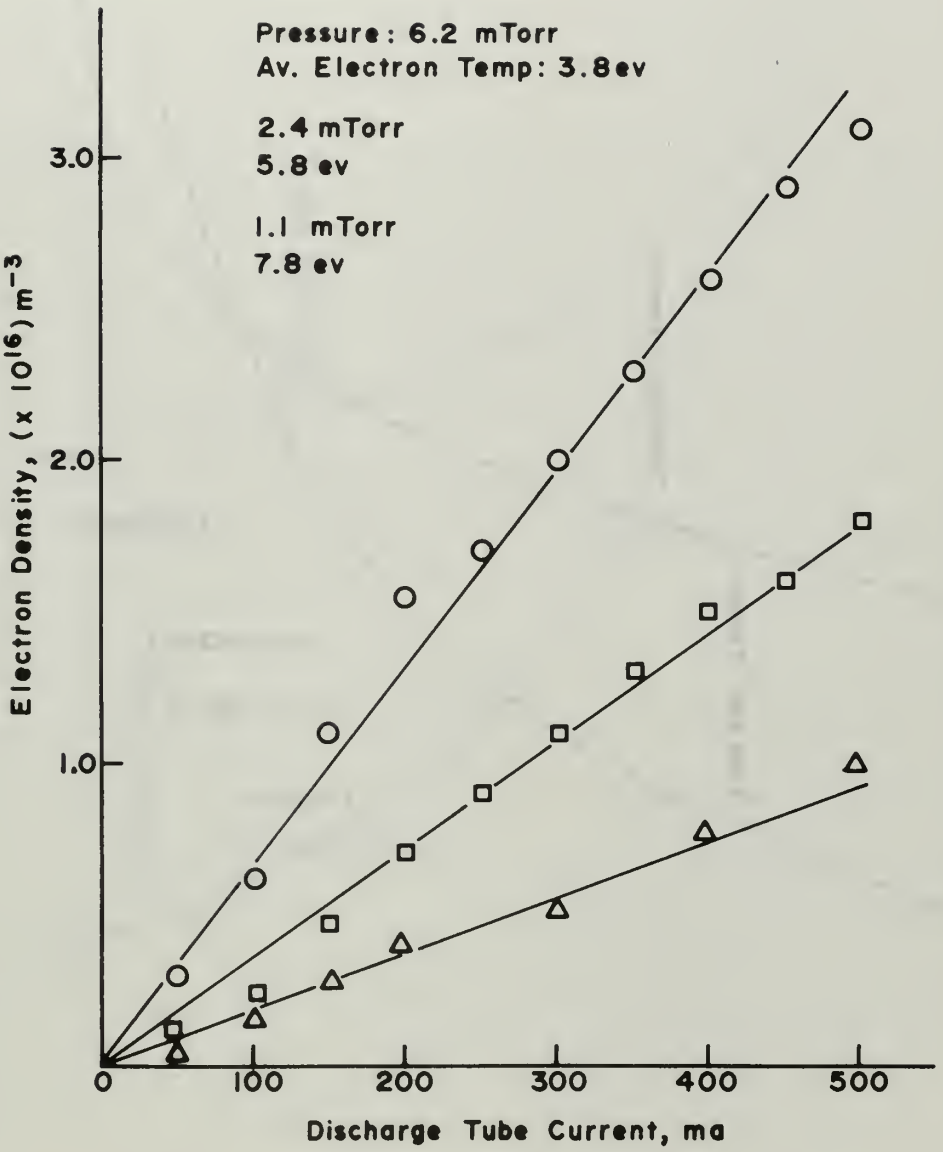

Figure 33

Electron density at center of 3.5 cm OD tube versus discharge tube current, argon

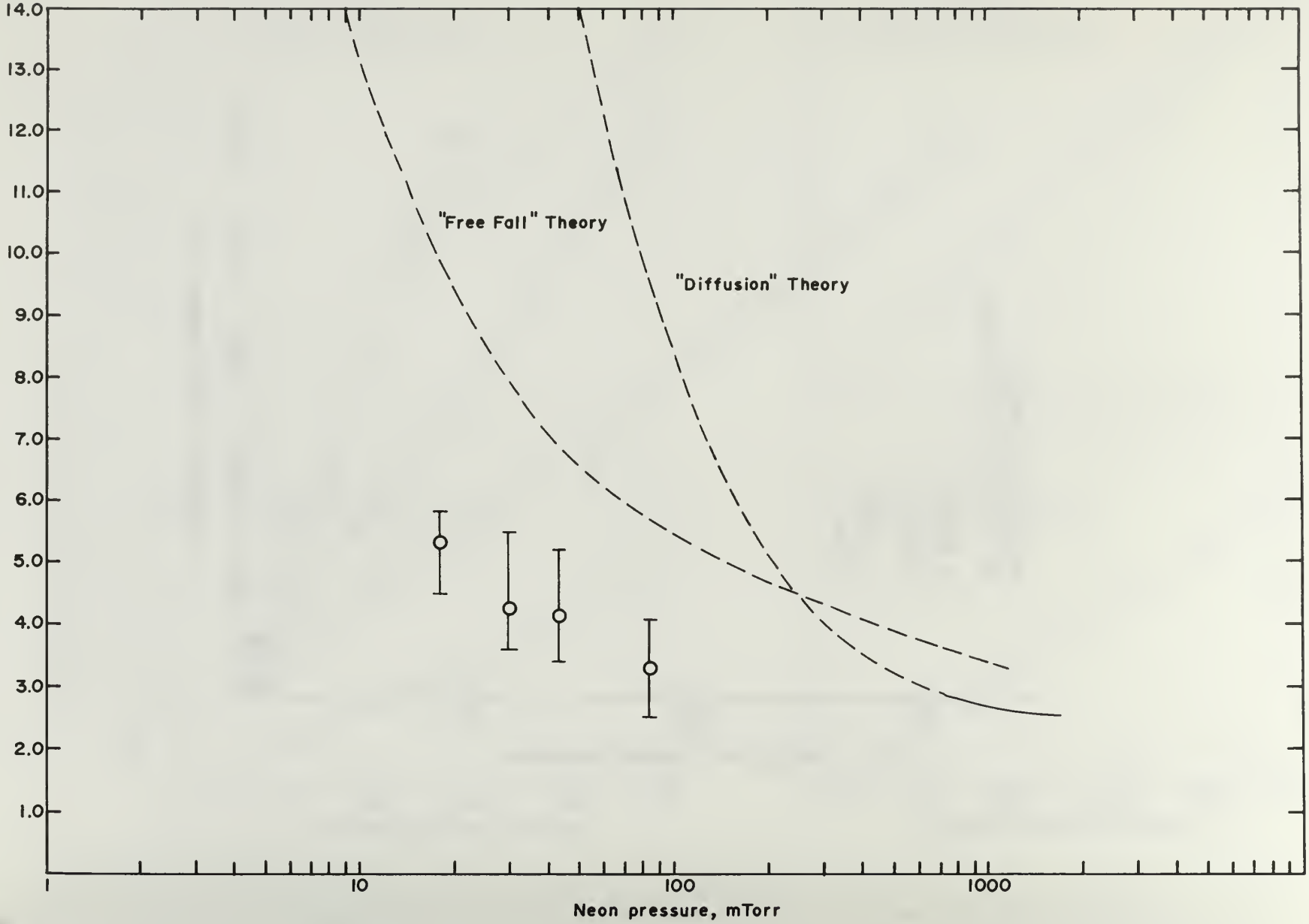

Figure 34

Electron temperature versus pressure, neon, 3.5 cm OD tube

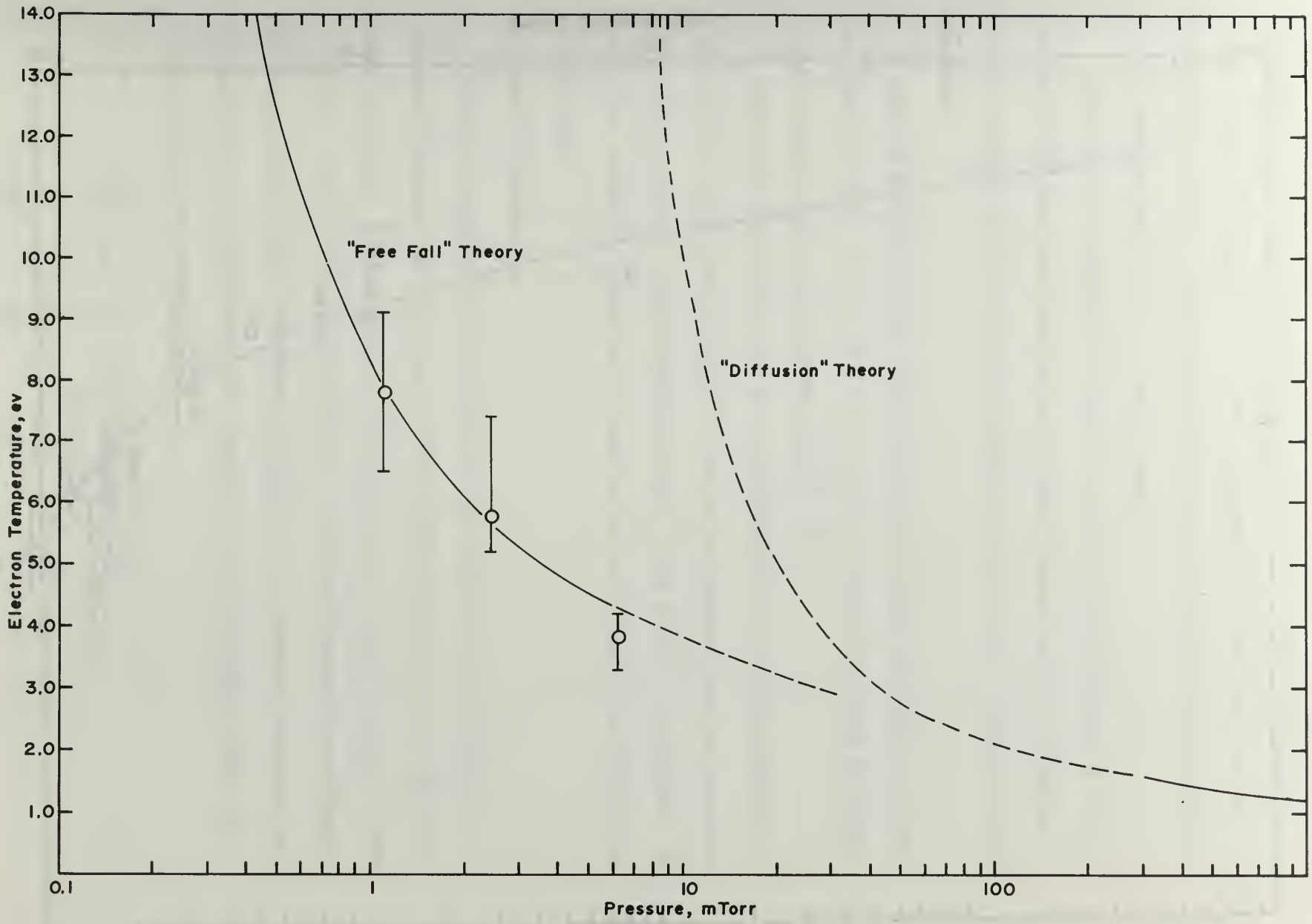

Figure 35

Electron temperature versus pressure, xenon, 3.5 cm OD tube

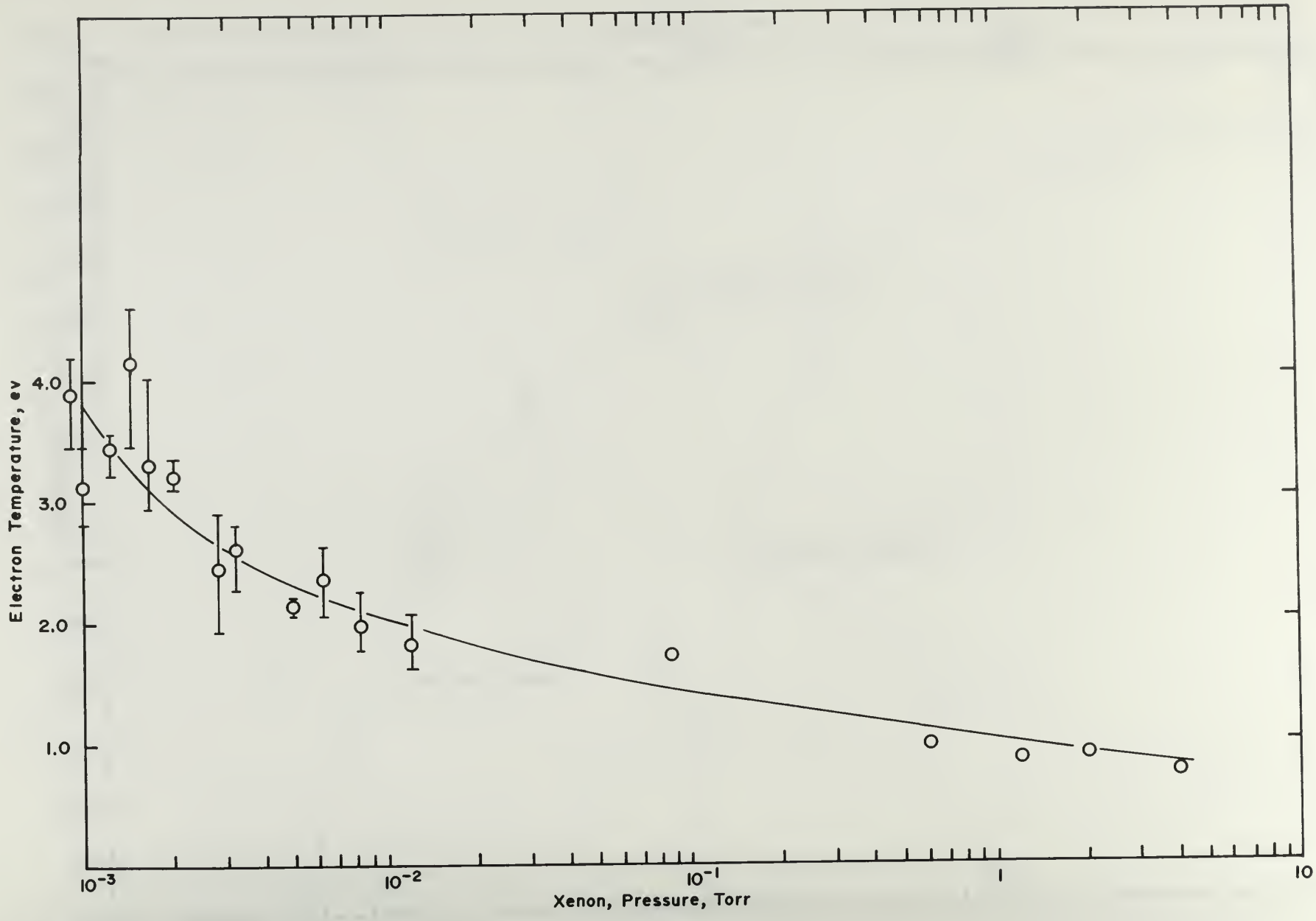

Figure 36

Electron temperature versus pressure, argon, 3.5 cm OD tube

continuation of the measurements were possible to lower pressures in neon, it would be expected that the experimental points would rejoin the free-fall theory curve when ion mean free paths were long compared to the tube radius, i.e., at about 3 mTorr.

The flags on the points in Figs. 34, 35, and 36 represent the extremes of temperatures observed at a given pressure as the discharge current was varied from a few milliamperes up to several hundred milliamperes.

Several radial profiles were determined in neon and xenon. These are shown in Figs. 37, 38, and 39. The dolid curves in these drawings are the theoretical profiles from Parker. [22]

The experimental profiles do not contradict the theoretical profiles and by comparison of Figs. 37 and 38 it appears that the observed profiles follow the trend suggested by Fig. 4 as r_w^2/λ_D^2 is lowered. The probe data cannot be taken very close to the wall due to the finite size of the probe.

2. Cavity Diagnostics

Electron densities of a plasma can be measured by the shift is resonant frequency of a microwave cavity upon insertion of the plasma into the cavity. [58] A first order perturbation theory usually is used to obtain a theoretical interpretation of the experimental measurements. The perturbation theory relates the shift of the resonant frequency of the cavity $\Delta\omega$ to the dielectric constant ϵ of the medium within the cavity through the expression

$$\frac{\Delta\omega}{\omega} = \frac{1}{2} \frac{\int (\epsilon_0 - \epsilon) E_0^2 \, d\mathcal{V}}{\int \epsilon_0 E_0^2 \, d\mathcal{V}} \tag{46}$$

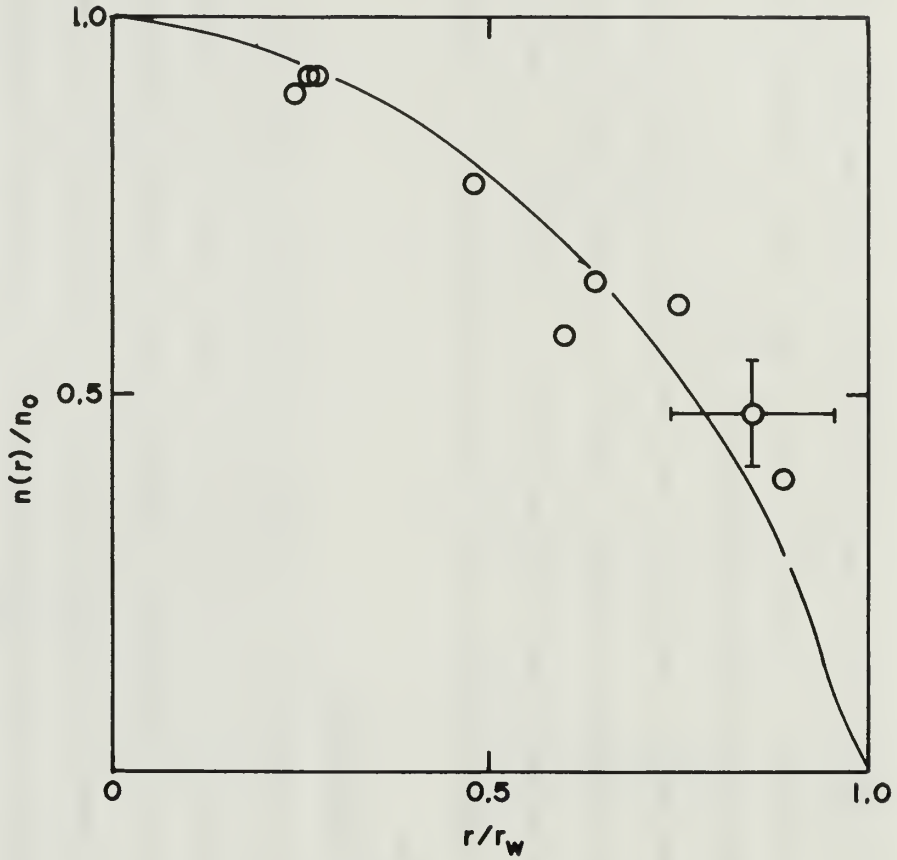

Figure 37

Normalized radial profile of electron density, xenon, $r_w^2/\lambda_{DO}^2 \simeq 2 \times 10^4$

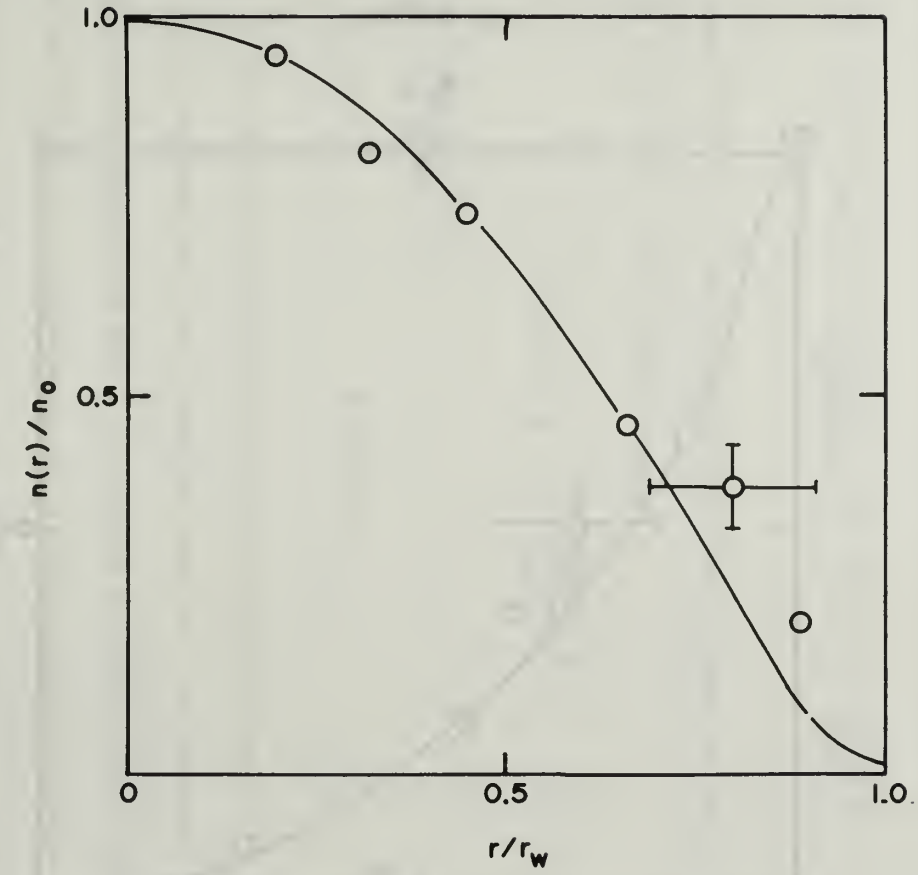

Figure 38

Normalized radial profile of electron density, xenon, $r_w^2/\lambda_{De}^2 \approx 4 \times 10^3$

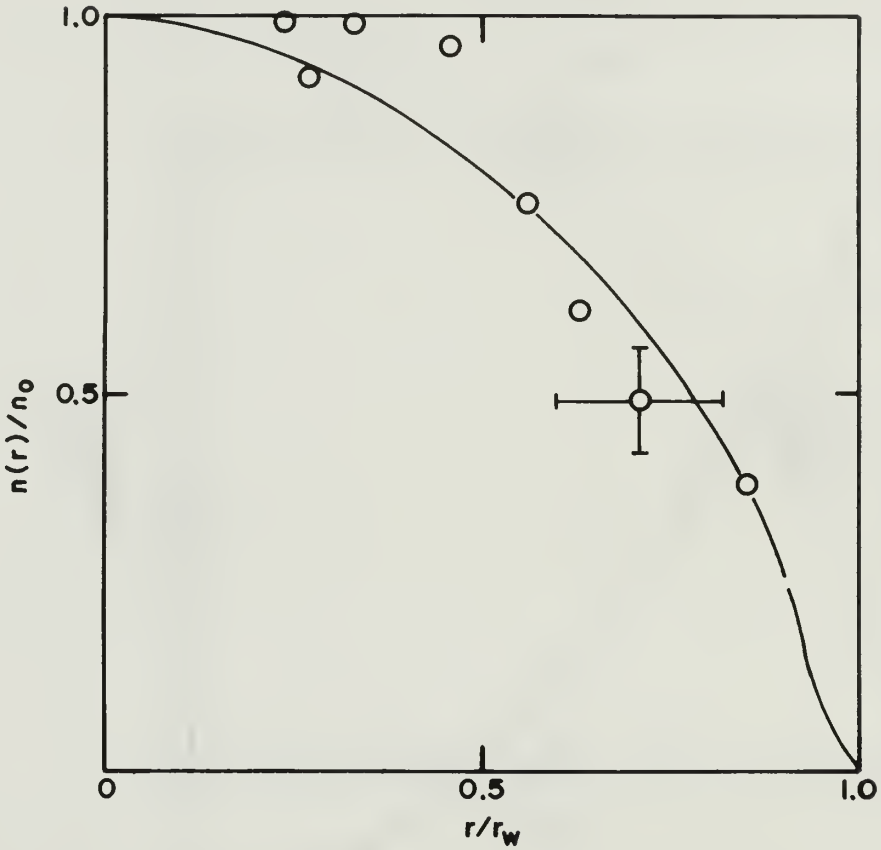

Figure 39

Normalized radial profile of electron density, neon, $r_w^2/\lambda_{DO}^2 \simeq 9 \times 10^3$

where E_o is the microwave electric field in the absence of the perturbation. The integration is over the volume of the cavity. In the region where collision frequency ν_c is much smaller than the radian frequency of the field ω, i.e.,

$$\nu_c \ll \omega \tag{47}$$

the imaginary part of the complex plasma conductivity exceeds the real part and the dielectric constant of the plasma is given by

$$\epsilon = \epsilon_o \left(1 - \frac{ne^2}{m_e \epsilon_o \omega^2}\right) = \epsilon_o \left(1 - \frac{\omega_p^2}{\omega^2}\right) \tag{48}$$

If we assume that the electron density of the plasma is only a function of radius r we have in the plasma region

$$\epsilon = \epsilon_o \left(1 - \frac{\omega_p^2(r)}{\omega^2}\right) \tag{49}$$

Within the glass tubing

$$\epsilon = K\epsilon_o \tag{50}$$

where K is the relative dielectric constant of the glass.

We will consider only the specific case of a cylindrical cavity operating in the TM_{010} mode which is chosen for application here since the electric field is a maximum in the location of the plasma. The geometry of the cavity has been illustrated in Fig. 21. For this specific mode the unperturbed field can be written

$$E_o = A\, J_o\left(\frac{\beta_{01} r}{a}\right) \tag{51}$$

and the electric field is entirely in the axial direction. J_o is the zeroth order Bessel function and β_{01} is the first root of $J_o(x)$.

Application of Eq. (46) shows that the total shift in the resonant frequency of the cavity is made up of two parts, the first for the plasma and the second for the glass. If ω is the shifted resonant frequency and ω_{oo} is the resonant frequency of the empty cavity:

$$\frac{\omega-\omega_{oo}}{\omega_{oo}} = \left[L\int_0^{r_w}\frac{e^2}{m\omega^2}\, n(r)\, A^2 J_0^2\left(\frac{\beta_{01} r}{a}\right) 2\pi r dr \right.$$

$$\left. -L\int_{r_w}^{b}\epsilon_0 (K-1)\, A^2 J_0^2\left(\frac{\beta_{01} r}{a}\right) 2\pi r dr\right] \Big/ 2\epsilon_0\int_0^a L A^2 J_0^2\left(\frac{\beta_{01} r}{a}\right) 2\pi r dr \tag{52}$$

If we calculate first the shift due to the glass alone we find (if ω_o is the shifted resonant frequency for glass alone):

$$\frac{\omega_o-\omega_{oo}}{\omega_{oo}} = \frac{-(K-1)}{2a^2 J_1^2(\beta_{01})}\left\{ b^2 J_1^2\left(\frac{\beta_{01} b}{a}\right) - \right.$$

$$\left. r_w^2 J_1^2\left(\frac{\beta_{01} r_w}{a}\right) + b^2 J_0^2\left(\frac{\beta_{01} b}{a}\right) - r_w^2 J_0^2\left(\frac{\beta_{01} r_w}{a}\right)\right\} \tag{53}$$

If ω is the resonant frequency with both the glass and the plasma:

$$\frac{\omega-\omega_{oo}}{\omega_{oo}} = \frac{\bar{n}e^2}{m\epsilon_0\omega^2}\,\frac{1}{2J_1^2(\beta_{01})}\,\frac{r_w^2}{a^2}\left[J_1^2\left(\frac{\beta_{01} r_w}{a}\right)+J_0^2\left(\frac{\beta_{01} r_w}{a}\right)\right]$$

$$\frac{-(K-1)}{2a^2 J_1^2(\beta_{01})}\left\{ b^2 J_1^2\left(\frac{\beta_{01} b}{a}\right) - r_w^2 J_1^2\left(\frac{\beta_{01} r_w}{a}\right)\right. \tag{54}$$

$$\left. + b^2 J_0^2\left(\frac{\beta_{01} b}{a}\right) - r_w^2 J_0^2\left(\frac{\beta_{01} r_w}{a}\right)\right\}$$

Here we have assumed that

$$\omega_p^2(r) = \frac{e^2}{m\epsilon_0}\left[\bar{n} + n_1(r)\right] \cong \frac{\bar{n}e^2}{m\epsilon_0} \tag{55}$$

Now subtracting Eq. (53) from Eq. (54) we have

$$\frac{\omega-\omega_o}{\omega_{oo}} = \frac{\bar{n}e^2}{m\epsilon_0\omega^2}\,\frac{1}{2J_1^2(\beta_{01})}\,\frac{r_w^2}{a^2}\left[J_1^2\left(\frac{\beta_{01} r_w}{a}\right)+J_0^2\left(\frac{\beta_{01} r_w}{a}\right)\right] \tag{56}$$

Nickel [23] has shown that to the order of accuracy of the perturbation theory

$$\frac{\omega - \omega_0}{\omega_{00}} = \frac{\omega - \omega_0}{\omega_0} \tag{57}$$

Furthermore, he has shown the right hand side of the equation to be more appropriate for measurements of the dielectric constant of a dielectric rod. Therefore, we can write:

$$(\omega - \omega_0)\,\omega_0 = \frac{\bar{n} e^2}{m \epsilon_0} \frac{1}{2 J_1^2(\beta_{01})} \frac{r_w^2}{a^2} \left[J_1^2\left(\frac{\beta_{01} r_w}{a}\right) + J_0^2\left(\frac{\beta_{01} r_w}{a}\right) \right] \tag{58}$$

This is the formula which has been used for density measurements with the cavity in this experiment.

If actual numbers are put in the formula we find for the small tube where:

$a = 4.15$ cm

$b = 0.5$ cm

$r_w = 0.4$ cm

that

$$\bar{n} = 0.732\, f_0 \Delta f \quad m^{-3} \tag{59}$$

where f_0 is the resonant frequency with the glass tube but without a plasma and Δf is the frequency shift due to the plasma (both in Hertz). For the larger tube where:

$a = 4.15$ cm

$b = 1.76$ cm

$r_w = 1.56$ cm

$$\bar{n} = 0.0578\, f_0 \Delta f \quad m^{-3} \tag{60}$$

In actual practice it was found that the perturbation theory was inadequate for density measurements in the larger tube. The evidence for this conclusion is that the cavity gave average densities about 30% of the central densities measured with the Langmuir probe in the larger tube. This is inconsistent with both theoretical predictions of the radial profile by Parker [22] and experimental measurements of it with the probe. (Figs. 37, 39 and 39.)

In order to investigate this departure from the perturbation theory, the actual fields present in the cavity were measured. This was done by a rather indirect method of inserting an acrylic rod into the cavity and measuring the relative frequency shift per unit length of rod inserted, since this shift is proportional to the electric field squared. The result for a 3/4 inch diameter rod is shown in Fig. 40. It is seen that rather than a uniform field in the axial direction, the field is much larger near the center than at the ends. This can be accounted for by the large diameter of the holes in the end of the cavity, ($\sim$36 mm). The slight assymetry can be accounted for by the fact that the portion of the rod inserted perturbs the field slightly.

The radial fields in the cavity were also measured. This was done by inserting a 3 mm glass rod in the cavity (with the glass tube present) and measuring the fractional frequency shift as the tube was moved radially. The result is shown in Fig. 41 together with the field predicted by Eq. (51). It is apparent that the field is significantly different from the theoretical unperturbed field and further accounts for the inadequacy of the perturbation theory in this case.

A similar study of the axial field in the cavity with 1 cm end holes shows a more uniform field. The result is shown in Fig. 42 for

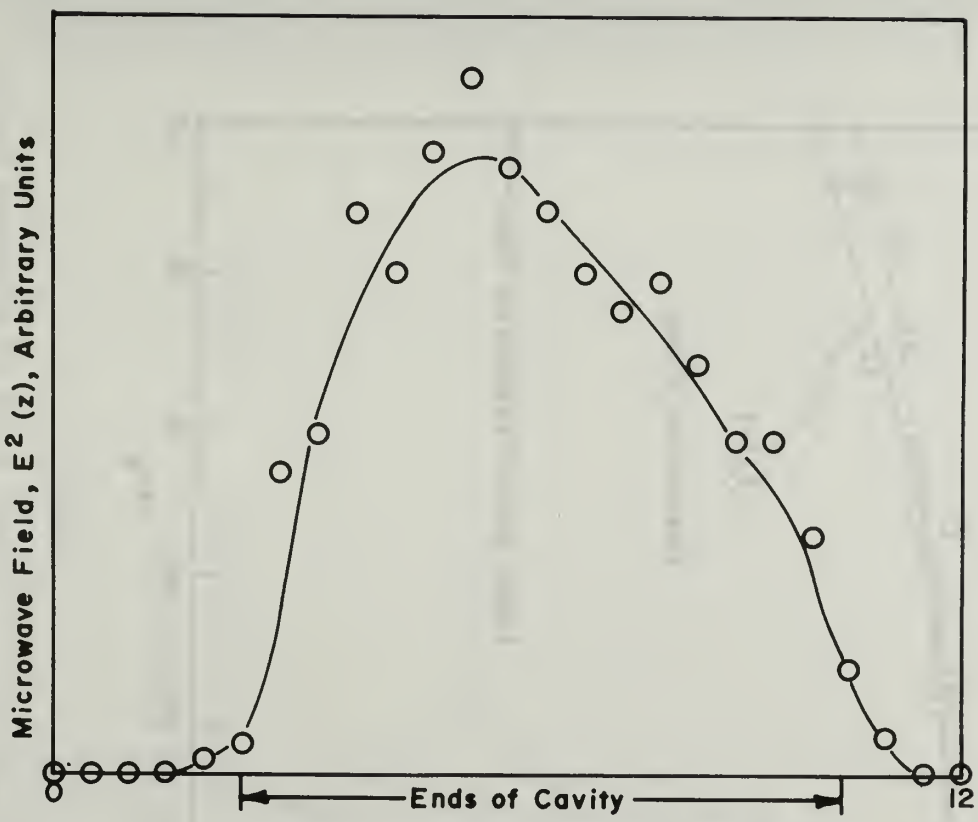

Figure 40

Axial variation of electric field of microwave cavity, cavity diameter 8.3 cm, end hole diameter 3.6 cm

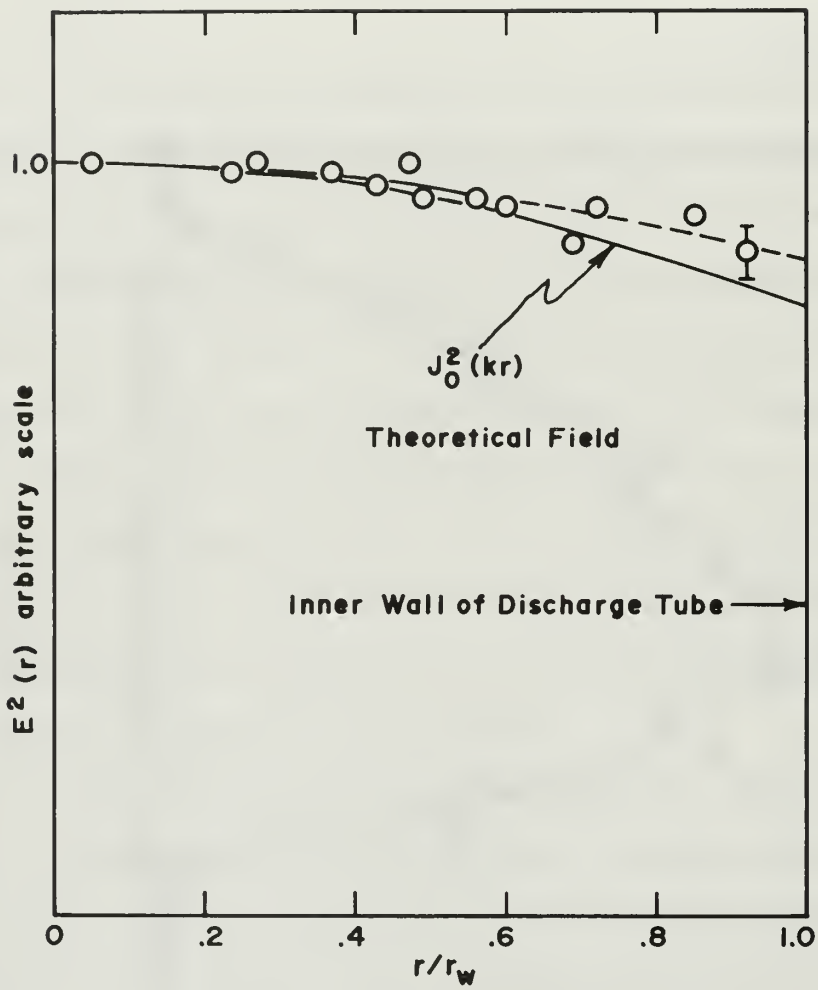

Figure 41

Radial variation of electric field of microwave cavity, cavity diameter 8.3 cm, end hole diameter 3.6 cm

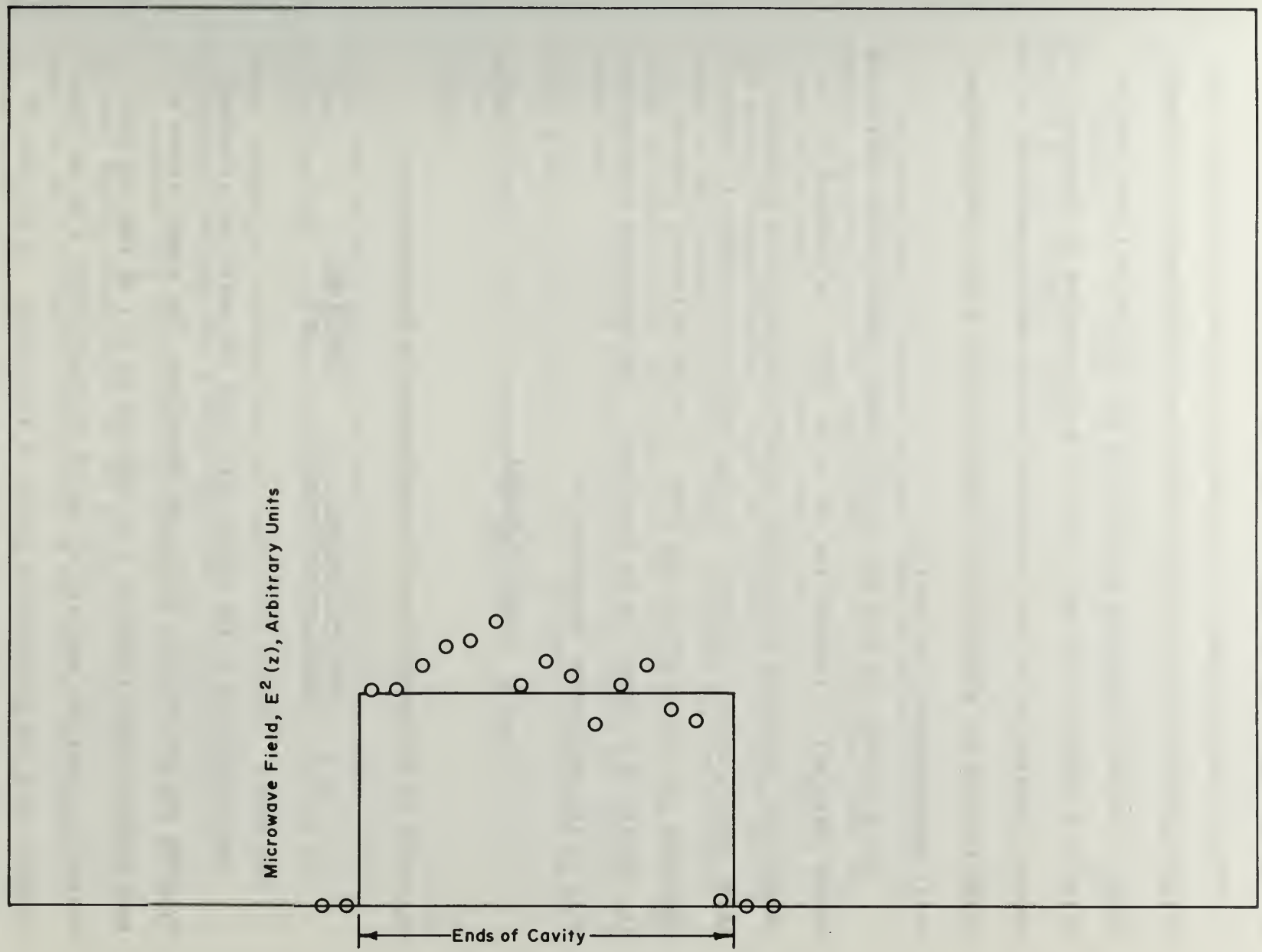

Figure 42
Axial variation of electric field of microwave cavity, cavity diameter 8.3 cm, end hole diameter 1.0 cm

a 4 mm test rod of Pyrex inserted into the cavity.

From these experiments it appears that the use of the larger end holes results in a serious distortion of the electric field of the TM_{010} mode. A recent theoretical treatment of the effects of finite size end holes in a cavity in the TM_{010} mode has been presented by Thomassen. [59] However, application of the corrections for end effects presented in this paper increase the constant in Eq. (59) by only a factor of 1.07 which still underestimates the density.

The fact that the tube was large, however, permitted an alternative method which will circumvent the use of Eq. (59). As proposed by A.L. Gardner [60] it should be possible to calibrate the cavity frequency shift using a known dielectric. A long dielectric cylinder is used to represent the free electrons and from its known dielectric constant ϵ the density of a plasma can be calculated. The equivalent electron density of the calibration dielectric is

$$n' = \frac{-m\omega^2(\epsilon-\epsilon_0)}{e^2} \tag{61}$$

Therefore on the assumption of a uniform density distribution

$$n = \frac{-\Delta\omega\ (\text{WITH PLASMA})}{\Delta\omega\ (\text{WITH DIELECTRIC})} \quad \frac{m\omega^2(\epsilon-\epsilon_0)}{e^2} \tag{62}$$

The calibration of the cavity with large end holes was attempted by using two dielectrics, Teflon and Styrofoam. Two sample pieces of each substance were turned to 1 cm rods and to 31.1 mm rods and the dielectric constants measured by use of the cavity with 1 cm end holes in which case the perturbation theory is quite good. In the case of Teflon a value of K = 1.98 was measured and for Styrofoam the K was

measured as 1.05. Using the larger pieces of the same material and the larger end holes the sensitivity of the cavity was determined for each dielectric. The results of applying Eq. (62) gave the following results:

Teflon: $$\bar{n} = 2.33 \times 10^{14} \, \Delta f(\text{PLASMA}) \tag{63}$$

where $\bar{n}$ is in m^{-3} and Δf in MHz.

Styrofoam: $$\bar{n} = 2.72 \times 10^{14} \, \Delta f(\text{PLASMA}) \tag{64}$$

The large (16%) difference between these two values can be attributed to the fact that such large pieces of the dielectric affect the fields in the cavity to different extents and thus the reliability of this method is questionable. Since the accuracy of the probes was assessed at 14% (assuming the probe theory is valid), the cavity method offers no advantage over the probe, thus the cavity was not used for the larger tube. It should be noted however that the direct calibration method gives an electron density in closer agreement with probes than the perturbation theory or the perturbation theory corrected for end effects.

A further uncertainty in the application of the cavity to the larger tube is the effect on the field on a non-uniform radial profile. Calibration with a uniform dielectric may be expected to produce different effects on the field than the non-uniform plasma. A more ideal calibration technique for a large cavity has also been suggested by A. L. Gardner. [61] The calibration dielectric should be shaped to have the same density distribution of the plasma to be measured. Furthermore, the total frequency shift should be the same as the plasma produces in order that the fields are perturbed in the same manner. This might be accomplished by arranging slices of dielectric material of the

proper cross-sectional shape along the axis of the column and arranging the spacing of the slices to give the desired frequency shift. Simple calculations would lead to a more exact calibration constant than can be obtained by the use of a solid uniform dielectric. Such a procedure has not been undertaken.

In connection with the use of the cavity for diagnostics in the case of the small tube, several experimentally important points should be mentioned. The cavity inside walls should be clean and smooth for the best Q. Furthermore, a good surface electrical connection should be maintained at the ends of the cavity as the surface currents must flow across this joint for the TM_{010} mode. The length of the probes for coupling to the cavity should be kept small in order to prevent loading and reduction of Q.

When taking density data for comparison with resonance measurements, the frequency shift was recorded as a function of discharge current and densities were calculated from Eq. (59). For densities at currents between values at which measurements were made, linear interpolation was employed.

VI. RESONANCE STUDY RESULTS

In this section are presented the results of the experimental studies of the Tonks-Dattner resonances.

Using the procedures described in Section IV, resonances were observed on the x-y recorder for neon, argon and xenon in the large 3.5 cm diameter tube and for xenon in the small one cm diameter tube. As previously noted these traces could be made when the amplitudes of the simultaneously occurring moving striations were small. Typical traces of the sort obtained are shown in Figs. 43, 44, and 45 for neon, argon, and xenon respectively. These data were taken with an rf millivoltmeter so that the ordinate is rf voltage. In Fig. 45 the zero of voltage is shown indicating an 88% absorption of rf power at the peak of the main resonance.

Experiments in which the minima in the reflected signal were observed show close agreement of the resonances with those in which minima in the transmitted signal were observed. Fig. 46 shows two resonance curves, one taken by each of these methods. The currents for the resonances agree within 4% which was comparable to agreement between values obtained for the same method on successive sweeps of the current.

Fig. 47 shows x-y recorder traces of a resonance measurement taken by the ratio meter observing maxima in the reflected signal from a waveguide horn directed at the small tube. The vertical scale is proportional to reflection coefficient P, $P = \frac{VSWR-1}{VSWR-1}$ where VSWR is the voltage standing wave ratio. The three curves are for different scales of sensitivity. The percent reflection for full scale deflection is indicated on the curves.

Data obtained from traces of the type just described were used to

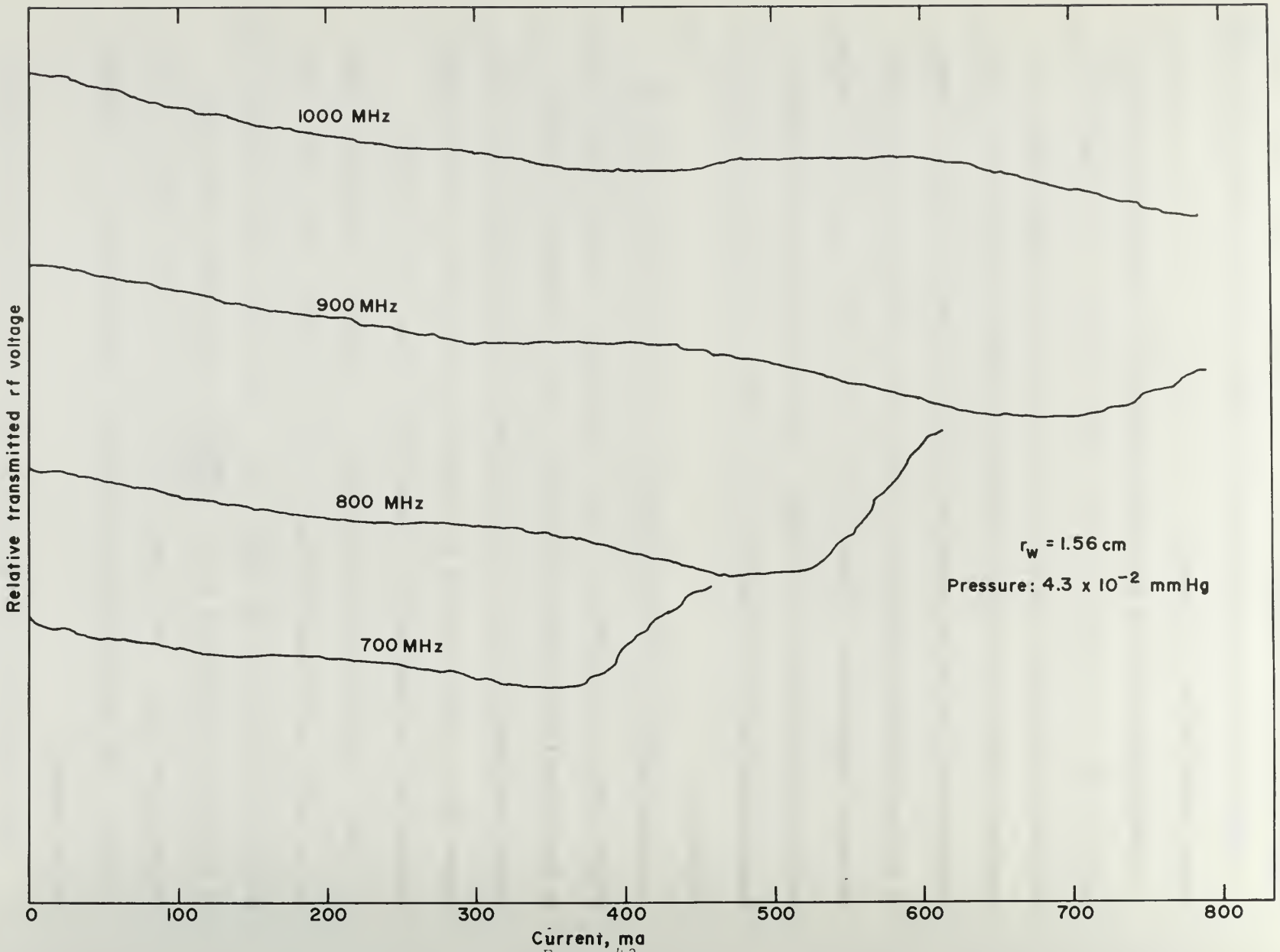

Figure 43

Resonances in neon, K_{eff} = 1.82, relative transmitted rf voltage versus discharge tube current

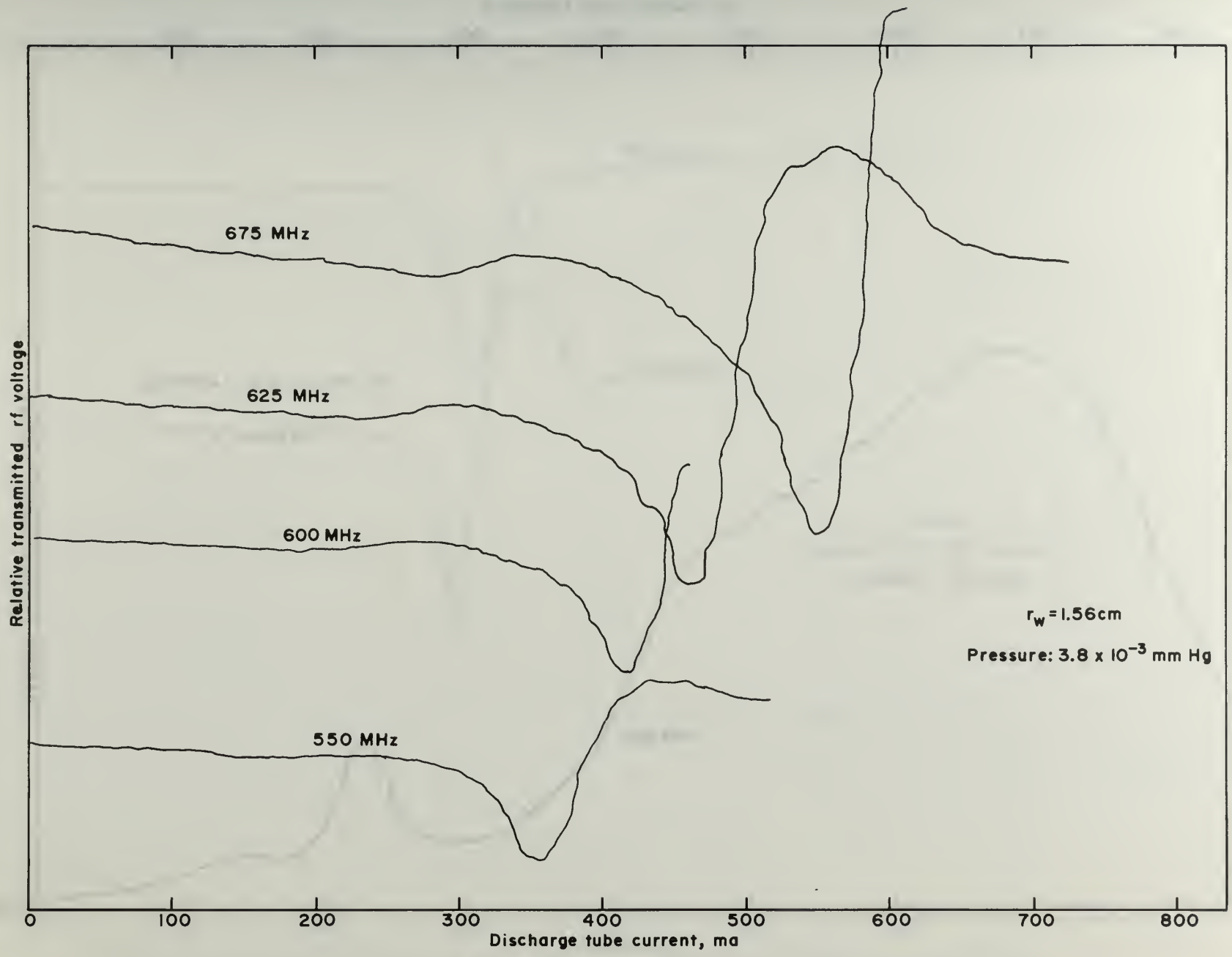

Figure 44. Resonances in argon, K_{eff} = 1.82, relative transmitted rf voltage versus discharge tube current

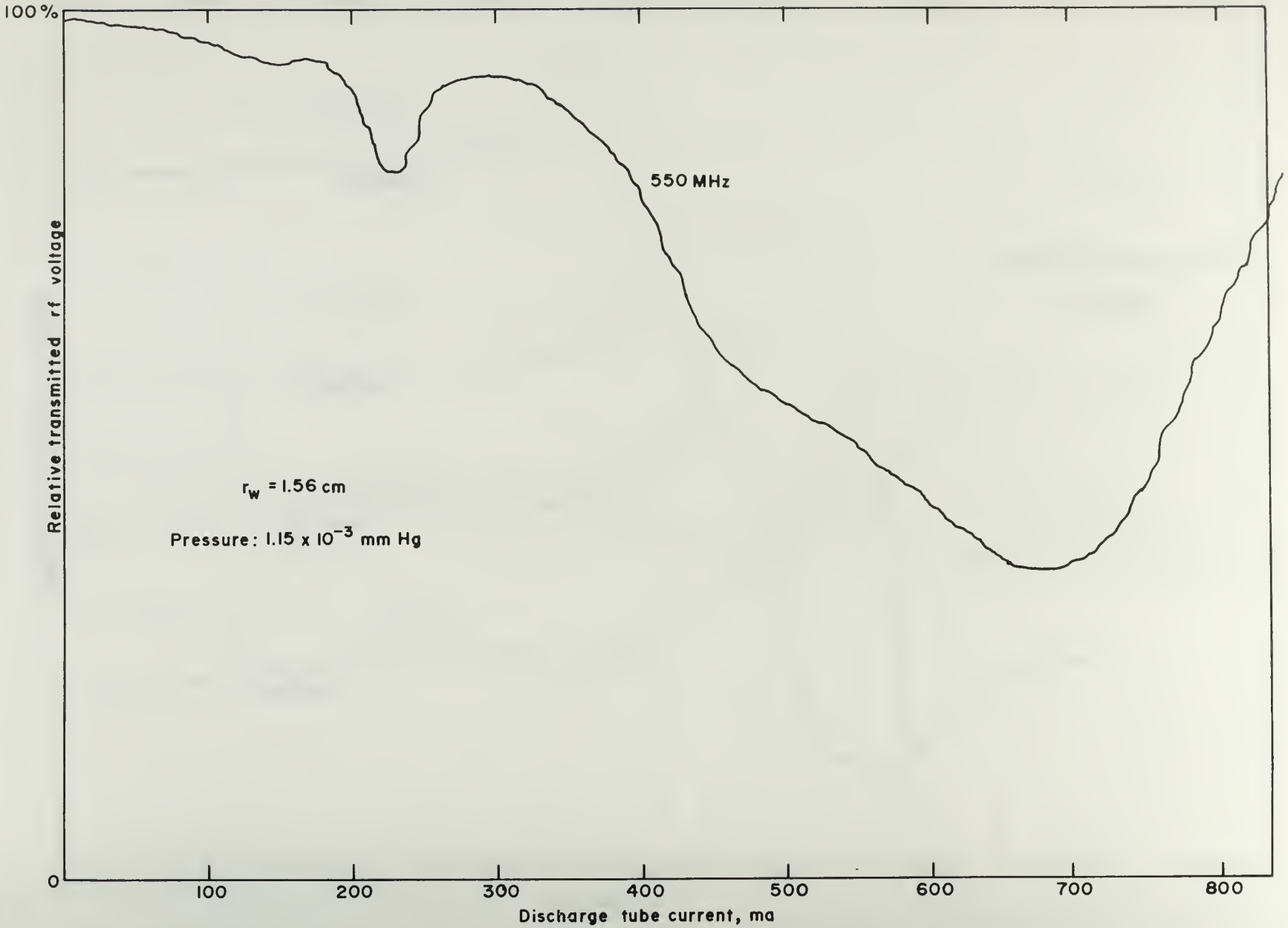

Figure 45. Resonance in xenon, K_{eff} = 3.74, relative transmitted rf voltage versus discharge tube current

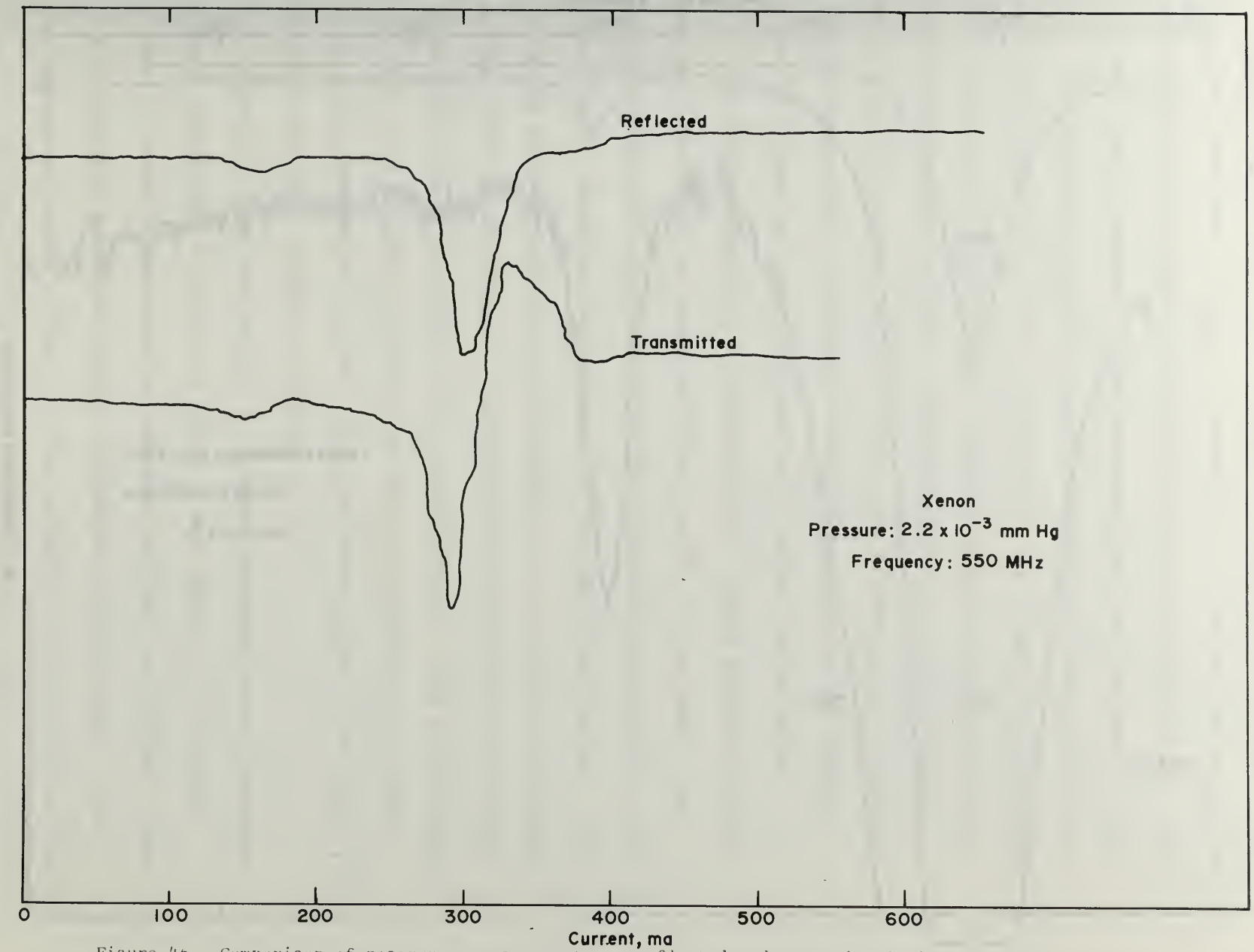

Figure 46. Comparison of resonance measurements on reflected and transmitted signals, xenon

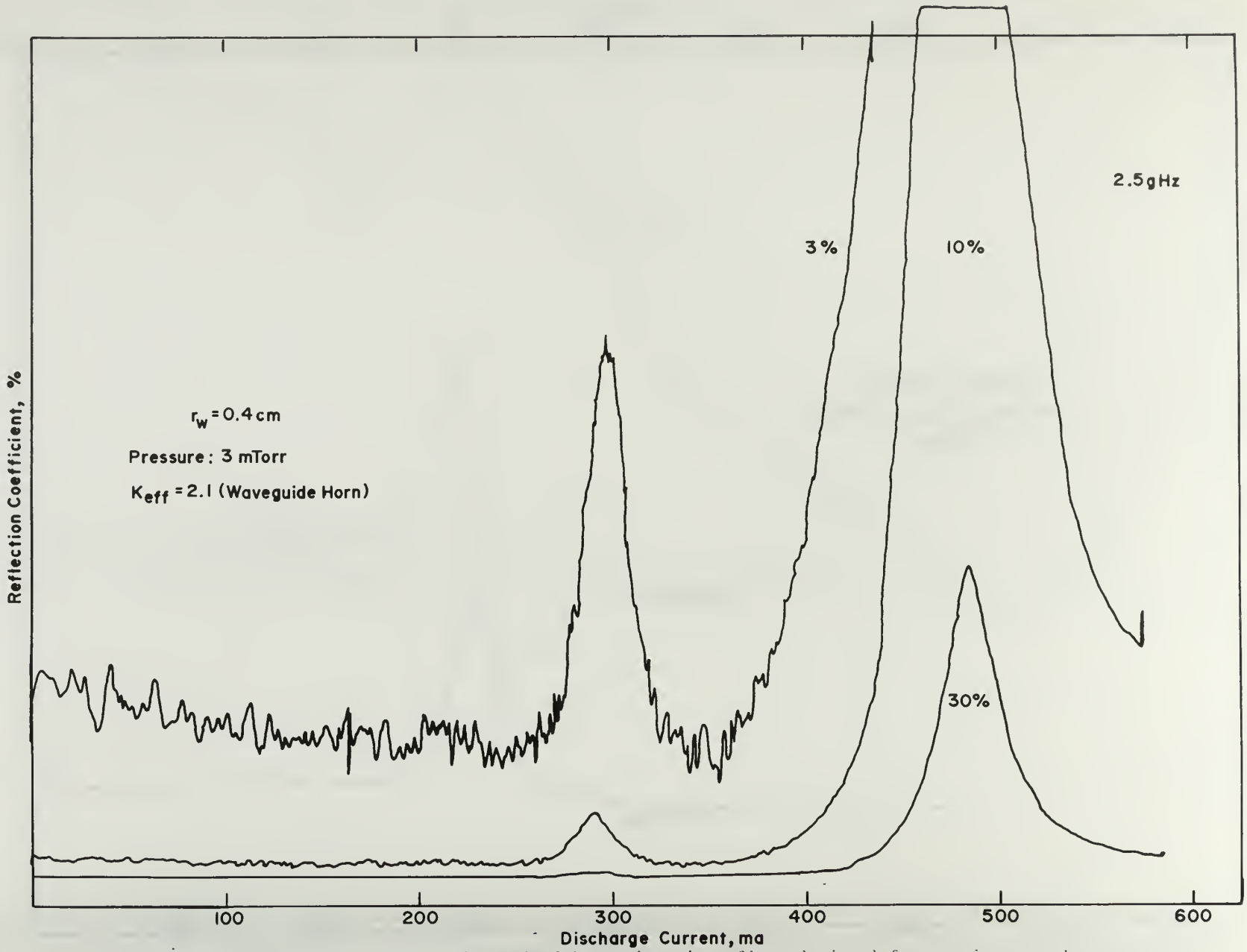

Figure 47. Resonances in xenon determined by maximum in reflected signal from a microwave horn, reflection coefficient versus discharge tube current

obtain resonant frequency as a function of discharge tube current. These data have been shown in Figs. 48 through 55. In one case for argon, the main quadrupole resonance was clearly visible on the high current side of the main dipole resonance. These resonance peaks are indicated on Fig. 48. The quadrupole resonance was only observed when using the small dipole device with a $K_{eff} = 3.74$. This effect was observed by Nickel [23] who noted that for devices smaller than three times the tube diameter, the quadrupole resonances were sometimes excited by a dipole device. This is possibly due to the fact that a more uniform electric field is applied when using a large device and eccentricities of the plasma-electrode system are more pronounced for a smaller radius device.

The electron density and temperature for a given pressure and current were determined as described in Section V. For the small tube, density measurements were made using the microwave cavity method, and consequently, densities are averages over the tube cross-section. For the probe measurements, density measurements are in terms of the density at the center of the column. (The probe was located as near the center as possible except for radial profile measurements.) From these diagnostic data it is possible to present the data on resonances in a manner which allows comparison with the theory of Parker, Nickel, and Gould. [21] This has been done in Figs. 56 through 61.

Figure 56 shows the results of resonant frequency versus discharge current information from Fig. 50 (neon, p = 21 mTorr, $r_w = 1.56$ cm) plotted in terms of dimensionless parameters ω^2/ω_{po}^2 and r_w^2/λ_{DO}^2, where λ_{DO} is computed using the density information plotted in Fig. 32 and the temperature values of Fig. 34. The variables here are based on densities at the center of the column. The theoretical results are also

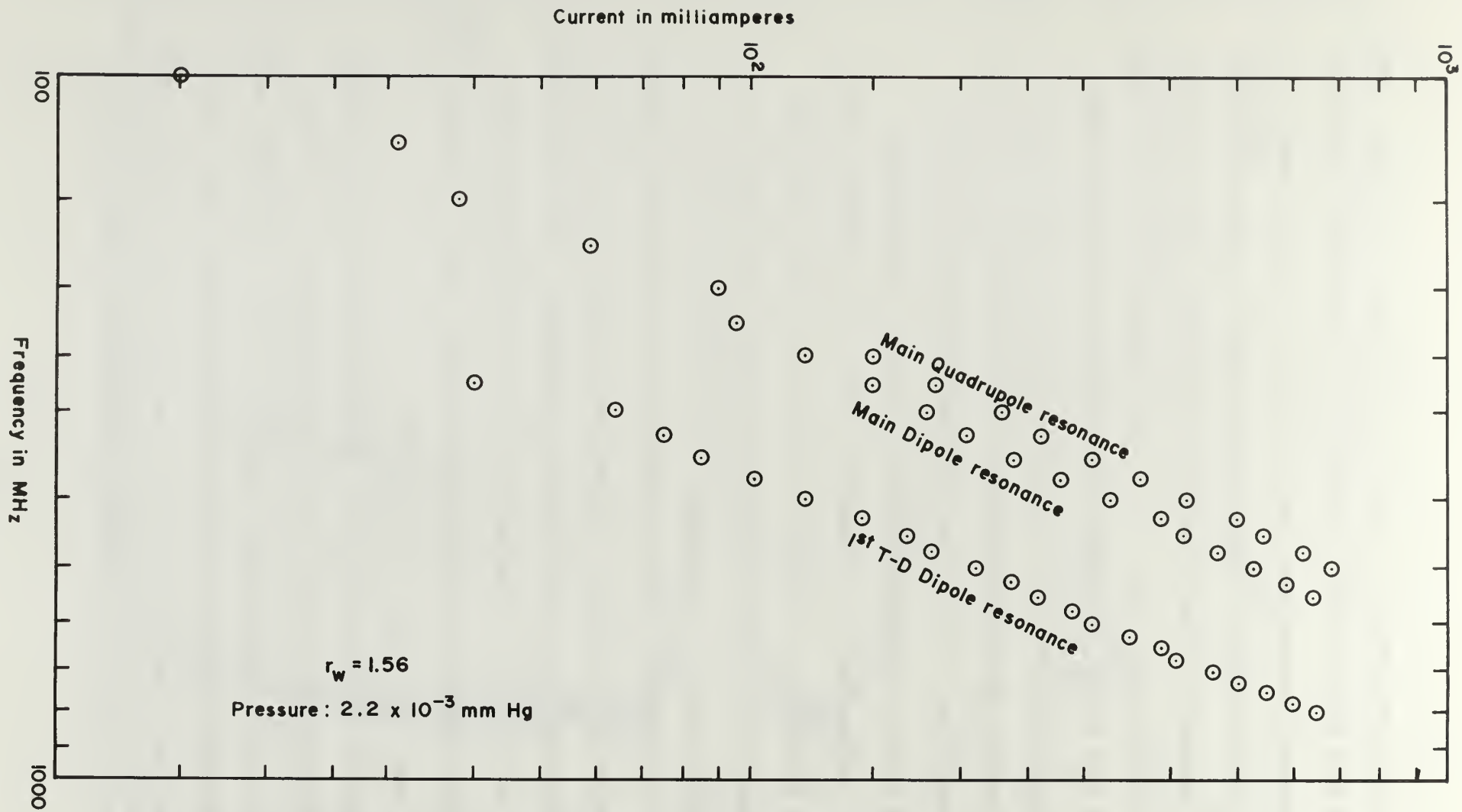

Figure 48

Current for resonance versus resonant frequency, argon, K_{eff} = 3.74, 2.2 mTorr

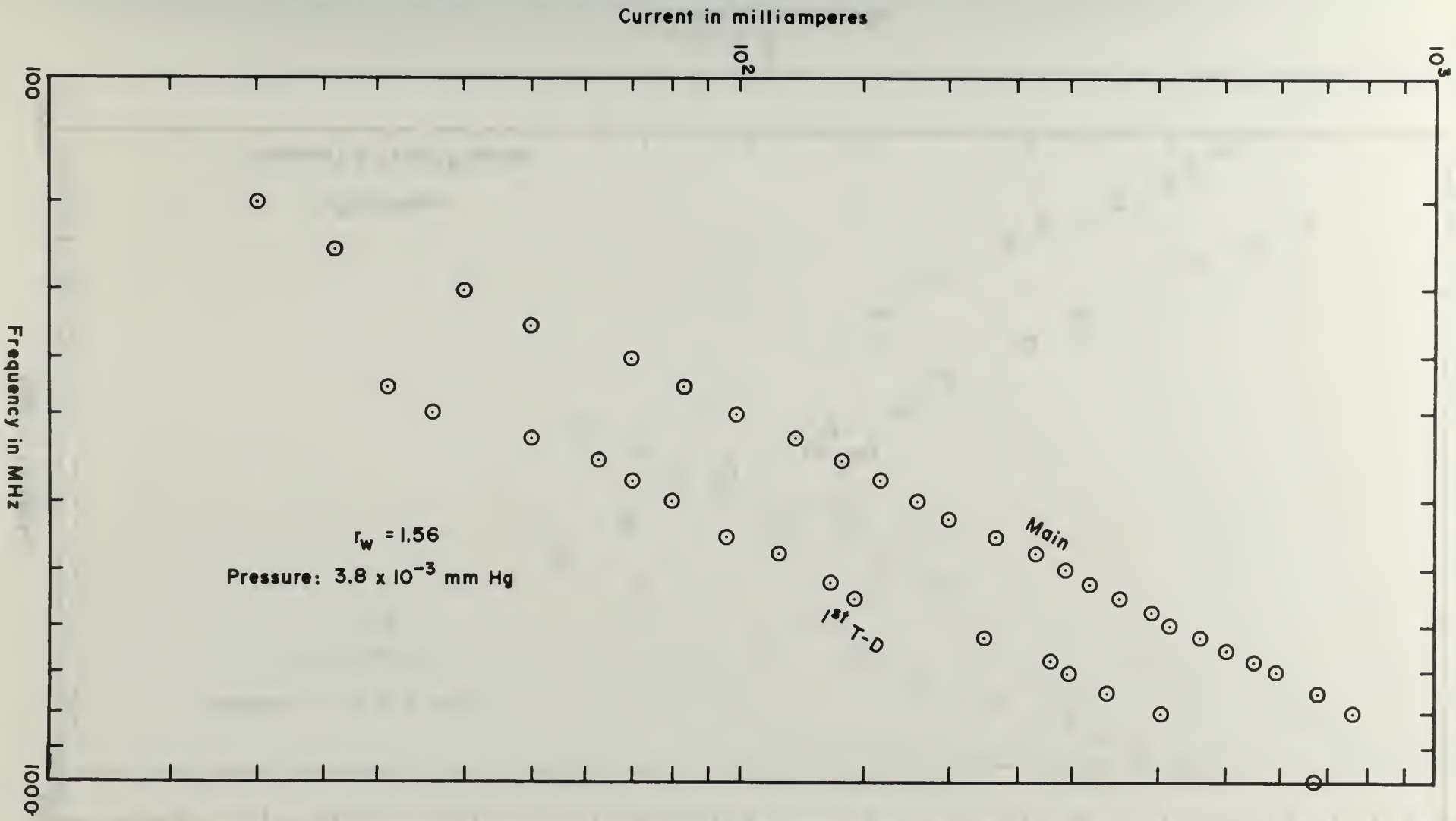

Figure 49

Current for resonance versus resonant frequency, argon, K_{eff} = 1.82, 3.8 mTorr

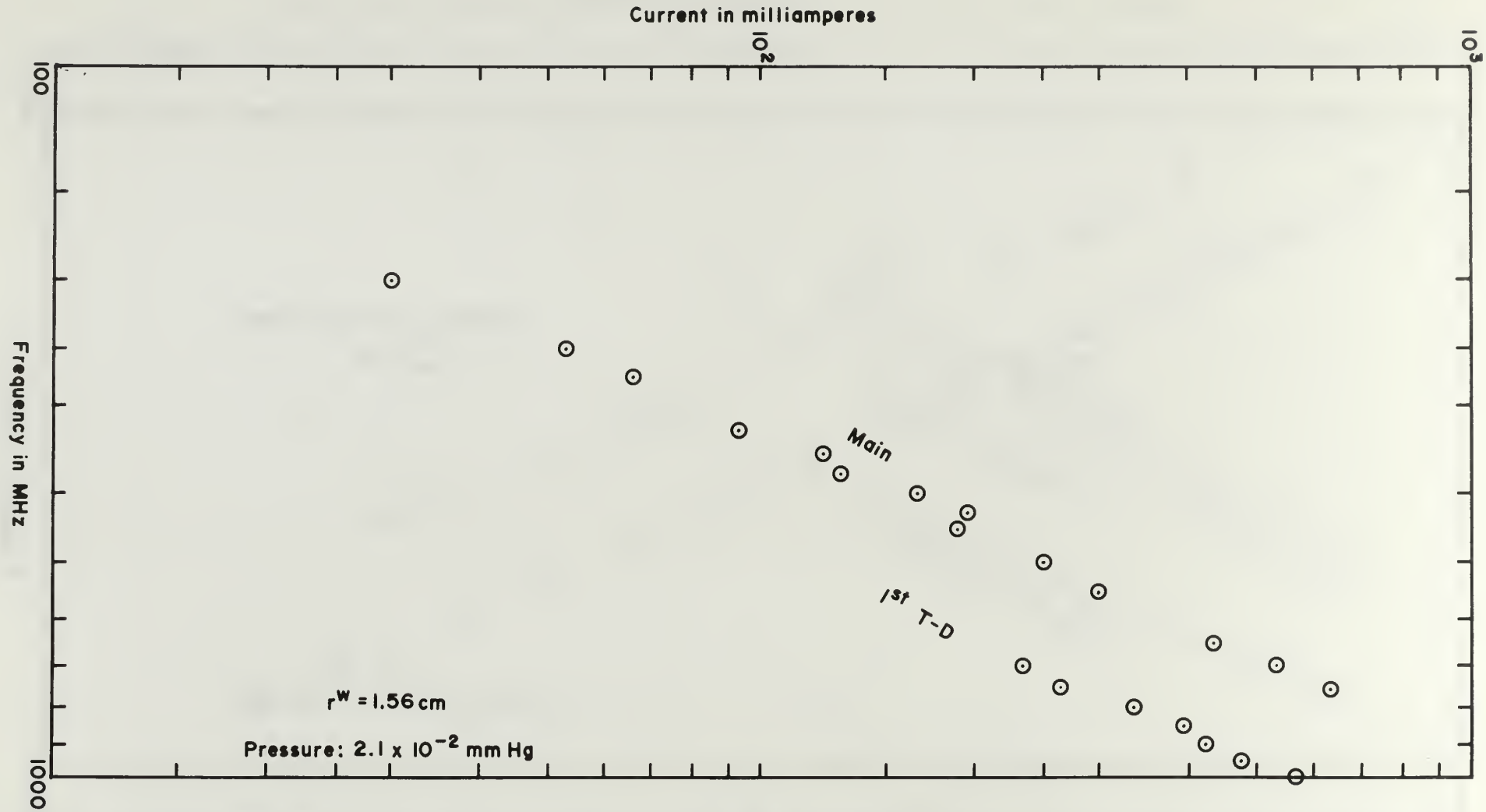

Figure 50

Current for resonance versus resonant frequency, neon, K_{eff} = 1.82, 21 mTorr

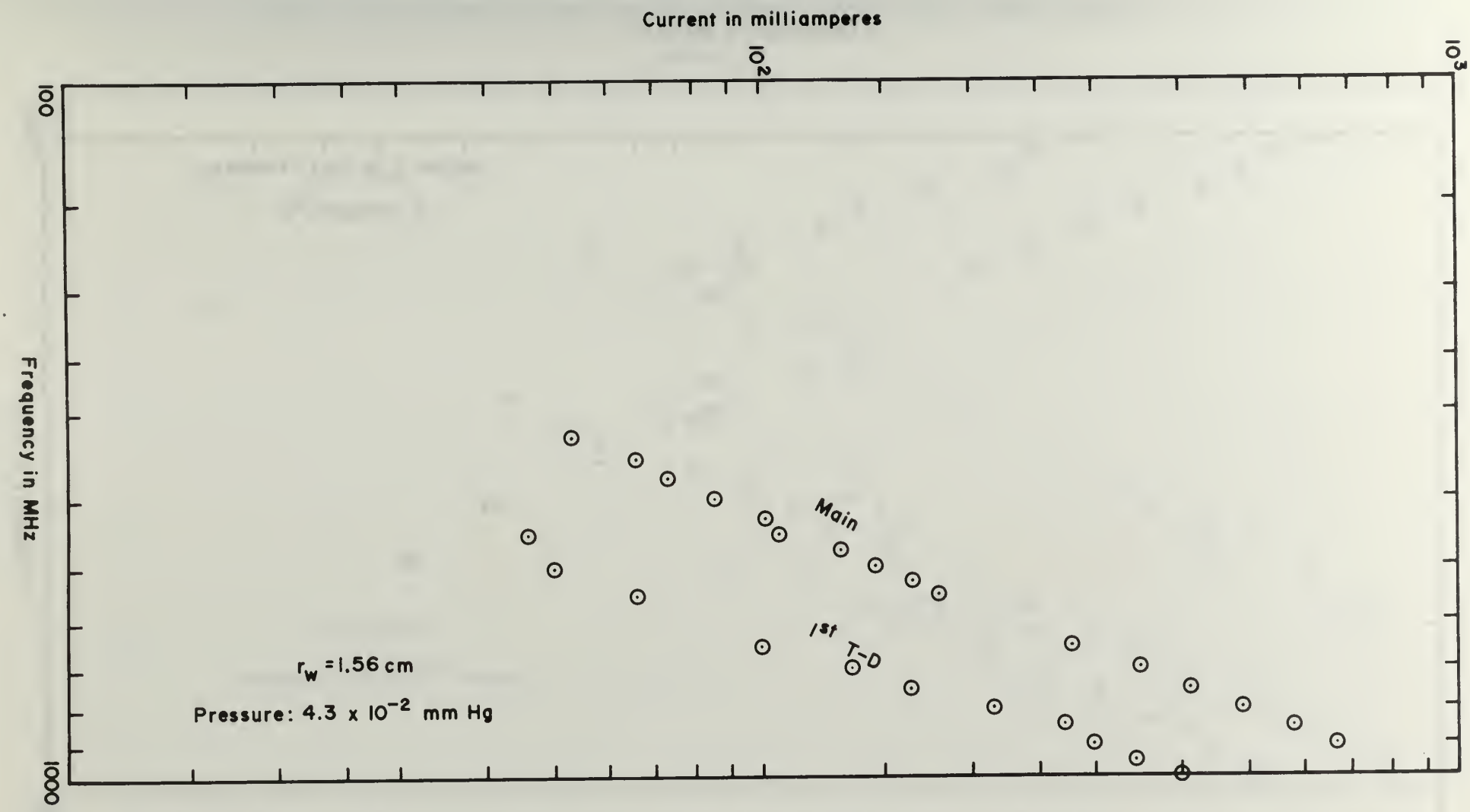

Figure 51

Current for resonance versus resonant frequency, neon, K_{eff} = 1.82, 43 mTorr

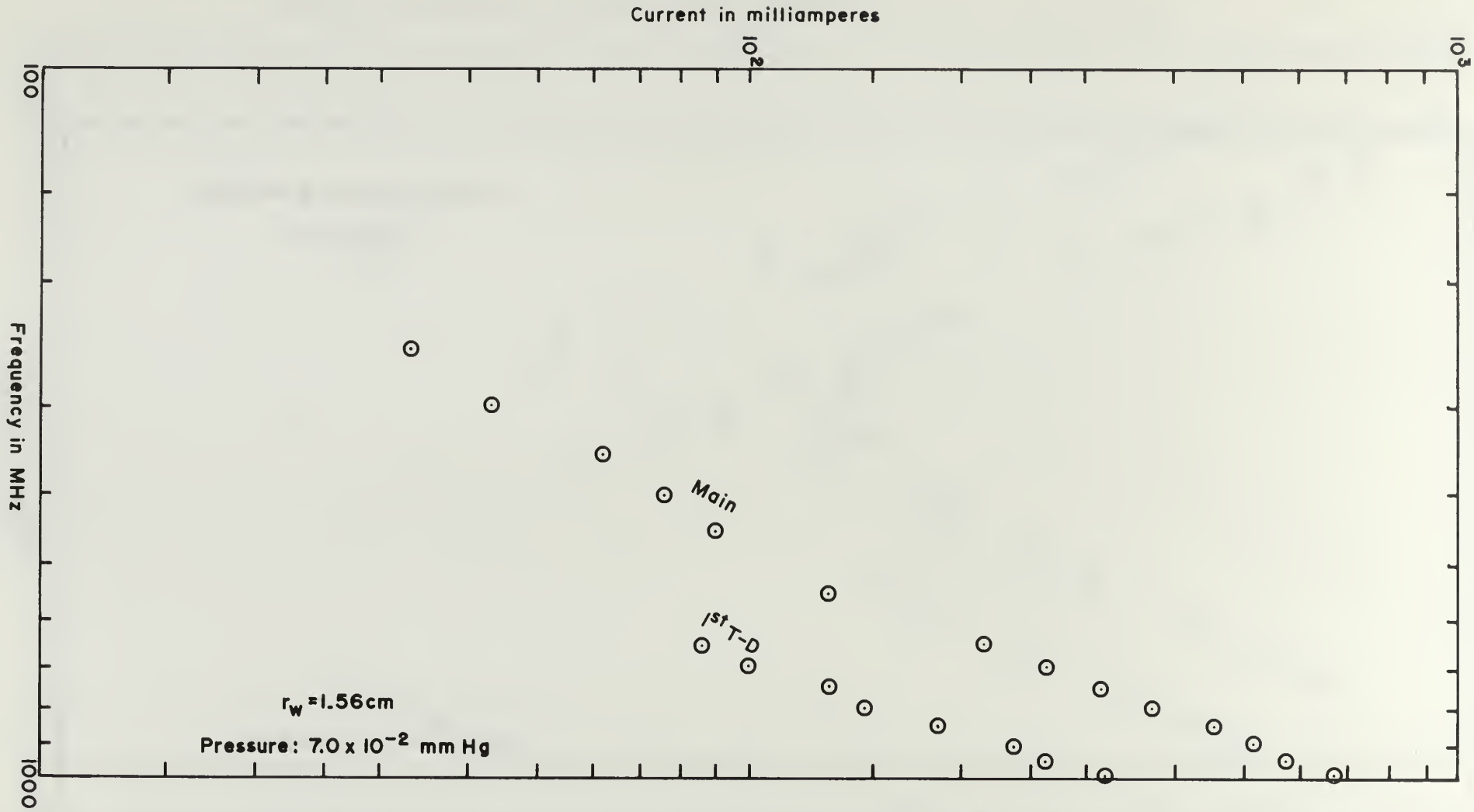

Figure 52

Current for resonance versus resonant frequency, neon, K_{eff} = 1.82, 70 mTorr

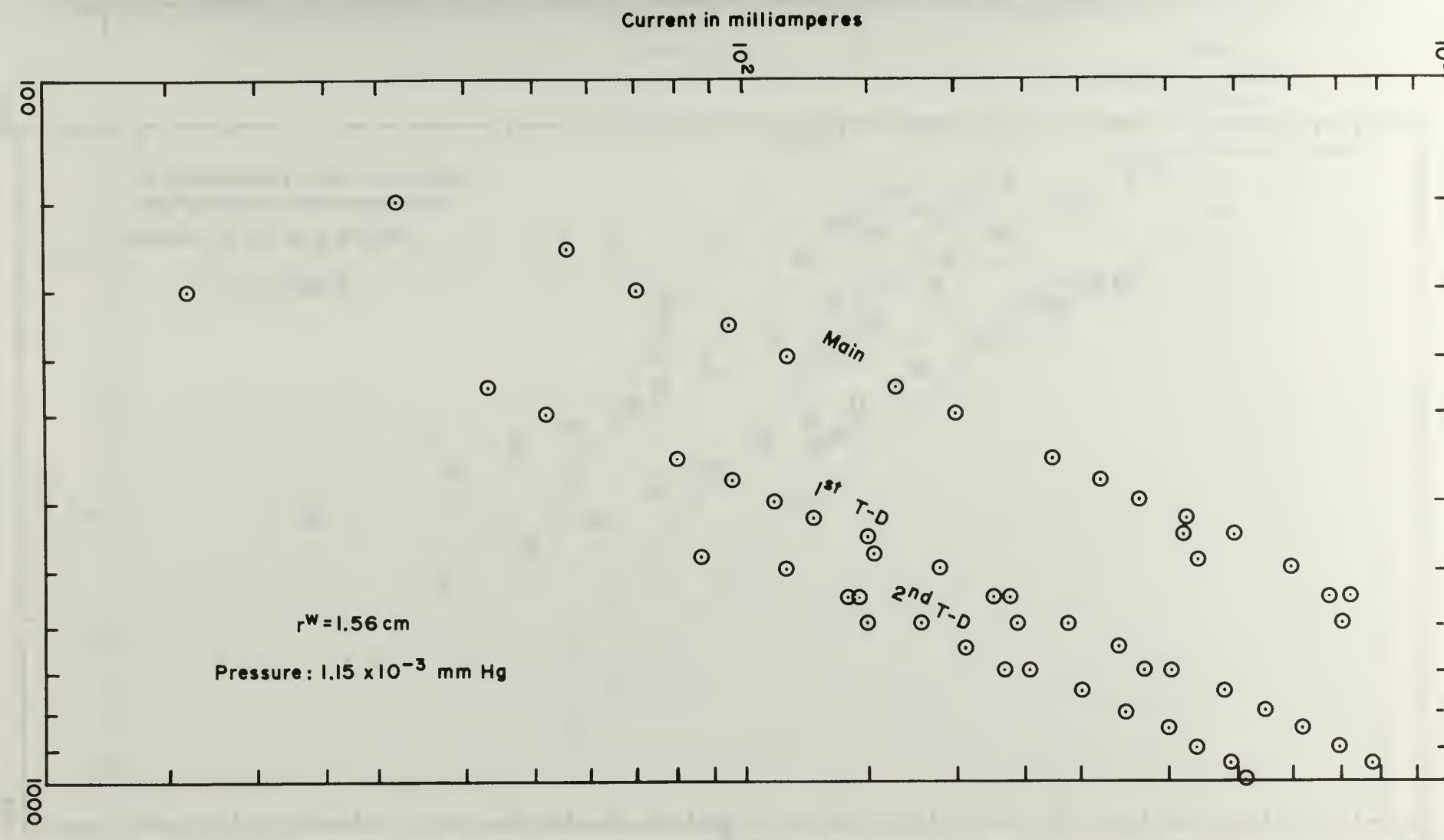

Figure 53

Current for resonance versus resonant frequency, xenon, K_{eff} = 3.74, 1.2 mTorr

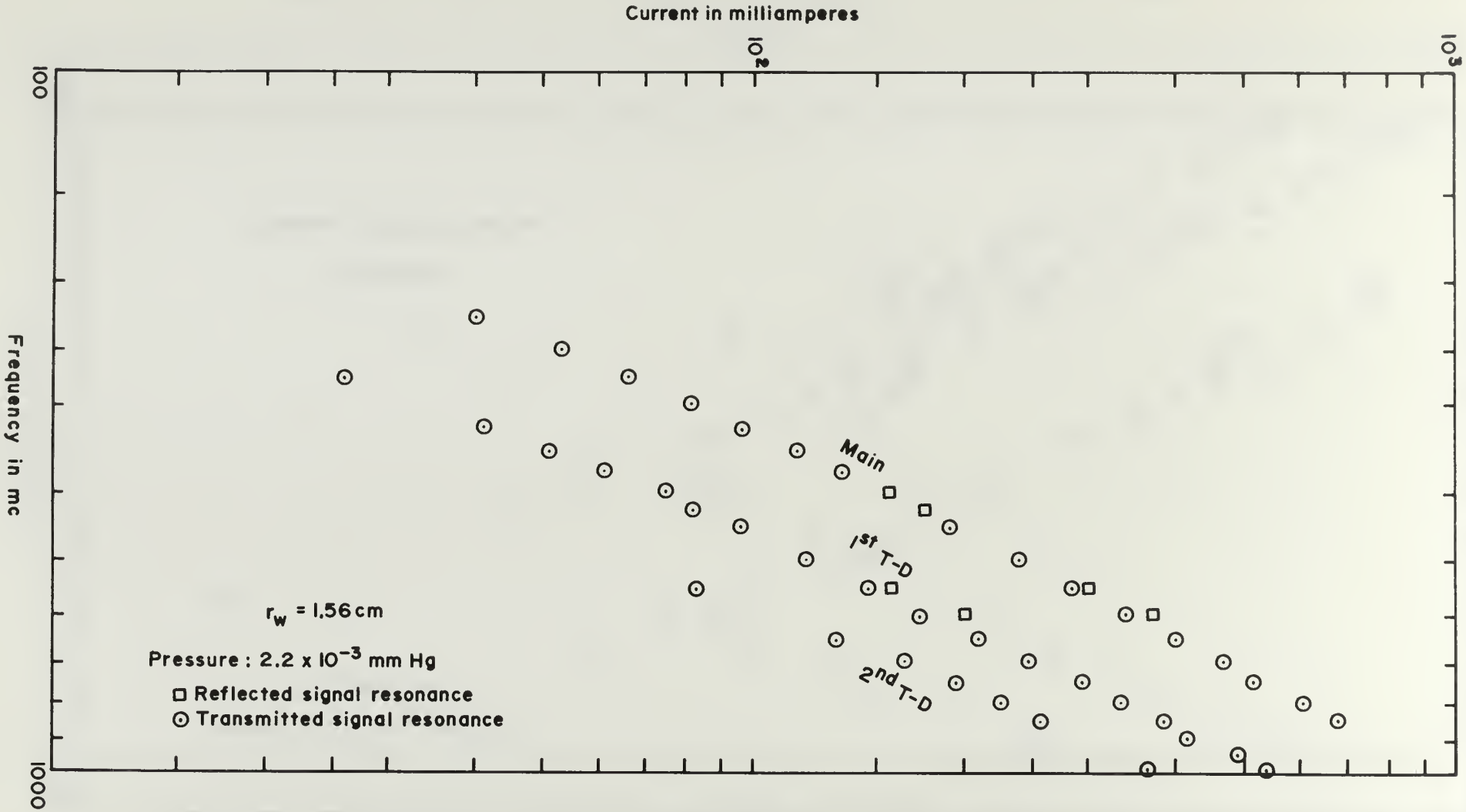

Figure 54

Current for resonance versus resonant frequency, xenon, K_{eff} = 1.82, 2.2 mTorr

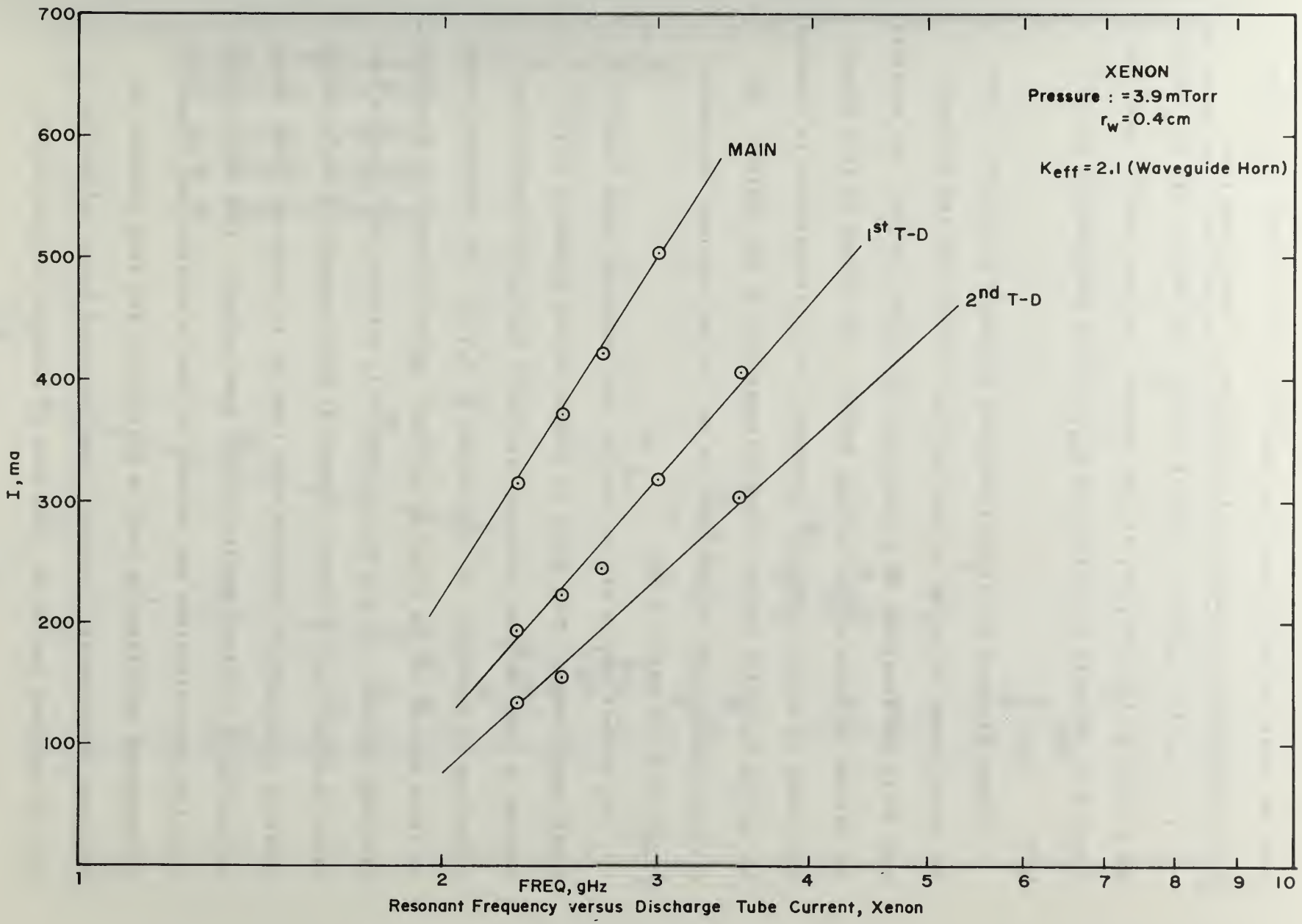

Figure 55. Current for resonance versus resonant frequency, xenon, K_{eff} = 2.1 (waveguide horn), 3.9 mTorr

based on these variables since the numerical data of Parker [22] allow the transformation of theoretical conditions to these quantities.

In a similar manner the results of Figs. 48, 49, 51, 52, 53, and 54 are plotted in Figs. 56, 57, 58, 59, and 60. The neon results have been combined on a single plot since the K_{eff} for all measurements was the same.

Figure 61 shows the results obtained for xenon in the small tube. The three groups of points at the right were taken with the microwave horn while the remainder were taken with the dipole device. The variables are defined in terms of the average density. The points on this figure were taken at several different pressures, but this variation is accounted for by the inclusion of the electron temperature in the abcissa. The electron temperatures ranged from 2.8 to 7 ev and resonant frequencies ranged from 250 MHz to 4 GHz.

The error flags in Fig. 61 are for the estimated error based on a single measurement. This error is largest at low values of $r_w^2/\bar{\lambda}_D^2$ because of the $\pm$ 0.3 MHz accuracy with which the cavity resonant frequency can be measured. At high values of $r_w^2/\bar{\lambda}_D^2$ the estimated error is large because of the clean-up pressure variation resulting from high discharge current. It has been attempted to maintain the pressure constant in observing resonances, however at high currents of about 500 ma there is a decrease in pressure with time due to clean-up. This causes a lowering of electron density for the same current. This high current operation was maintained for as short a time as possible and diagnostic measurements were taken as near as possible to the same pressure as resonance measurements. However, some increased error and scatter of data is expected due to the high rate of clean-up at high current.

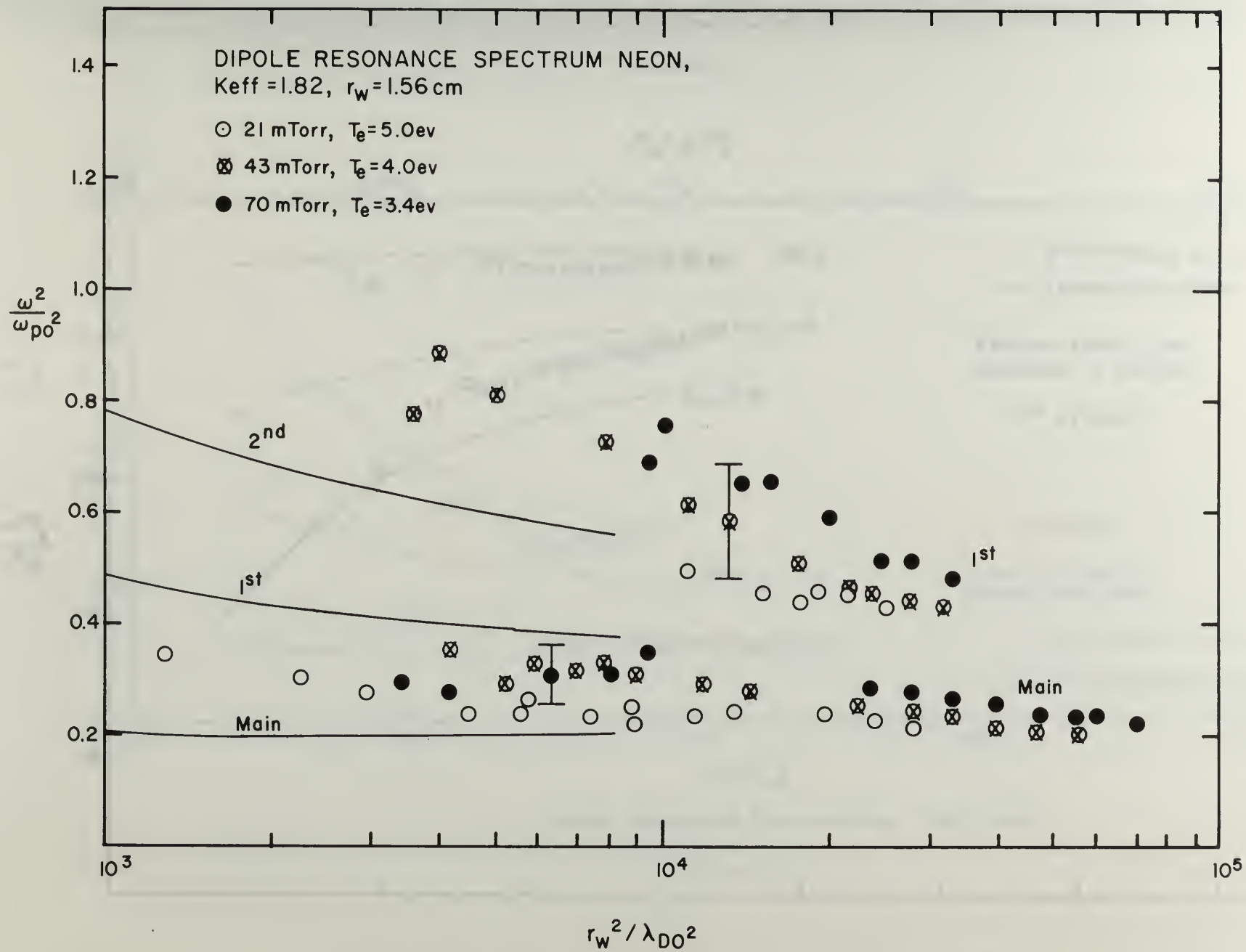

Figure 56. Dipole resonance spectrum, neon, K_{eff} = 1.82

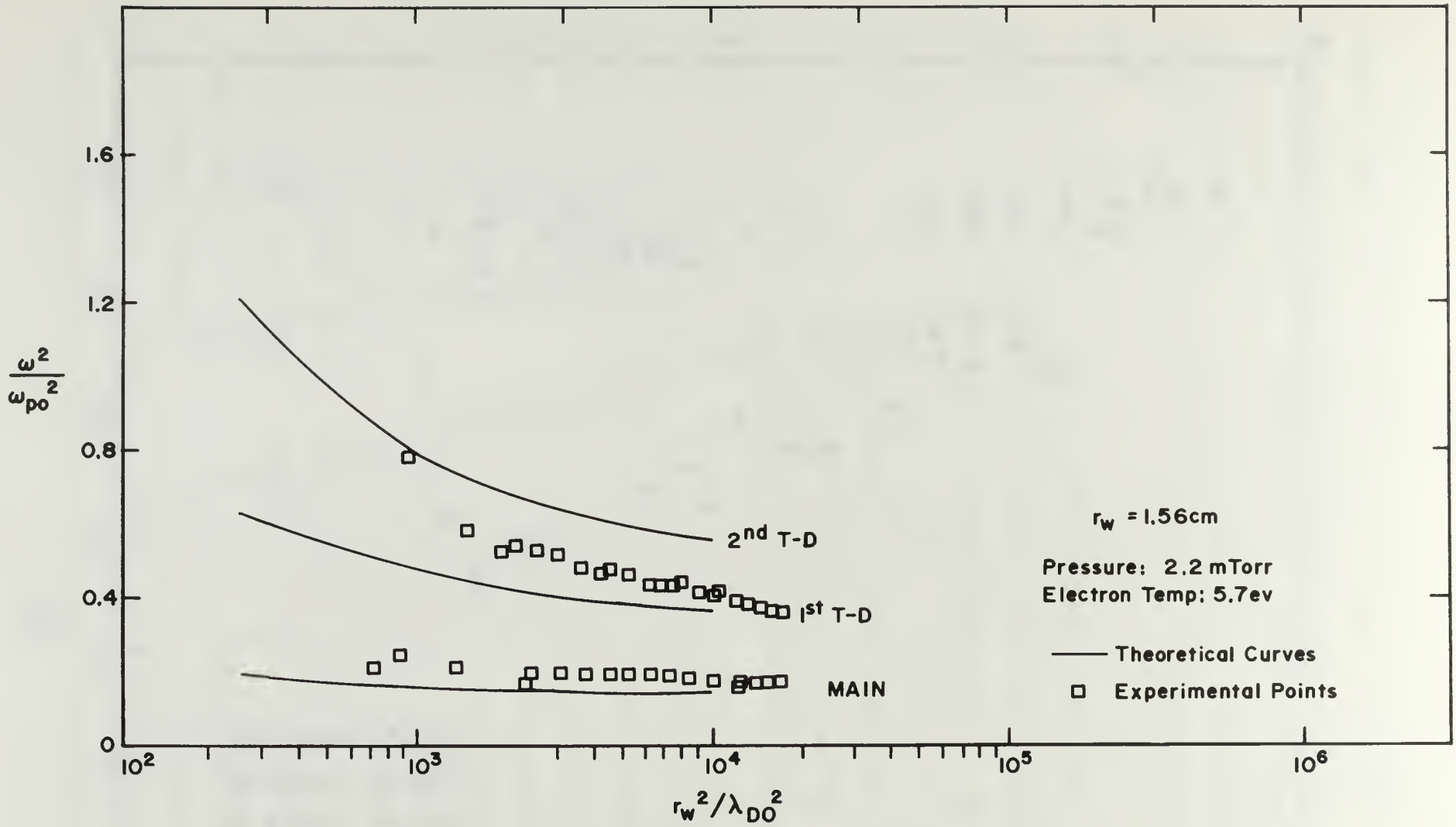

Figure 57

Dipole resonance spectrum, argon, K_{eff} = 3.74

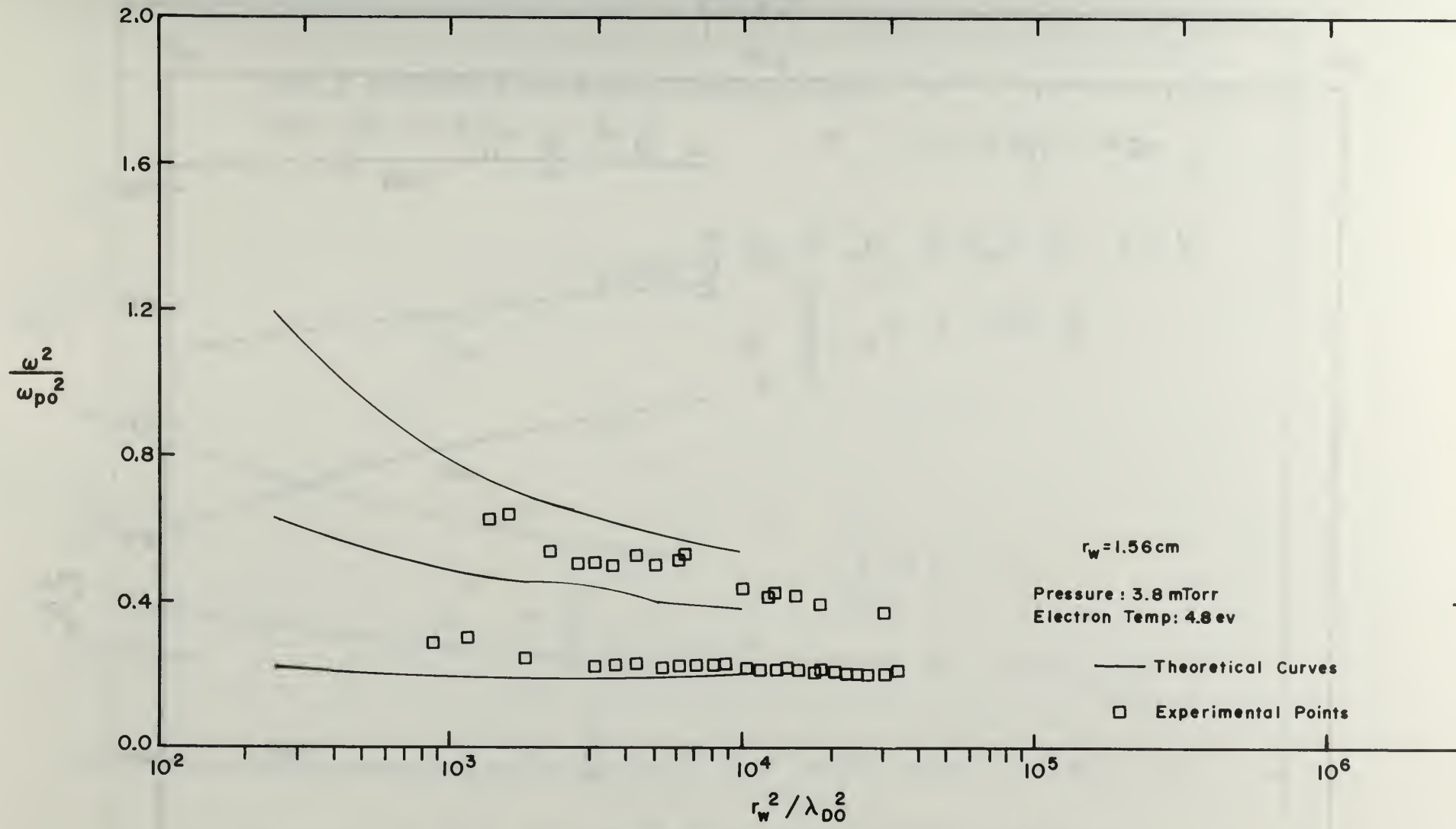

Dipole Resonance Spectrum K_{eff} = 1.82, Argon

Figure 58

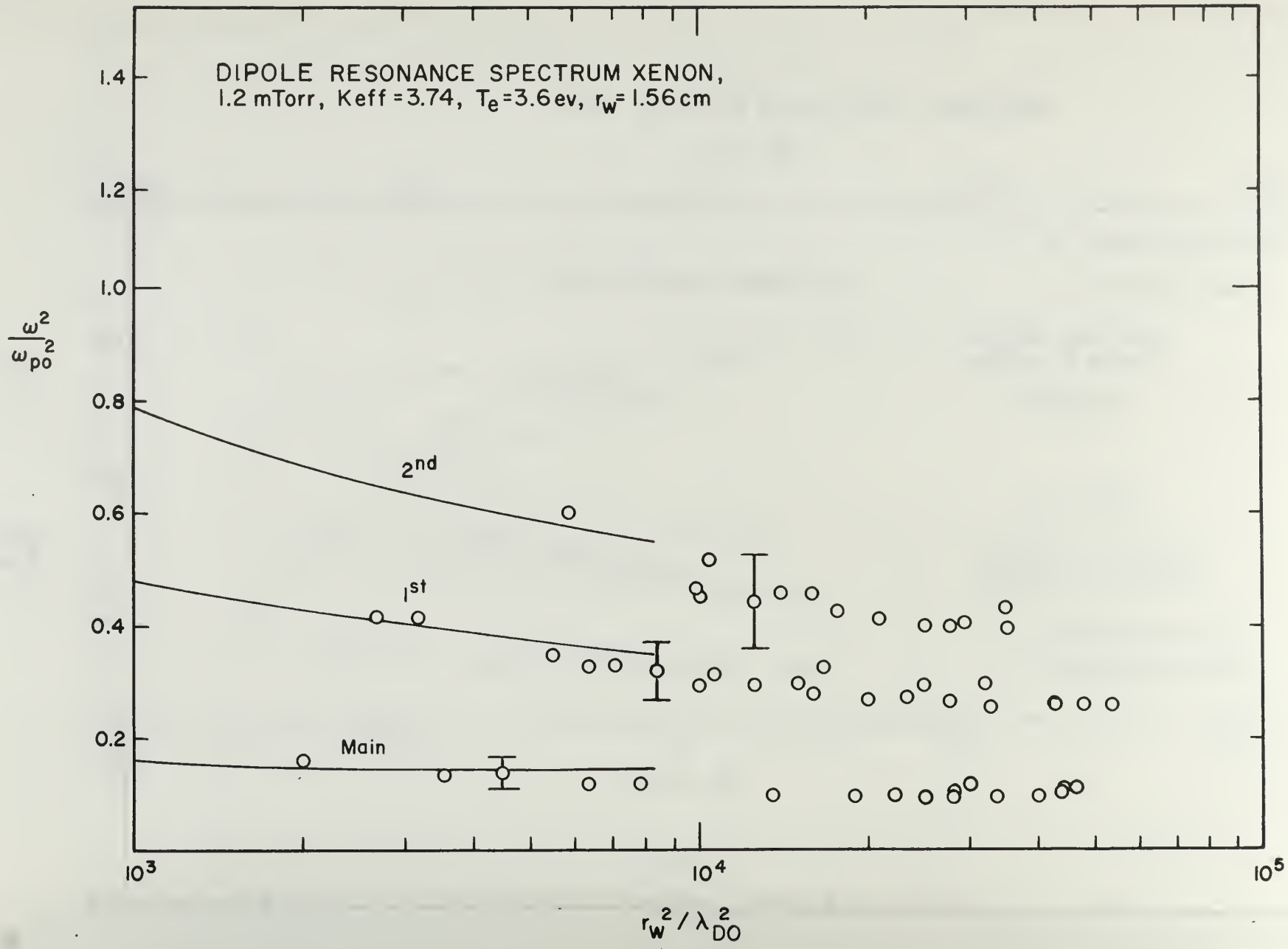
DIPOLE RESONANCE SPECTRUM XENON,
1.2 mTorr, Keff = 3.74, T_e = 3.6 ev, r_w = 1.56 cm
1.4
1.2
1.0
0.8
0.6
0.4
0.2
$\frac{\omega^2}{\omega_{po}^2}$
2nd
1st
Main
10^3
10^4
10^5
r_w^2 / λ_{DO}^2

Figure 59

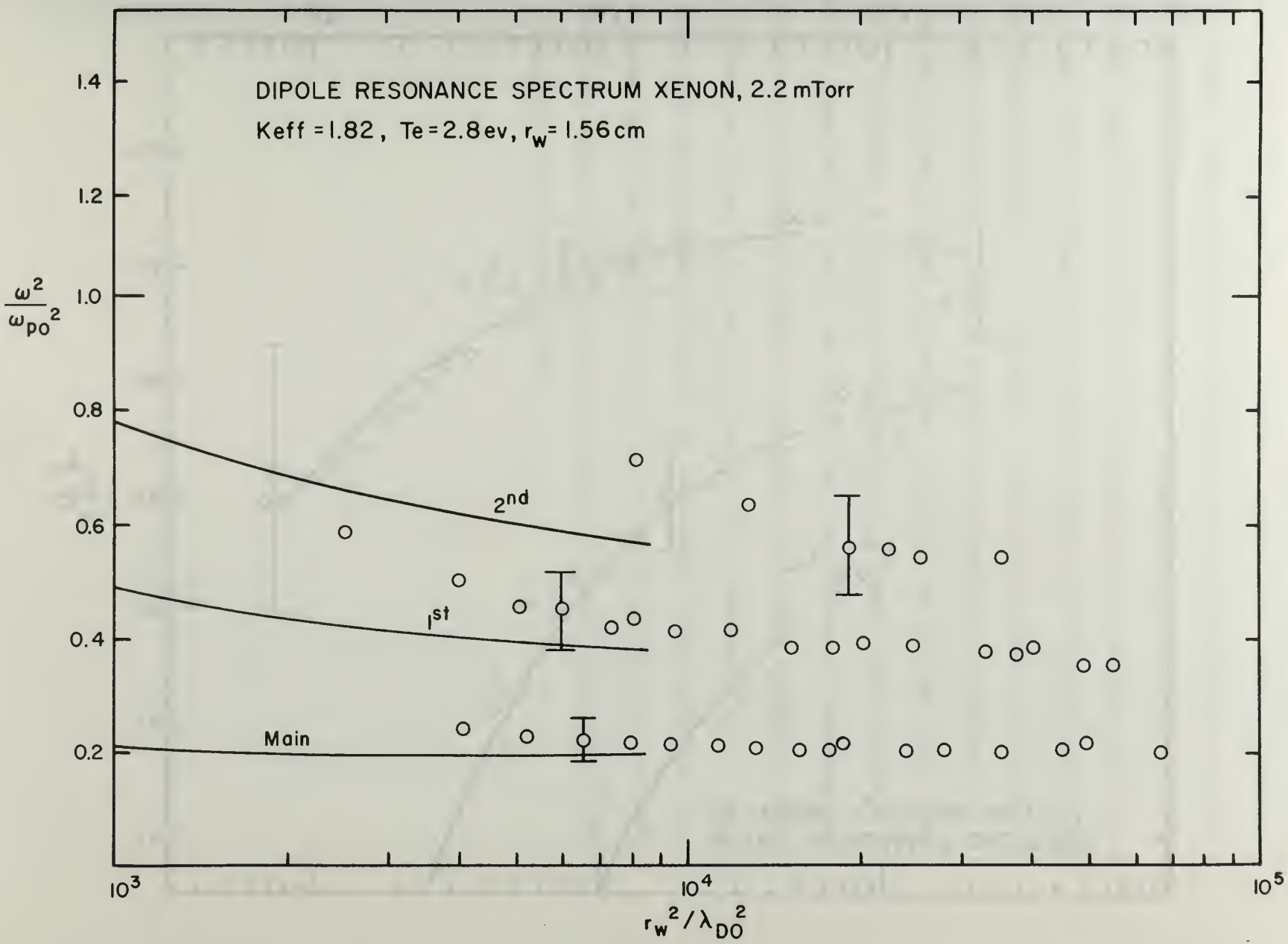
DIPOLE RESONANCE SPECTRUM XENON, 2.2 mTorr
Keff = 1.82, Te = 2.8 ev, r_w = 1.56 cm
$\frac{\omega^2}{\omega_{po}^2}$
1.4
1.2
1.0
0.8
0.6
0.4
0.2
2nd
1st
Main
10^3
10^4
10^5
r_w^2/λ_{DO}^2

Figure 60

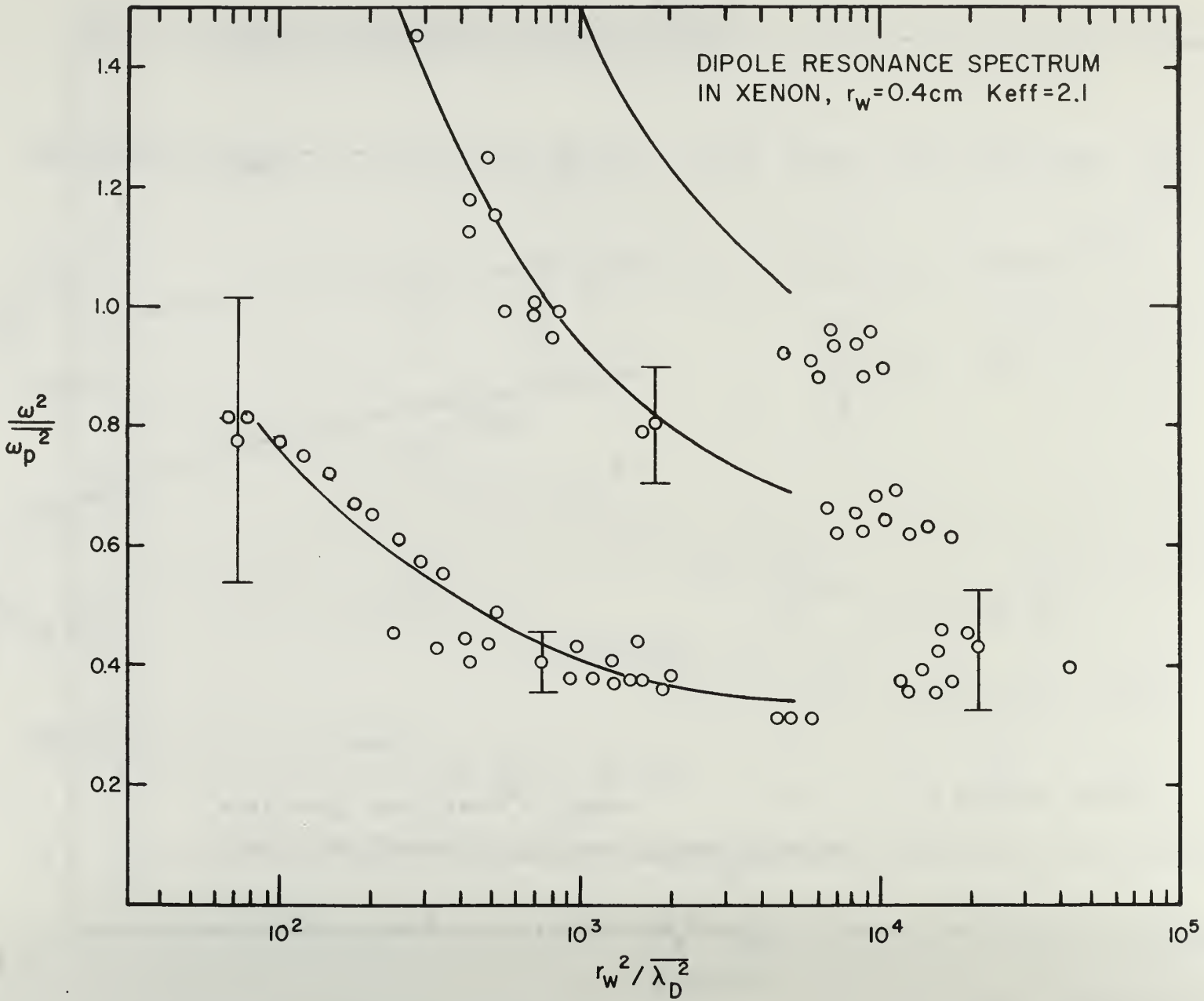
DIPOLE RESONANCE SPECTRUM
IN XENON, r_w=0.4cm Keff=2.1
1.4
1.2
1.0
0.8
0.6
0.4
0.2
$\frac{\omega^2}{\omega_p^2}$
10^2
10^3
10^4
10^5
$r_w^2/\overline{\lambda_D^2}$

Figure 61

For the case in which moving striations have been taken into account, results have been obtained for the case of xenon at 4.3 mTorr and for neon at 27 mTorr pressure. In the case of xenon the resonance measurements were synchronized to four different parts of the striation corresponding to maximum and minimum light intensity and to two points midway between these two. For neon, only resonances at the maximum and minimum of light intensity have been observed. These resonances were obtained by the method described in Section IV. The resonances have been displayed in Figs. 62 and 63. It is seen that the resonances for minimum light intensity occur at lower frequencies than those for maximum light intensity, indicating a lower electron density at minimum light intensity. Within experimental error, the differences in resonance frequencies obtained in the different parts of the moving striations correspond to the differences in densities as determined by probe measurements. It is also noted that the resonances observed at the minimum light intensity were broader than those observed for the crests of the striations. In these resonance curves, it is the frequency which is varied while keeping the discharge tube current constant.

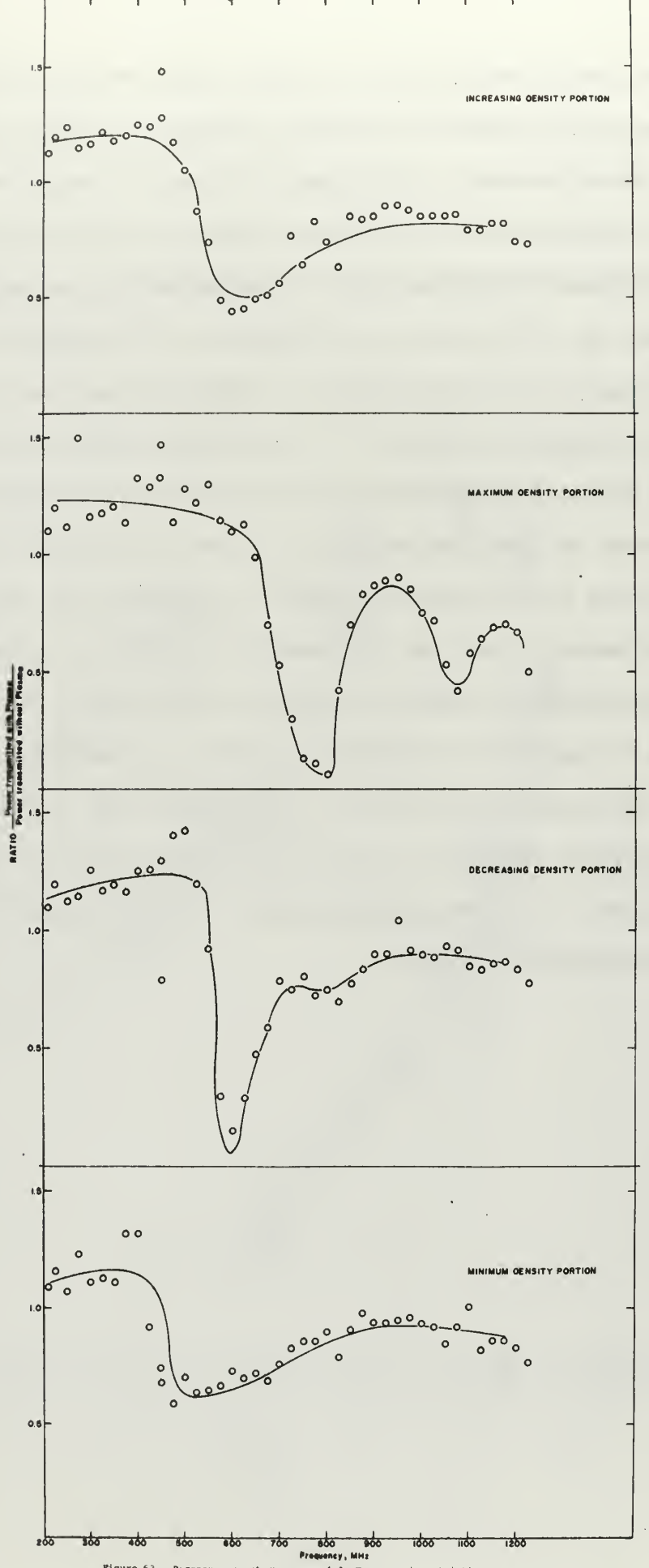

Figure 62. Resonance spectrum, xenon 4.3 mTorr, moving striations present and transmitted signal measurements made in synchronization to moving striation phase

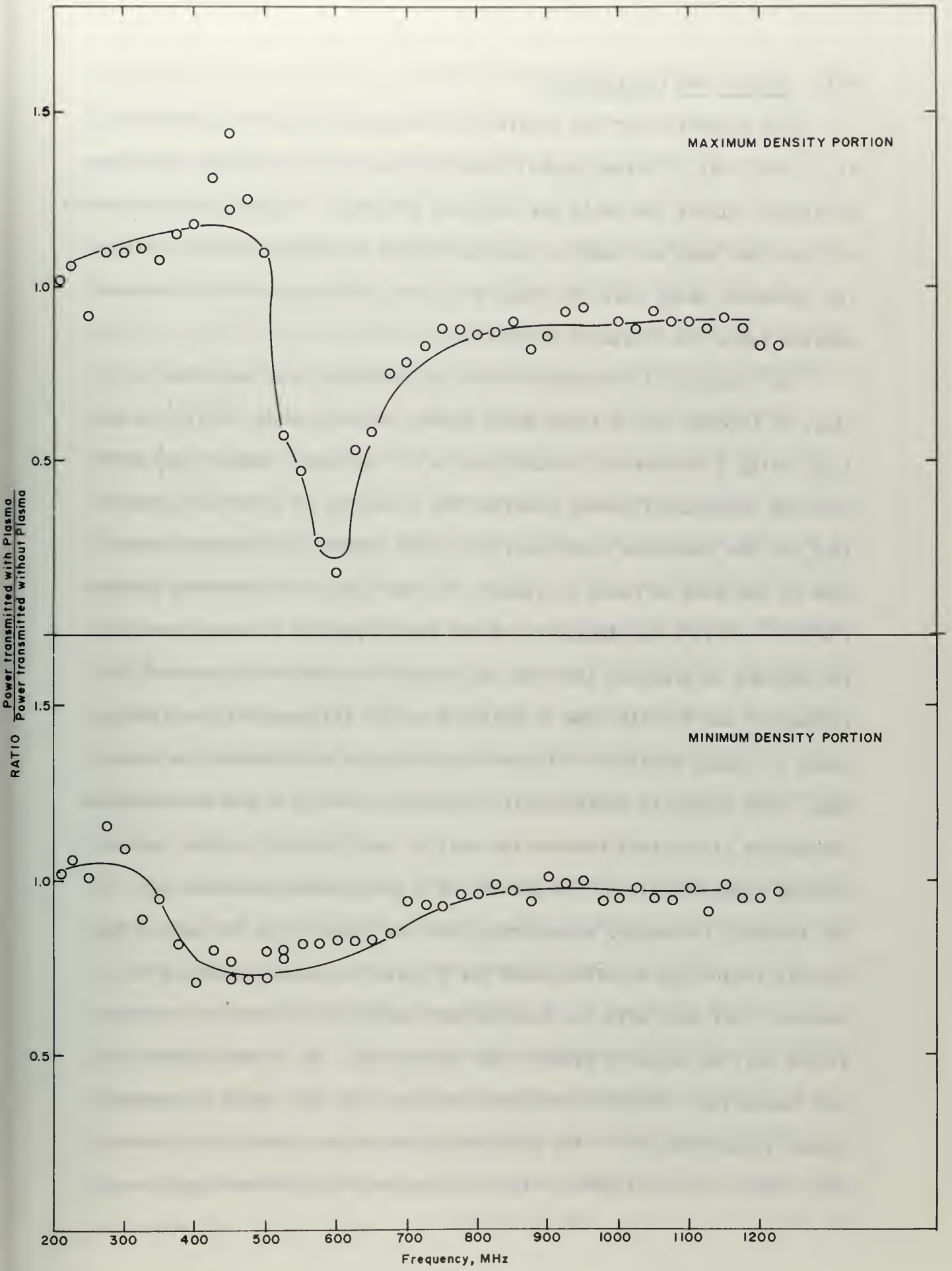

Figure [illegible]. Resonance spectrum, neon, 27 mTorr, moving striations present and transmitted signal measurements synchronized to moving striation phase

VII. SUMMARY AND CONCLUSIONS

Upon inspection of the results for resonances shown in Section VI it is seen that the experimental results agree quite well with the theory of Parker, Nickel and Gould for the case of xenon. However, the resonances in argon and neon are seen to occur at higher frequencies than predicted, the agreement being worse for neon where the resonances occur at approximately twice the frequency predicted.

The theoretical resonance conditions which hav been employed in Figs. 56 through 61 are those which parker, Nickel and Gould [21] calculated using a theoretical radial profile for mercury. Parker [22] gives also the theoretical radial profiles for a variety of other ion species (but not the resonance conditions for these gases); however, the influence of ion mass on these is slight. In the case of low density plasmas ($r_w^2/\lambda_D^2 \cong 10^2$) the departure of the radial profile of neon from that for mercury is greatest (for the ion species studied in the present experiments) and in this case an estimate of the influence of the differences in radial profiles on theoretical resonant frequencies has been made. The region in which density variations occur for the Tonks-Dattner resonances is confined between the wall of the tube and a point corresponding approximately to the cut-off of a longitudinal electron wave (at the resonant frequency) propagating into the plasma from the wall. This cut-off radius can be established for a given resonance occurring in mercury. For neon with the same central density, the density at this radius will be slightly higher than for mercury. If it is assumed that the theoretical resonance frequency for the same mode would be shifted upward proportionally to the increase in the square root of density at this radius, the influence of the ion species on the theoretical resonant

frequency can be estimated. On these assumptions, it is calculated that for the same central density as for mercury the shift in the theoretical ratios of ω^2/ω_p^2 for neon resonances would be increased by about 8% over those in mercury in the worst case, i.e., for $r_w^2/\lambda_D^2 \cong 10^2$. As r_w^2/λ_D^2 increases to larger values the ion mass has increasingly less influence on the theoretical radial profiles and at high values of r_w^2/λ_D^2 ($\geq 10^5$) the difference almost vanishes. Since most of the data taken in the present experiments was obtained for parameters corresponding to r_w^2/λ_D^2 greater than 10^3, and thus was obtained under more advantageous conditions than those discussed, it can be said that the theoretical resonance conditions used are not inappropriate for the gases to which comparison is made, particularly since experimental error in the density measurements is on the order of 15%. This negligible influence of ion mass on the theoretical resonance conditions for higher values of r_w^2/λ_D^2 has also been pointed out by Lustig. [62] In terms of observable parameters, a value of r_w^2/λ_D^2 of 10^3 would correspond to an electron density of about 10^{15} m^{-3} for the 1.56 cm radius tube and nearly all data was taken for values in excess of this amount, i.e., for values of r_w^2/λ_D^2 greater than 10^3.

If the experimental conditions in the positive column were such that the assumptions of the theory for the radial profiles just discussed were not fulfilled, it would not be expected that the true radial profile would match the theoretical profile (regardless of the question of the influence of ion mass). The experimental determinations of the radial profile (as shown in Figs. 37, 38, and 39) are not sufficiently accurate to determine the existence of any deviation from the theoretical profile in the columns studied. However, calculations show that the ion mean free paths for neon in the range of pressures of Fig. 56 are on the order of

one cm which is smaller than the tube radius r_w for the large tube in which the results were obtained. Thus one of the assumptions of the Parker, Nickel and Gould theory is not met. There is about an 80% probability that an ion makes a collision before reaching the tube wall if it is created at the center of the tube. Some additional evidence for ion collisions in neon is that electron temperatures as shown in Fig. 34 are below those predicted by a free-fall theory for which it is assumed that ions drift to the wall without making collisions. Argon does not show any indication of this decreased electron temperature in the pressure range studied (which is about an order of magnitude below the neon pressure range).

It is concluded that the influence of ion collisions may be sufficient to distort the profile from the theoretical to the point that the theoretical resonance conditions do not apply, at least for neon. It should be pointed out here that operating pressures for neon were about an order of magnitude higher than for argon or xenon and unfortunately, the ion mean free paths for neon could not be increased in the experiments because lowering the tube pressure caused the transition to the collapsed discharge in neon. Some additional evidence for the existance of ion collisions in neon is that for successively higher pressures the resonances occur at higher frequencies, indicating a higher density at the wall of the column for the same central density, and as the pressure is lowered the theoretical resonance conditions are more nearly approached. An extrapolation of the data in Fig. 56 indicates that the theoretical resonance conditions are approached at approximately 5 mTorr, a pressure at which operation was not possible in neon, but at which ion mean free paths are on the order of 3 cm, compared to the tube radius of 1.56 cm.

An estimate of the ion mean free paths for the operating conditions of Figs. 57 through 61 for xenon and argon gives on the order of 4.8 cm and 2.8 cm for xenon and argon respectively. Therefore, it can be said that the requirement of long ion free paths is better satisfied for these two gases and the results should more nearly approach the theory. This is borne out in the results, xenon most nearly approaching the theoretical prediction.

In summary, it can be said that the resonance results in the rare gases shown in Figs. 56 through 61 while not precisely confirming the theory of Parker, Nickel and Gould would seem to approach the theory in the limit of long ion mean free paths. In these results, xenon most nearly satisfies this criterion and the agreement with theory is likewise best. To demonstrate this conclusion, the ratios of the observed resonant frequencies squared to resonant frequencies squared predicted by Parker, Nickel and Gould, plotted against the ratios of tube radius r_w to ion mean free path, λ_i are shown in Fig. 64. In the limit of small λ_i the resonances approach the predicted frequencies. All points in Fig. 64 are for a r_w^2/λ_D^2 of about 10^4. Also shown are some points from Nickel's 23 data for mercury for the same value of r_w^2/λ_D^2 .

A conclusion that can be reached concerning the damping of the resonance is that the dominant mechanism in the case of the rare gases studied is the density variation produced by moving striations. This factor alone would seem sufficient to explain the results of Messiaen [35] and of Kojima, et.al. [39] whose results showed fewer and broader resonances in the rare gases in which they observed resonances. The Q of the resonances observed in the maximum density portion of a striation shown in Fig. 62 is about three times greater than that in which striations

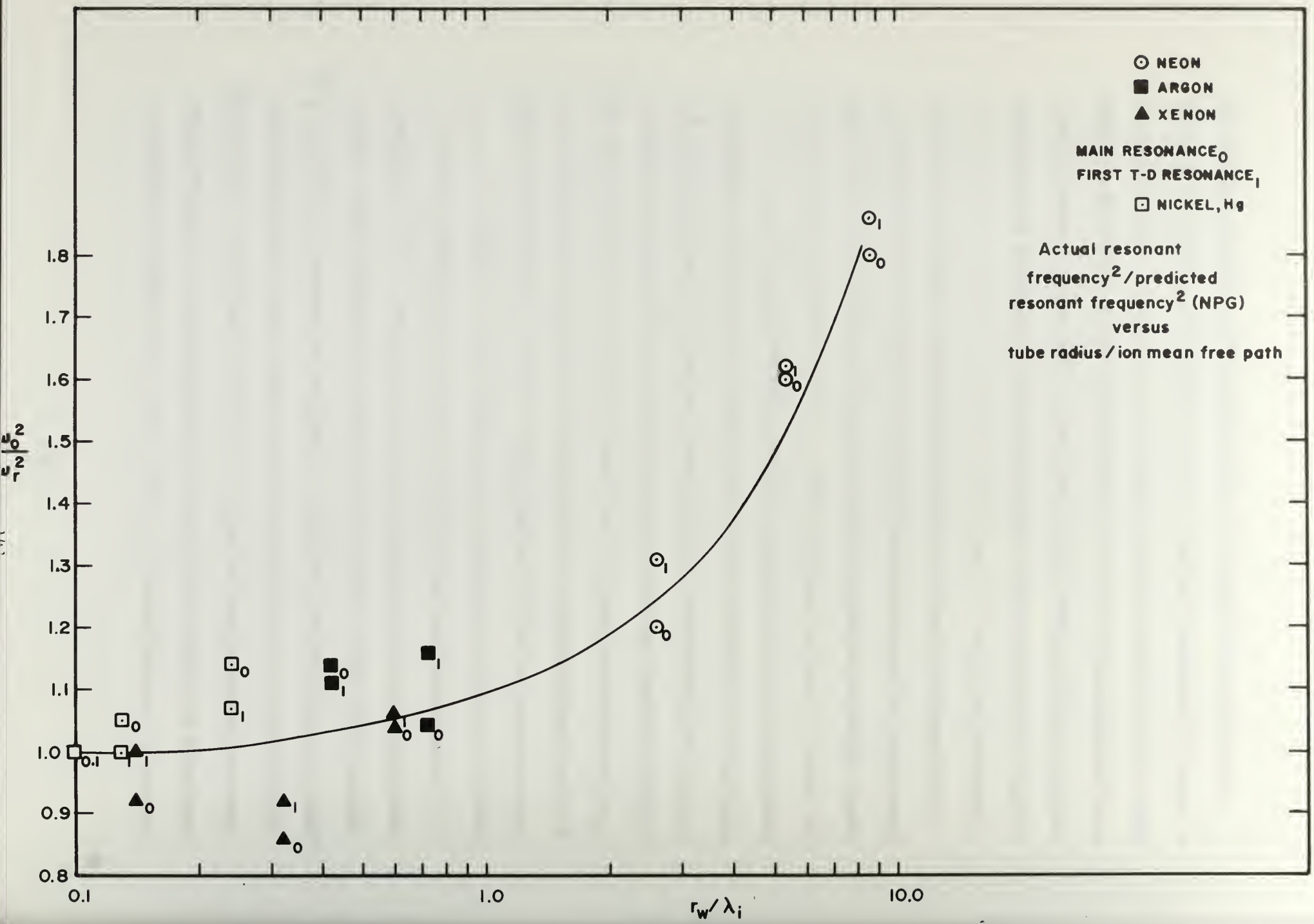
NEON
ARGON
XENON
MAIN RESONANCE$_0$
FIRST T-D RESONANCE$_1$
NICKEL, Hg
Actual resonant frequency^2/predicted resonant frequency^2 (NPG) versus tube radius/ion mean free path
$\frac{\omega_0^2}{\omega_T^2}$
r_w/λ_i
0.8
0.9
1.0
1.1
1.2
1.3
1.4
1.5
1.6
1.7
1.8
0.1
1.0
10.0

are not taken into account (e.g. Fig. 45), the Q being about 6.4 in the first case and about 2.5 in the latter. Q's here are determined from the difference of frequency of the one-half power points of the resonance in one case and by the frequency difference necessary to shift the resonance by the width of the half power points in the other case.

Part of the axial density variation occurring due to moving striations is removed by the technique leading to Fig. 62 since the transmitted rf is sampled only when approximately a quarter of the striation is illuminated by the strip-line field. This reduces the total axial variation of electron density to something on the order of 10% for these resonances, in which case the axial density variation can still be the dominant broadening mechanism. It is believed that the differences in damping between the resonances observed for different parts of the striation can be explained by the way in which the density varies about the part of the striation to which the measurements are synchronized. If the trough of the striation is sharper than the crest, the resonance observed in the trough will be broader than that for the crest, since the axial variation will be greater. That this is actually so is confirmed somewhat by Fig. A6 (Appendix A) which shows a somewhat smaller axial density gradient at the maximum light intensity portion of the striation than at the minimum.

Other mechanisms which would be expected to lead to broadening of the resonances are electron-neutral collisions and Landau damping. Electron-neutral collisions can be expected to broaden the resonances since the coherence of electron oscillations is lost when they are interrupted by a collision. [25] Landau damping [63] is collisionless damping due to the velocity of the electron longitudinal waves being comparable to the

thermal velocities of the electrons supporting the oscillations. If there are more electrons with velocities less than the wave velocity than there are electrons with velocities greater than the wave velocity, particles are trapped by the moving wave with a resultant transfer of energy out of the waves and into the electrons.

If the line widths of Fig. 62 are corrected for the electron-neutral collision frequency, a corrected line width results that is still about an order of magnitude greater than that predicted by Huggins and Raether [64] as resulting from Landau damping. This seems to indicate that there is a damping mechanism operative in Fig. 62 that is in excess of that due to electron-neutral collisions and Landau damping and in fact seems to be due to axial density gradients. A 10% axial variation in the density of Fig. 62 could be responsible for a line width of about 40 MHz alone and this is in excess of the collision frequency.

Number density variations of 10% are not uncommon for mercury discharge tubes [65] so it would be expected that density fluctuations might be the dominant damping mechanism in other experiments performed on the resonances.

These conclusions are important in evaluating the use of the Tonks-Dattner resonances as a diagnostic method. In order to obtain meaningful electron density measurements from the resonances, one must be assured that the theoretical conditions are precisely satisfied. A probe determination of the radial profile is not sufficient in this regard as the region of greatest importance is that near the wall of the column where the probes lose their accuracy due to the disturbance they produce in the fields and due to their finite size. An indication of how near the wall the resonance effects may be confined is given in Fig.

A7 (Appendix A) where the cutoffs of the longitudinal modes have been marked with arrows. In order to predict the resonances accurately, the fields and densities in this region must be known. For such a determination to be made experimentally, the use of finely collimated electron beams seems indicated.

It appears that the situation is one in which knowledge of the sheath or of the gross plasma density profile alone is not sufficient, but rather one needs to know also how the fields vary in the transition region. In the range of long ion mean free path, the theoretical profile of Parker seems to fulfill this requirement but as ion collisions become important the "free fall theory" is no longer adequate. The requirement of long ion mean free paths becomes more severe as the diameter of the column increases and some earlier attempts to verify theories experimentally in mercury may have suffered from the existance of collisions of ions near the wall, especially in large diameter tubes.

In this connection, the use of the variable $\omega^2/\overline{\omega_p^2}$ is somewhat misleading. While the electron density at the wall may be higher than predicted by the theoretical profile of Parker [22] due to collisions and thus may cause higher frequency resonances, the average plasma frequency is also higher and the errors tend to cancel. If the central density is used as in the case of Figs. 56 through 60, the effect of collisions is more readily recognized.

In order for any experimental determinations of the damping of the resonances to be meaningful, a means must be found to eliminate the effects of low frequency density variations. The plasma electron density varies through an ion oscillations cycle and conditions may also exist under which ion oscillations affect the amplitude of electron oscilla-

tions, besides altering the electron plasma frequency itself. [66] This indicates that suppression of the ion oscillations (moving striations) is desirable. The region of transition between positive and negative striations as mentioned in Appendix A is not sufficient for this purpose as the axial extent of this region is not large enough for resonance measurements to be made over what must be an axially uniform column. Suppression of moving striations has been accomplished in the vicinity of the Pupp limit by eliminating feedback paths with local cavity excited discharges in the Torr range of pressures but such a procedure may not be feasible at low pressures.

VIII. RECOMMENDATIONS FOR FUTURE WORK

1. A thorough experimental investigation of the unified probe theories of several workers [49,50,51,52] is suggested. Comparison with independent means of measuring electron densities would be desirable.

2. An experimental measurement of the radial profile of electron density in the vicinity of the wall should be made. A finely collimated electron beam might be employed since the disturbing influence of a Langmuir probe is too great in this region.

3. The theoretical influence of non-free-fall conditions on the radial profile of electron density seems indicated. For experimental utility, such a treatment should include a wide range of Debye lengths.

4. Using experimentally derived radial profiles or theoretical profiles which take into account non-free-fall conditions, the theoretical Tonks-Dattner resonance conditions should be derived and compared with experiment.

5. A means of eliminating moving striations from a low pressure rare gas discharge should be sought. Such a procedure seems mandatory before any quantitative measurements on the damping of the Tonks-Dattner resonances can be made.

APPENDIX A

MOVING STRIATION STUDIES

Low frequency noise is a well known phenomenon present in low pressure (1 - 50 mTorr) gas discharges and has been reported by many experimenters. However, the occurrence of moving striations in these discharges has been reported only recently [67] although their occurrence in the torr range of pressures has long been known. At the outset of the present work it was not suspected that moving striations were present in these columns but in a search for the cause of the broadening of the resonances observed in the x-y recorder data, it was discovered that at certain currents and pressures coherent oscillating signals could be detected in the floating potentials of probes inserted into the plasma. Subsequently, use of a photomultiplier tube showed that a variation in light intensity accompanied these oscillations and the light intensity variations were propagating along the tube through the positive column.

One of the first features of the moving striations which was noted was that the currents at which the striations were regular in time varied radically from one pressure to another. At a given pressure, if the current were altered, the striations often became incoherent so that accurate measurement of their velocity became impossible even though it appeared that the incoherent variations were propagating through the column. This could be observed by triggering the oscilloscope beam using the probe floating potential and observing the movement of the corresponding variations in light intensity as the photomultiplier was moved away from the probe position. Even in the case where the noise was very great, the amplitudes of the probe floating potential and light intensity variations were about the same as when the striations were coherent and phase shift

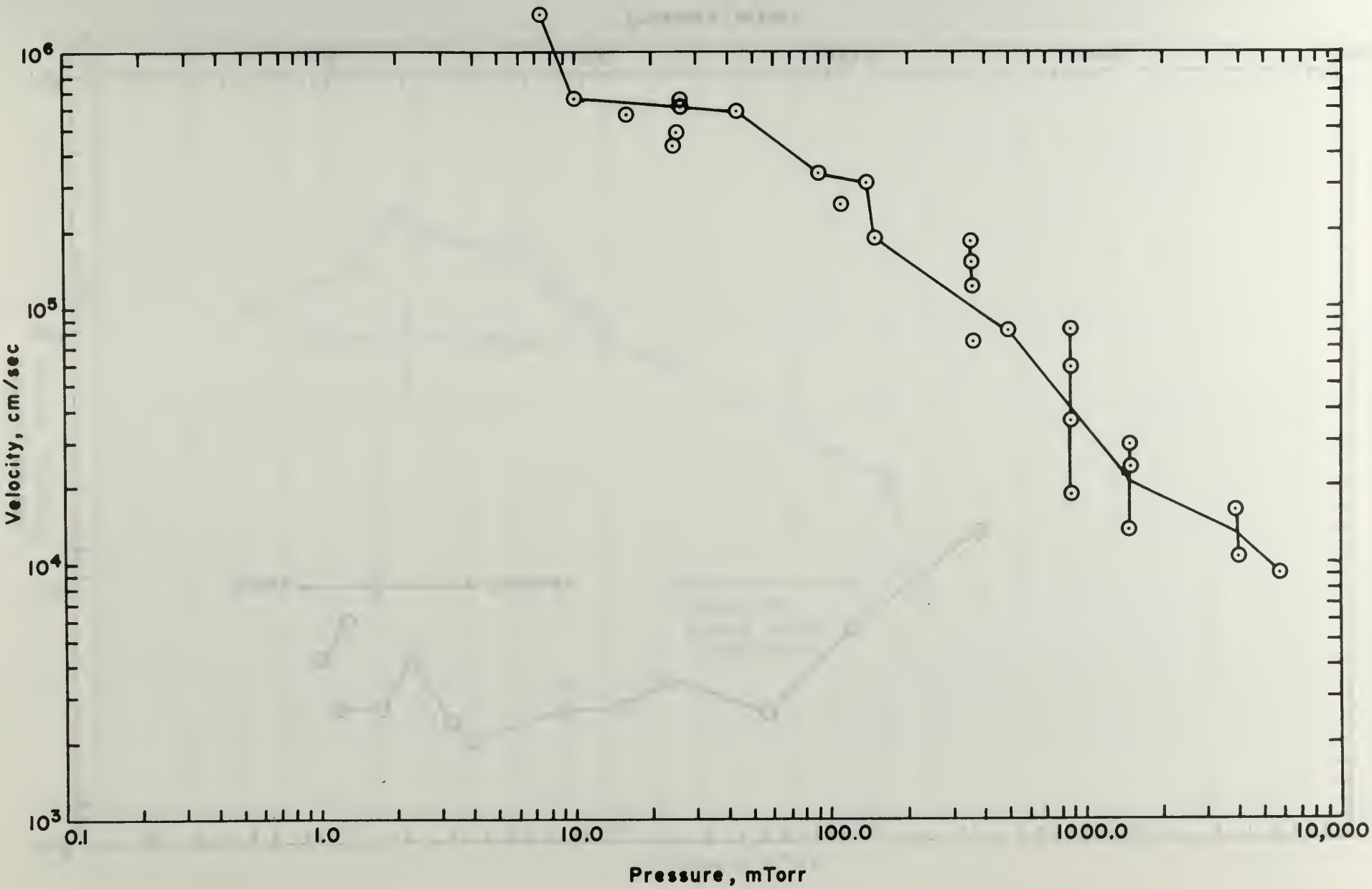

Figure A-1

Moving striation velocity in neon as a function of pressure, 3.5-cm OD tube

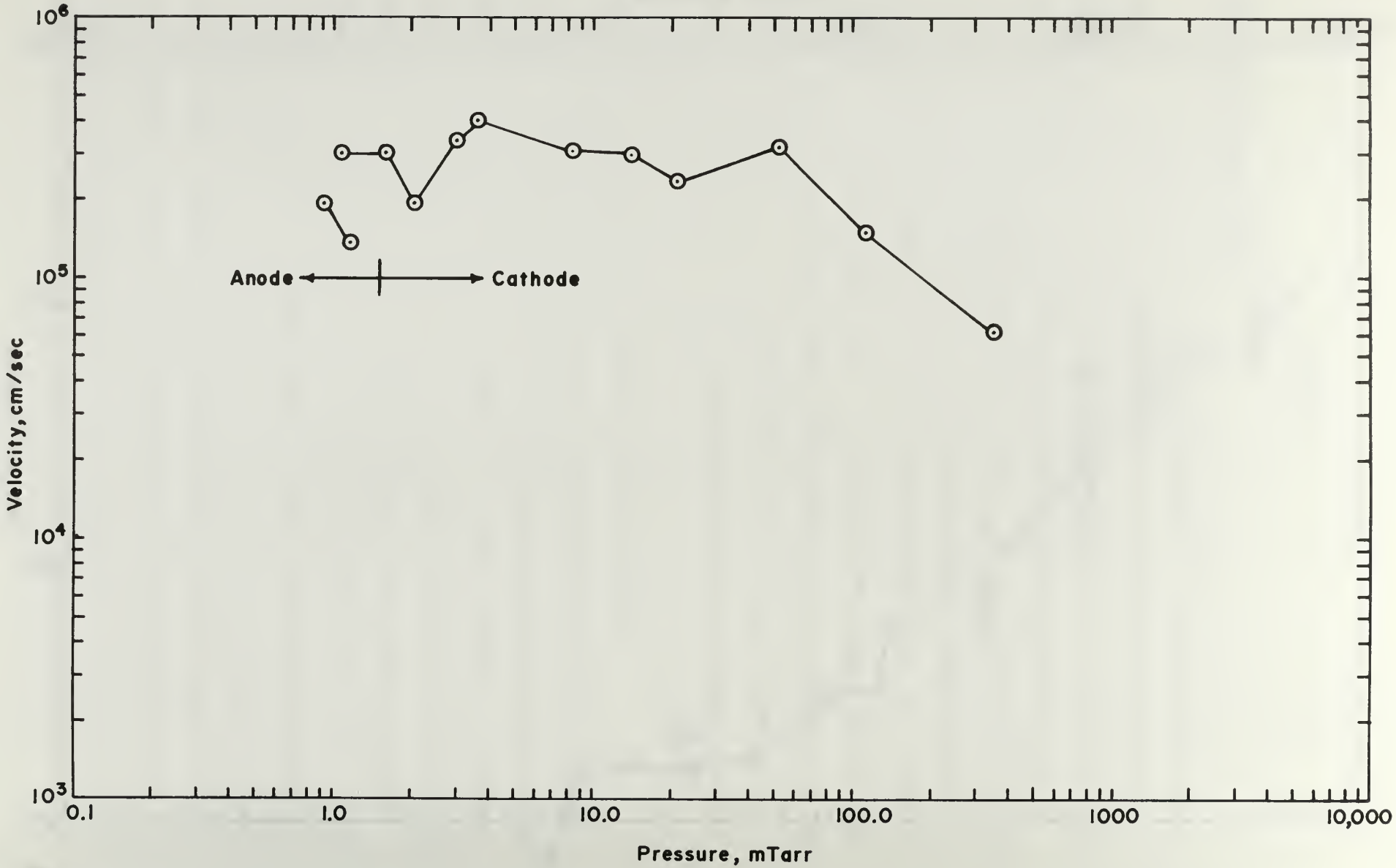
Velocity, cm/sec
10^6
10^5
10^4
10^3
Anode
Cathode
0.1
1.0
10.0
100.0
1000
10,000
Pressure, mTarr

Figure A-2

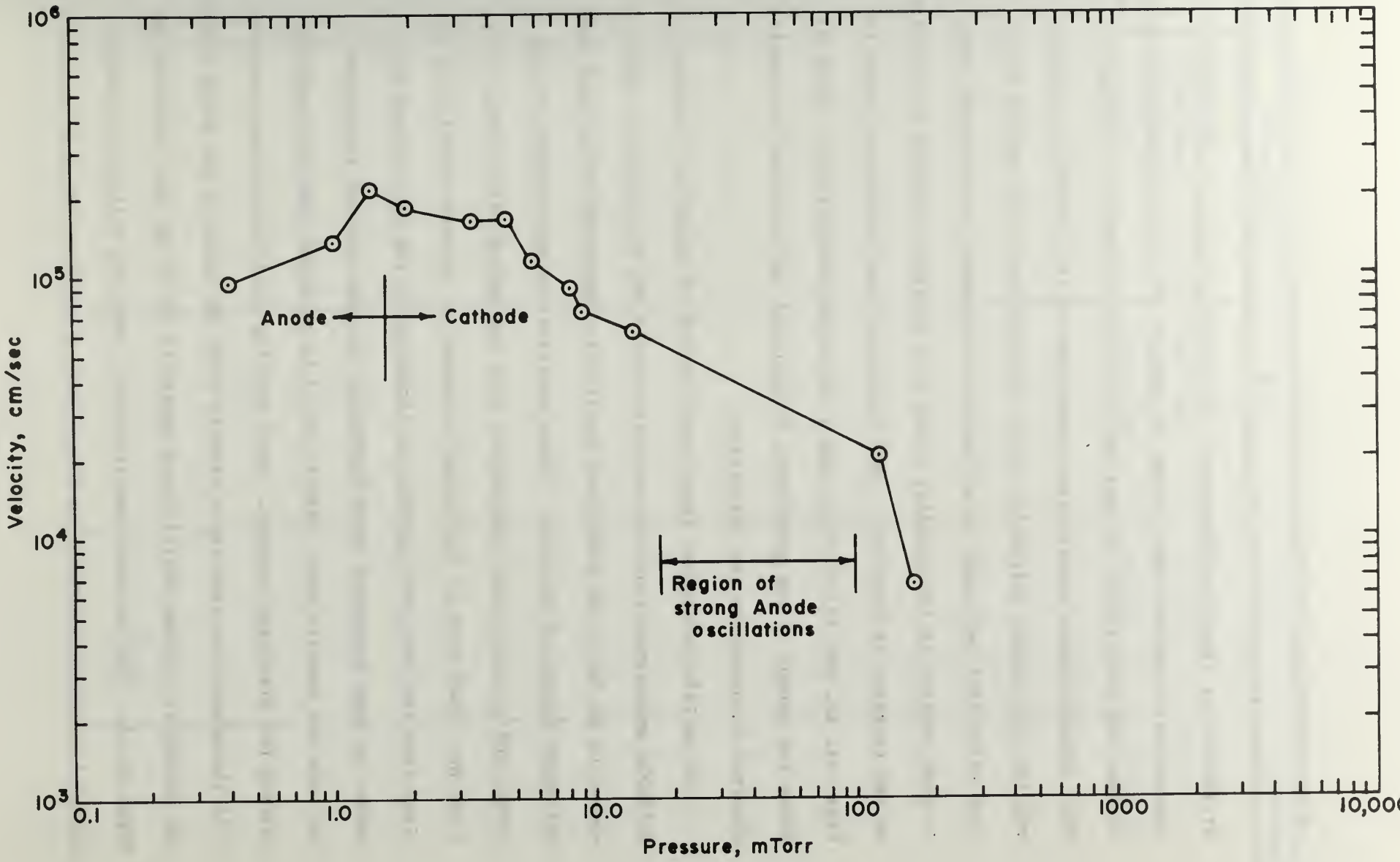

Figure A·3

Moving striation velocity in xenon as a function of pressure, 3.5 cm OD tube

of corresponding disturbances indicated movement.

There is a great deal of scatter in velocity data taken on moving striations at these low pressures. For a given pressure and current, the striation velocity may change as much as 20% from one observation to another and even larger changes may occur if the current is altered. This behavior makes quantitative comparison of the results on velocity studies with theory difficult. Many observations of the moving striation velocities were made as a function of pressure and although there is wide scatter in the results, there is a distinct increase in velocity as the pressure is decreased. The results of the studies are shown in Figs. A1, A2, and A3 for neon, argon and xenon respectively. Table A1 shows the ranges of the pressures, frequencies and wavelengths actually observed in obtaining the velocities.

At certain pressures, there were regions of operation for which reliable measurements on the velocities could not be obtained. This seemed to be due to an additional oscillation mechanism associated with the anode region of the tube. These oscillations were random in frequency and at much lower frequencies than the moving striations, i.e., $< 10^2$ Hz. They were at low enough frequency to be seen visually in the light from the tube and appeared as darkening in the glow around the anode. At some pressures these darkening regions extended throughout the tube but usually their effects could be confined near the anode by raising the discharge current. Even when the oscillations were not visible throughout the tube their effects could be noted in the probe floating potential. These oscillations appear to be of the type reported by Pupp, et.al., [68] as anode oscillations. They are believed to result from a buildup of positive ion concentration at the anode which causes

GAS	Pressure mTorr	T_e ev	ν kHz	Wavelength cm
Xe	~0.4 < 165	~5.7 > 1.5	6.6 < 216	7 < 18
Ar	.93 < 350	8.5 > ~1.5	9 < 25	11 < 18.1
Ne	7.1 < 5780	3.8 >	1 < 72	6.5 < 20
Xe small tube	5 < 100	3.7 > ~1.5	4 < 40	2.9 < 10.6

Table A-1

ions to move away from the anode under the influence of the longitudinal field. Electrons will now be accelerated into the anode drop resulting in increased ion production. The ion concentration builds up again and the cycle repeats periodically.

An attempt was made during the course of this work to eliminate these oscillations by the use of a special anode first used by Pupp. The anode consisted of a flat tungsten spiral in the center and located near the front face of a tantalum cylindrical shell. Pupp and others have reported reduction of the effects of the anode oscillations when an auxiliary discharge was run between the spiral and the shell in the Torr range of pressures. At the low pressures encountered in the work reported here, however, this method was found to be completely unsatisfactory in eliminating the anode oscillations. Due to the long mean free paths at these pressures, only a small current could be drawn between the tungsten spiral and the outer tantalum cylinder of the Pupp anode. At voltages up to 1 kv, only a few milliamperes were obtained between the tungsten spiral and the tantalum cylinder even when operating the spiral as a hot filament. (The spiral was operated at bright red heat in this case. Possibly higher temperatures would have increased the emission, however, at the temperatures used, tungsten was evaporated onto the wall of the discharge tube darkening the glass.) An attempt was made to increase the current by placing the anode assembly in a longitudinal magnetic field but for fields up to 250 gauss the current was increased by only 20% and no significant effect was produced on the anode oscillations. It had been thought that a magnetic field would trap some electrons and allow more ionization between the spiral and the shell. At present, no successful method has been devised which will eliminate these anode

oscillations which are especially troublesome in argon and xenon at pressures around 10 mTorr.

Moving striations were also noted in xenon in the smaller discharge tube, although with somewhat smaller amplitudes than in the larger tube. Velocity data has been obtained for this tube and is shown in Fig. A4. The average wavelength of striations in the smaller tube was significantly smaller than for the large tube, viz., 5.5 cm (compared to about 14 cm in the larger tube). The velocity data is in fair agreement with that for the larger tube shown in Fig. A3.

The velocity data shown in Figs. A1, A2, A3, and A4 are in fair agreement with results published by Alexeff and Jones, [67] and most of the details of the observations are consistent with those reported by these workers who attempt to make connection between the self-excited moving striations of a rare gas discharge and ion acoustic waves. The theory of ion acoustic waves is modified to include the effects of ion-neutral collisions. Over a range of from a few mTorr to several Torr, quantitative agreement is found between the ionic sound wave velocities predicted by the theory and the experimentally observed velocities of moving striations. Experimentally, the strong damping predicted by the theory is not observed.

The velocity of an ion acoustic wave can be shown from a simple theoretical treatment to be

$$V = \sqrt{\frac{\gamma k T_e}{m_i}} \qquad \text{(A·1)}$$

where γ is a constant dependent on the type of compression, T_e is the electron temperature, and m_i is the ion mass. This infers that should the electron temperature dependence be removed from velocity measure-

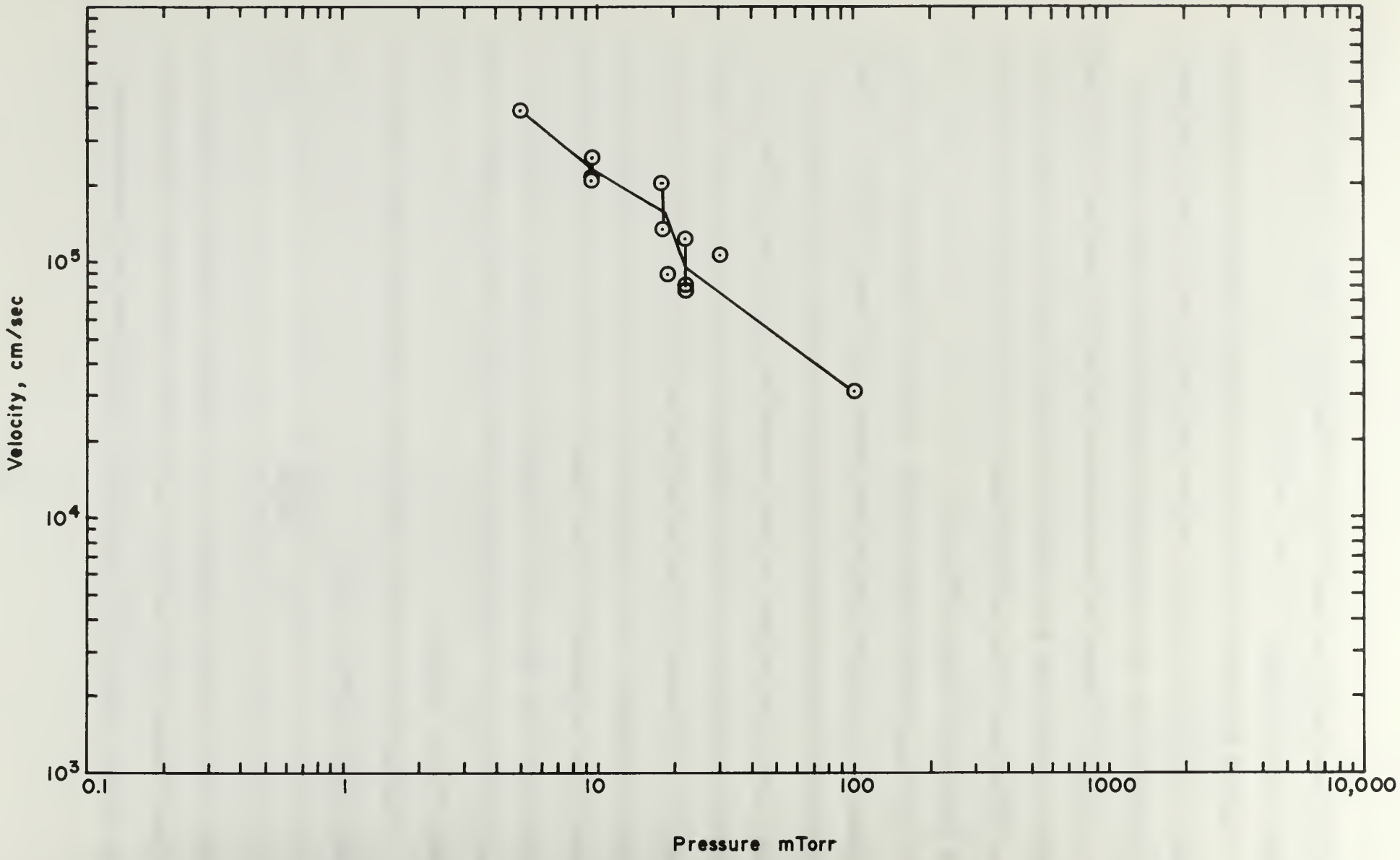

Figure A.4

Moving striation velocity in xenon as a function of pressure, 1.0 cm OD tube

ments, the velocity should vary as $\sqrt{\frac{1}{m_i}}$. In Fig. A5 are plotted the experimental velocities observed for the data in Figs. A1, A2, and A3 multiplied by $T_e^{-\frac{1}{2}}$. The solid lines are the velocities predicted by Eq. (A.1) for various values of γ . While there is still considerable spread in the results, there does seem to be a decrease in velocity with increasing mass. Furthermore, the spread of velocity measurements is considerably reduced when the electron temperature dependence is removed. The values of γ shown in Fig. A5 are those appropriate for adiabatic compression. The value $\gamma = 1$ applies for collisionless electrons and ions while the values of 5/3 and 3 are appropriate when collisions are sufficiently frequent compared to the time scale of the oscillations that the electrons and ions undergo one or three dimensional compression.

It should be emphasized that the agreement shown in Fig. 50 and in the results of Alexeff and Jones does not preclude the possibility of some completely different mechanism for the production of striations than ion acoustic waves. In particular, the theory of Pekárek and Krejčí [69,70] has been very successful in accounting for most properties of moving striations in the vicinity of the Pupp limit at higher pressures where ion-acoustic waves would suffer strong collisional damping.

Some remarks can be made on the observations made on negative striations, that is, striations moving from cathode to anode. These striations have been observed in the present work in argon and xenon, but none were observed for neon at pressures down to 7.6 mTorr. In the discharge tubes used in the present investigation the current was always space charge limited rather than emission limited. Emission limited operation causes an increase in the voltage drop across the tube and the cathode coating is sputtered away. Alexeff and Jones report that negative

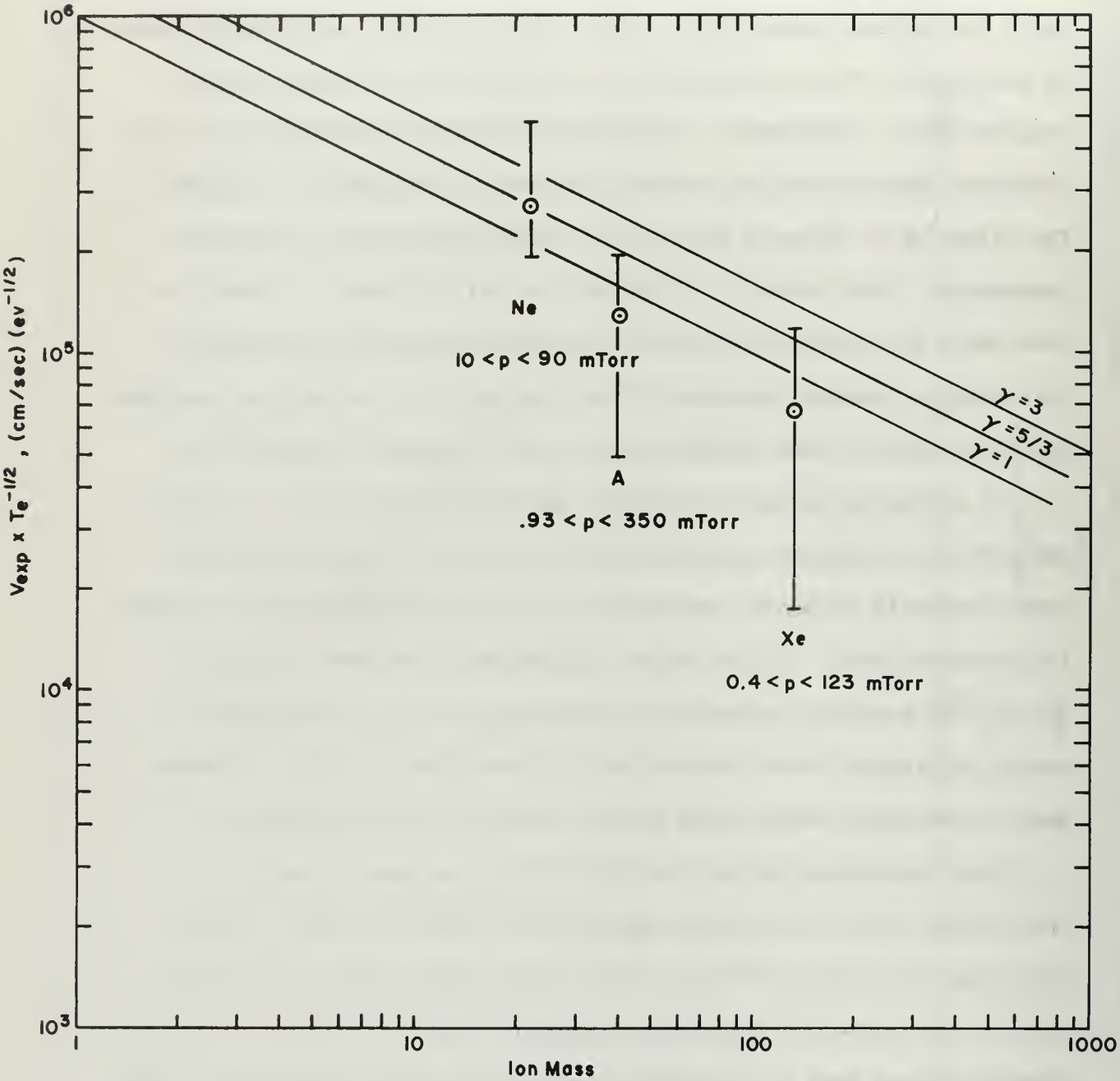

Figure A.5

Moving striation velocities versus ionic mass

striations could be produced at will by changing from the first of these conditions to the latter. It is possible that if emission limited current operation had been possible, the negative striations would have been seen in neon, and that the transition regions for xenon and argon would have agreed better with those reported by Alexeff and Jones.

In one case in argon both positive and negative striations were observed at the same time in different parts of the tube. At a pressure of 2.1 mTorr and 60 ma discharge current positive striations were noted between the anode and a point about 17 cm in front of the cathode. From that point to the cathode, the striations propagated in the opposite direction. At the boundary, the light intensity passed through a distinct minimum. This is an alternative to a vanishing velocity at the discontinuity between the two types of striations. (If the striations change directions, having a large velocity in one direction for some conditions and then having a large velocity in the opposite direction, somewhere in the itermediate region either the velocity must vanish or the amplitude of the variations must vanish.)

In one case at one mTorr in xenon, anode directed (negative) striations were detected between the cathode and the probe. Beyond the probe the light intensity varied with time but the variations did not propagate. The phase of the light intensity variations between the probe and the anode was the same as the moving striation phase at the probe. When the probe was withdrawn until only about one mm extended into the plasma, the moving striations propagated (at the same velocity) all the way to the anode. From these observations it appears that the velocity can become effectively infinite at and beyond some point in the discharge.

In one experiment the harmonics of the fundamental moving striation frequency have been detected by means of a lock-in-amplifier. From the

fact that the waveform of light intensity variations changes very little along the tube axis it is suspected that harmonics of the fundamental travel at the same velocity as the fundamental and thus the waveform, even if not sinusoidal, is preserved. This was confirmed within the accuracy of the equipment by the phase-sensitive detection of the higher frequency components. Table A2 shows frequency and wavelength data recorded for a moving striation in xenon at 19 mTorr. Actually, the observation of the waveform of moving striations probably provides a better test for the constant velocity of propagation than the phase-sensitive detection, since it is estimated that a 1% variation in the velocities of the harmonics could probably be seen in a change in the waveform from one end of the column to the other (unless the harmonic content were very small). It is possible that self-excited standing waves may also occur in the column as reported for mercury by Hirose, et. al., [71]; however, these were not investigated.

Some other observations can be reported concerning the studies on the striation properties. At low pressures in argon, there can occur regions of greatly differing light variation amplitude for anode directed striations. The signal near the cathode passes through a maximum in front of the cathode and may diminish to about a third of this amplitude near the anode.

In general, it can be said that at low pressures the moving striations are much more coherent near the cathode than near the anode. This seems to be primarily due to the anode oscillations discussed earlier.

There are certainly many questions remaining concerning the nature of moving striations at low pressures and no completely satisfactory theory presently exists which explains all their features. In particular,

Xenon Pressure	ν kHz	Wavelength	Velocity cm/sec	
19×10^{-3} Torr	22.5	4.1	9.0×10^{4}	
19×10^{-3} Torr	46	1.9	8.8×10^{4}	
19×10^{-3} Torr	70	1.2	8.4×10^{4}	

Table A.2

the modified ion acoustic wave theory still leaves unanswered the question of why the observed damping is not as great as predicted by theory in the region of a few tenths of a Torr.

In connection with measurements of the Tonks-Dattner resonances in different parts of the striation it was desirable to know how the plasma parameters varied from one part of the striation to another. A study was made of density and temperature variations through a moving striation in neon at 15 mTorr. The results of probe measurements and light intensity measurements are shown for this case in Fig. A6.

Although the accuracy of the data do not allow exact determination of the phase relation of the various parameters, it appears that the electron temperature maximum, particle density maximum and light intensity maximum are very nearly in phase, in constrast to the situation at higher pressures. [72] The total variation in electron temperature is slight and is only about 25% of the average. Density variations are larger and represent about 30% variation about the average. Light intensity variations are typically 2 to 5% of the average. It is usually assumed that small changes in light intensity are proportional to changes in electron temperature but this assumption does not seem to hold for the low pressure moving striations.

The radial profile of ion density has also been determined for one case of moving striations in xenon. Only the maximum and minimum density profiles were taken, it having been ascertained that these were in phase across the diameter of the tube in the presence of moving striations. The result is shown in Fig. A7 wherein the profiles have been normalized to the density on the axis. Also shown is the theoretical profile from the theory of Parker 22 discussed in Section II. It is

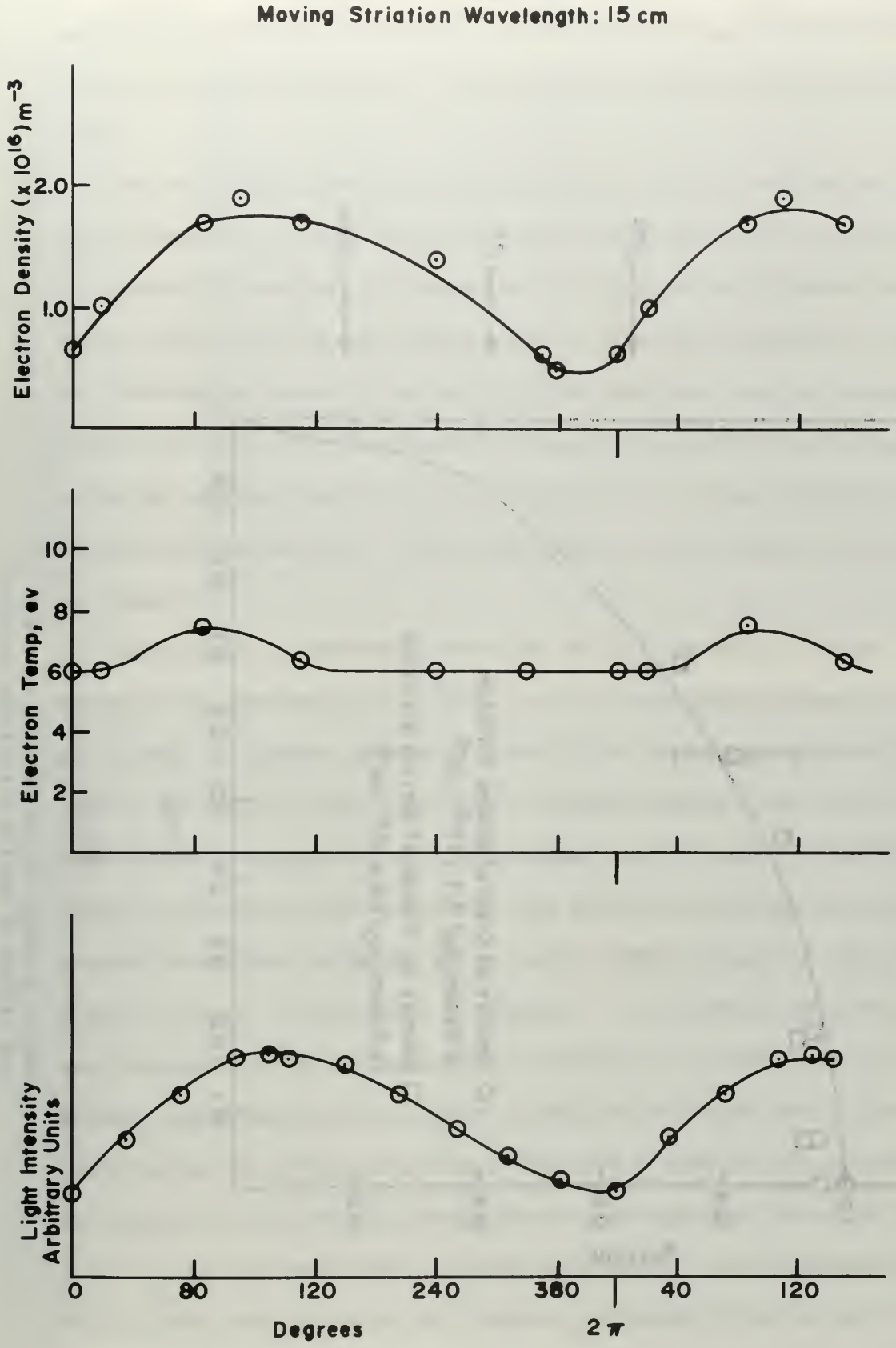

Figure A-6

Variation of plasma parameters through moving striations in neon, 15 mTorr, 235 ma discharge current

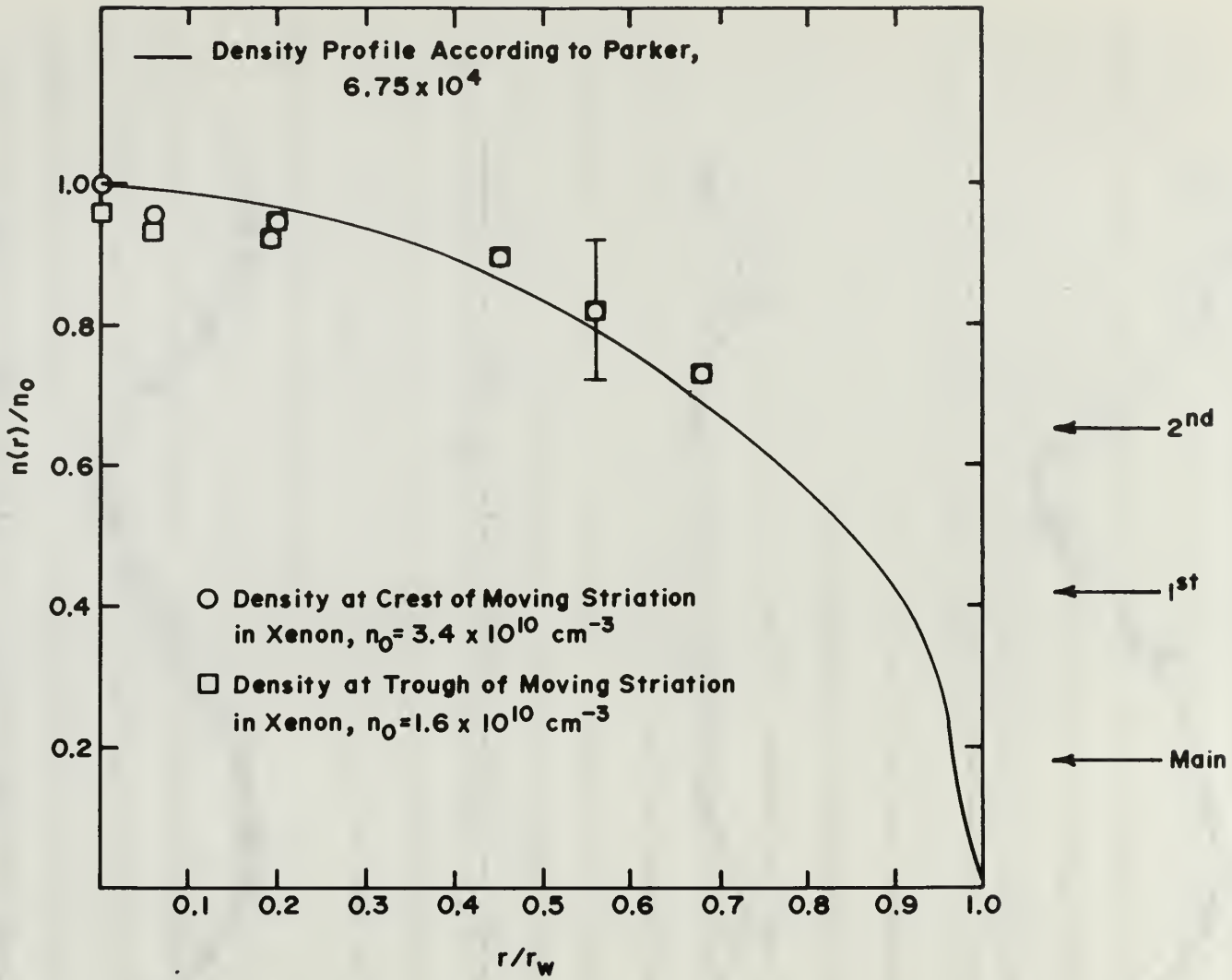

Figure A-7

Radial profile of ion density at crest and trough of moving striations in xenon

noted that the probe measurements could only be taken to within 0.7 r_w, a fact that is of importance in discussing the resonance results (Section VII).

The striking difference in the character of the Tonks-Dattner resonances observed in different parts of the striation (which was discussed in Section VI) prompted an investigation of plasma oscillations in different parts of the moving striations. It had been reported that there was evidence of strong plasma oscillations near the crest of moving striations. [73] This suggested that some feature of the spontaneously occurring electron oscillations present in the discharge might account for the differences noted above, (though later work suggested a different cause).

Accordingly a receiver system was set up to detect rf noise. The receiver was composed of a TS-403, 1.8 to 4 GHz, signal generator acting as a local oscillator; a General Radio 874-MR mixer and a General Radio 1216-A, 30 MHz i.f. amplifier with a 0.5 MHz bandwidth and 2 microvolt sensitivity. An experimental check showed that a signal of -62 dbm could be detected on the receiver. The plasma frequencies of the plasmas used here were estimated to be around 2 GHz so that the receiver would cover the range of the plasma frequencies. Video output from the receiver was displayed on the oscilloscope. In addition a photomultiplier tube movable along the column provided an input to the oscilloscope indicating the presence of moving striations. When the strip-line was connected to the input of the receiver, no signal could be detected above the noise level of the receiver at any pressure or current. This investigation was made to determine if there was a dipole radiation of the column in the vicinity of the plasma frequency. The input of the receiver was then

connected (through a capacitor) to the Langmuir probe which was 40 cm from the anode. With a neon pressure of 30 mTorr and a current of about 250 ma, moving striations were observed in the anode to cathode direction with a frequency of 40 kHz and wavelength of 12.5 cm. Under these conditions and with no external microwave source present, microwave signals were observed on the receiver with maxima occurring repetitively at the moving striation frequency. Figure A8 shows an oscillogram of the video output at the location of the probe. It is observed that the microwave signal maximum is not related to the phase of the moving striation at the probe. Rather it appears to originate at the anode and to be associated with an electron density maximum at the anode. This was determined by the fact that the microwave noise could also be picked up on an external probe placed close to the surface of the plasma column outside the glass. There was no phase change of the microwave signal maxima with respect to the light intensity variations observed at a fixed point indicating that the microwave signal is given off in bursts at the moving striation frequency but does not originate in the moving striation nearest the probe. The external probe consisted of a 2 cm, thin wire connected to the center conductor of a 50 ohm coaxial cable across the end of which a 50 ohm resistance was connected.

By placing the external probe and the photomultiplier tube at the anode where the microwave signal was most intense, it was confirmed that the microwave signal maximum coincided exactly with the light intensity maximum at the anode. Thus it appears that the microwave signal is greatest when the electron density maximum associated with the moving striation occurs at the anode. Since the microwave signal is actually most intense in the region a few mm beyond the anode in the glow which surrounds the

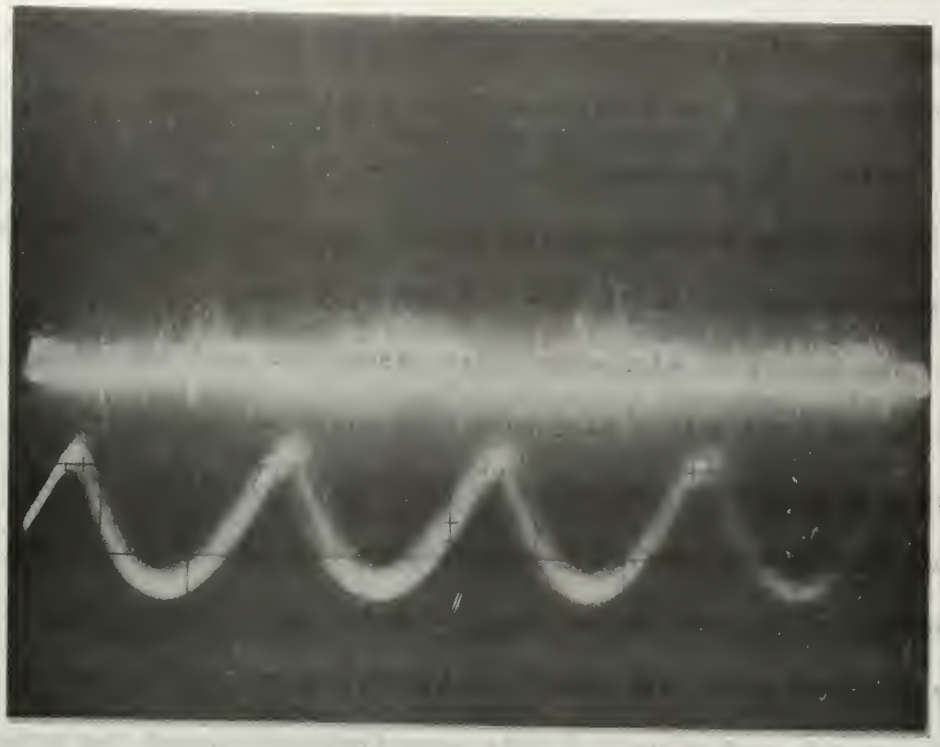

Upper Trace: Video output from i.f. amplifier terminals
Lower Trace: Signal from photomultiplier tube

Pressure: 25 mTorr; Discharge tube current: 360 ma
Local Oscillator Frequency: 3570 MHz
Moving Striation Frequency: 40 KHz
Moving Striation Wavelength: 12.2 cm
Horizontal scale: 10 sec/cm

Figure A8

Oscillogram of video output of microwave receiver with input from a Langmuir probe in a neon plasma

anode at this pressure, the origin of the microwave signal may be a two-stream instability caused by the electrons drifting past the anode and interacting with the electrons being accelerated back in the direction of the anode. The maximum signal received on the external probe was about 20 db above the minimum sensitivity of the receiver and covered a frequency range of at least from 1.8 GHz to 4 GHz.

The bursts of microwave noise associated with the striations could not be detected with a microwave horn aimed at the anode. An attempt was also made to detect the noise by placing a cylindrical cavity around the anode region with the tube axis through the cavity axis. The cavity was resonant at 2.4 GHz in the TM_{010} mode but when the cavity was coupled to the receiver which was tuned to this frequency, no signal was detected. Noise had been detected at this same frequency using the external pick-up probe. These results would seem to indicate that the oscillations were not of a type which couples efficiently to a free space mode.

The application of a magnetic field along the axial direction reduces the amplitude of the microwave signal picked up on the external probe. Figure A9a shows the variation in maximum height of video peaks shown on the receiver output as a function of the magnetic field at the anode. The probe was located in the plane of the field coil just external to the tube at the anode and remained fixed as the field was varied. As the field was increased the intensity of the glow at the anode was decreased. Figure A9b shows the variation of noise intensity with magnetic field with the coil and the external probe 21 cm from the anode. This plot (Fig. A9b) is magnified by a factor of 6.3 compared to the scale of Fig. A9a, and the maximum noise at 21 cm from the anode is down by a factor of about 5 compared to that at the anode. The signal is

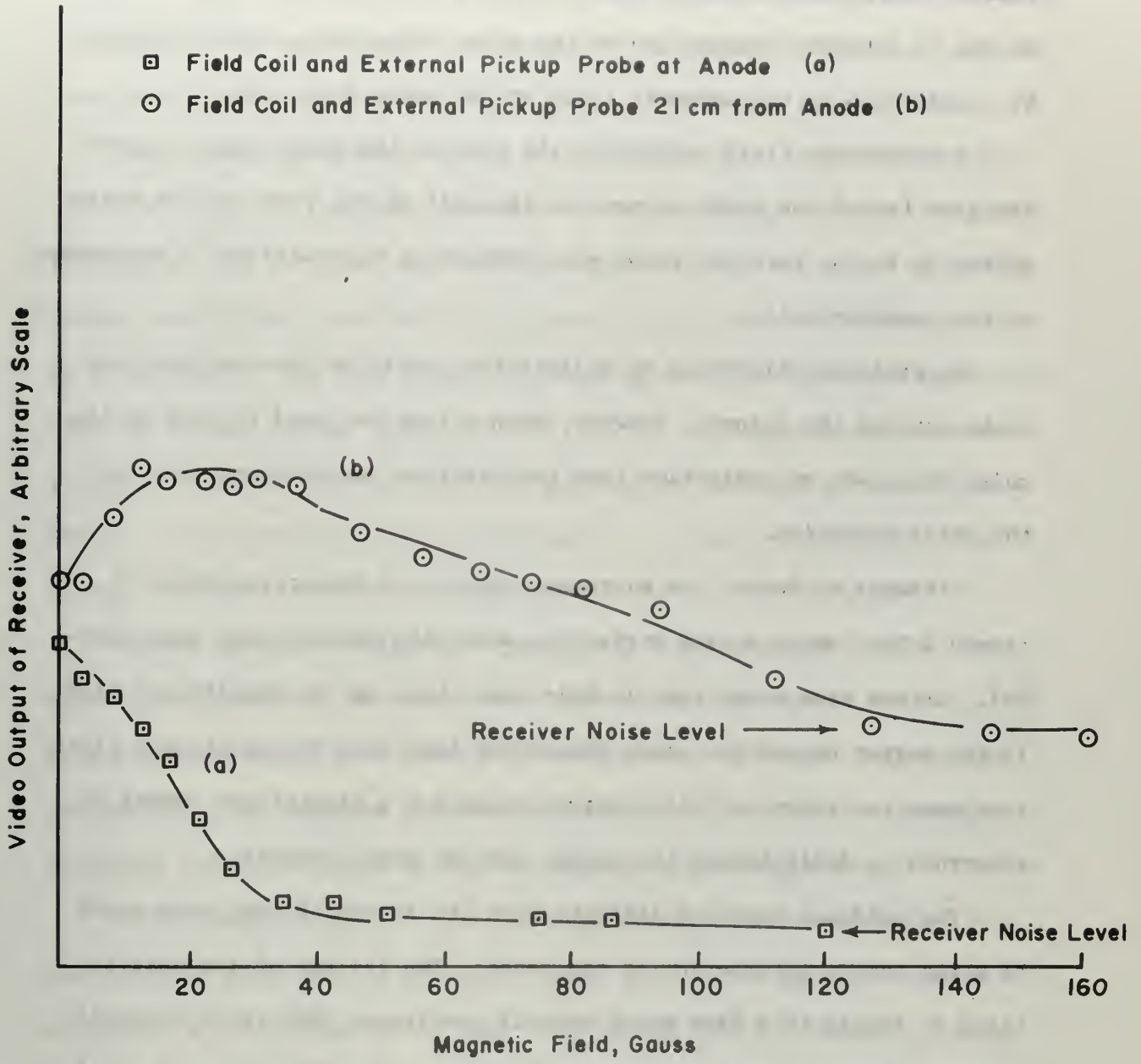

Figure A.9

Variation of microwave noise with an applied axial magnetic field

reduced to the minimum detectable with a magnetic field of about 120 gauss. There seems to be a slight maximum at about 30 gauss, which may be due to enhanced propagation of the noise along the column, followed by a reduction as the magnetic field at the anode increases.

A transverse field applied to the tube at the anode region caused the glow beyond the anode to move to the wall of the tube and the noise picked up by the external probe was enhanced at that wall while decreasing at the opposite wall.

No preferred direction of polarization could be detected with the probe outside the column. However, when a loop was used to pick up the noise there was an indication that polarization was preferentially in the axial direction.

Attempts to detect the microwave signals at higher pressures of around 1 Torr where moving striations were also present were unsuccessful. It was also noted that in this case there was no significant glow in the region beyond the anode suggesting that mean free paths for electrons were too short in this pressure range for a significant number of electrons to drift beyond the anode, even at high currents.

The evidence seems to indicate that the source of the noise could be a two-stream interaction at the anode. The failure of the oscillations to couple to a free space mode is consistent with their identification as longitudinal electron oscillations. The effect of the axial magnetic field would appear to be to focus the electron stream and cause the number streaming past the anode to decrease. The anode in this case is a tantalum cylinder but the wires supporting the shell are along the axis of the tube.

The noise detected in these experiments may be related to the noise

resonance detected by Lustig [74] whose experimental discharge conditions were very nearly the same as in the present experiment. While Lustig does not specifically mention the observation of moving striations, in the present experiment no method was found whereby they could be eliminated.

The striations themselves may have plasma oscillations associated with the crests as reported by Swartz and Napoli [73]; however, the sensitivity of the receiver used in this experiment was not great enough to detect such signals even when the magnetic field reduced the anode noise to a low level. Any such signals associated with the crests of the striation would have a power below -62 dbm or else they would have been detected. It seems that any such oscillations as detected by Swartz and Napoli are not present in this experiment, at least spontaneously. No attempt was made to pulse the discharge to excite oscillations.

Plasma electron oscillations generated in beam-plasma systems are often associated with low frequency fluctuations and several workers [75] have suggested there is a causal relation between the two. It has been pointed out also that the anode or cathode can be the site of both low frequency noise and noise around the electron plasma frequency.

It is noted in Fig. A8 that the high frequency noise picked up by the external probe was intermittent being recorded at the video output as pulses of a microsecond or less in duration. Such a feature of noise from a low pressure mercury discharge has been reported by Emeleus and Jones, [75] who thought that this could be due to large amplitude low frequency fluctuations giving an electron frequency deviation large compared to the bandwidth of the receiver. However, when they used a wideband detector, the discontinuities in oscillation intensity remained.

One of the main reasons for making the association between Lustig's

[74] results and those observed here is the reduction in amplitude of rf due to a magnetic field. It was not possible to verify the resonant character of the noise due to the fact that the receiver sensitivity was not constant with frequency due to the variation with frequency of the local oscillator output and the fact that the mixer input impedance was not that of the line. A balanced mixer and leveled power local oscillator would be necessary for such measurements. It was evident that there was some variation in power level of the noise with frequency but no quantitative data could be taken.

APPENDIX B

RESONANCE PROBE

In the course of this work several experiments have been performed in which the resonant increase of electron collection to a probe has been observed. This is the resonance probe technique which was first studied experimentally by Ikegami and Takayama. [76]

The phenomenon of probe resonance is best explained by illustrating the circuit with which it is observed. A schematic is shown in Fig. B1. The probe is biased so as to collect a small electron current. This bias is such that only the higher energy electrons reach the probe. Superimposed on the bias is an rf voltage which is varied in frequency. At frequencies ω very much lower than the plasma frequency ω_p the dc current increases with an applied signal $\delta V \sin \omega t$ over that without an applied rf signal in accordance with the well known relation

$$\delta j = j_{es} \left\{ I_o \left(\frac{e \delta V}{k T_e} \right) - 1 \right\} \qquad \text{(B·1)}$$

where j_{es} is the Langmuir probe current of Eq. (43), δj is the current increase, and I_o is the modified Bessel function of zeroth order. It is noted in this case that δj is independent of frequency.

As the applied frequency approaches the plasma frequency, there is a resonant increase in the current. Experimentally it is observed that this resonance occurs below the plasma frequency, and that the ratio of resonant frequency to plasma frequency depends on the geometry of the probe and the probe dc bias. An ideal resonance probe characteristic is shown in Fig. B2.

The theory of the resonance rectification probe has been developed by several workers for plane probes. [77,78]

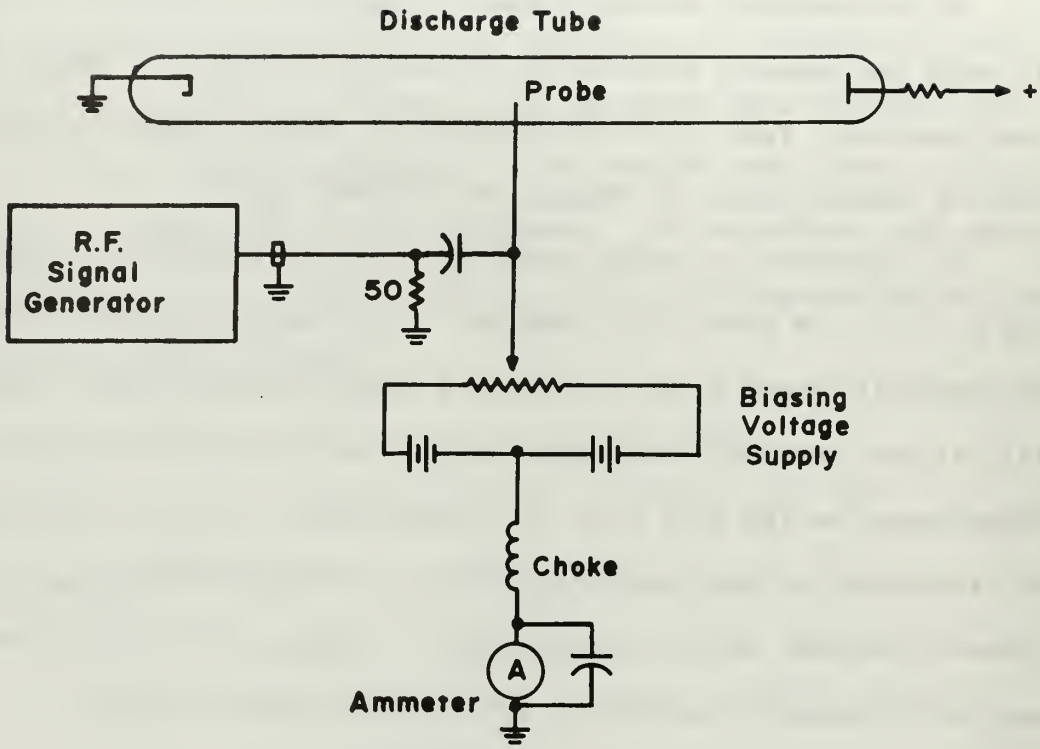

Figure B·1

Schematic of resonance probe circuit

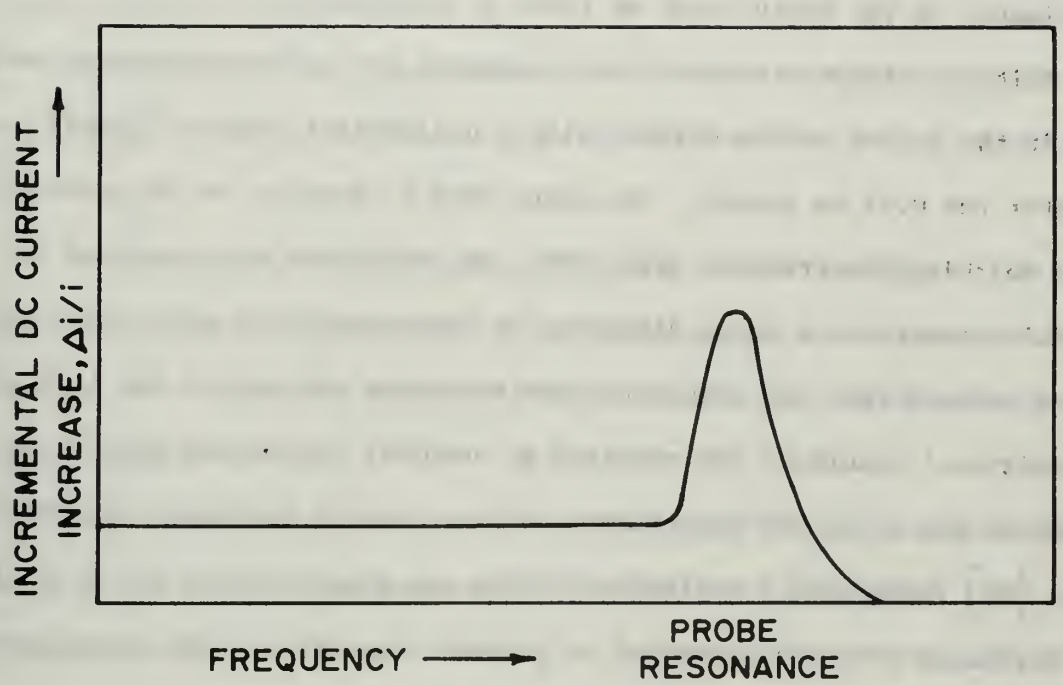

Figure B.2

Ideal resonance probe characteristic

It has been suggested that the resonance occurs between the capacitance of the probe sheath and the plasma inductance. Harp [79] has developed a simplified model of the spherical resonance probe and has shown good agreement between this model and experiment. A prediction of Harp's theory is that the radius of the probe must be large compared with the Debye length, λ_D.

No theoretical treatment of the resonance rectification probe exists for a cylindrical probe. Consequently any results obtained from our experiments on the device must be taken as qualitative.

Initial attempts to detect the resonance for a resonance probe were made in the 0.4 cm radius column using a cylindrical probe of 15 mil diameter and 0.62 cm length. The meter used to monitor the dc current was a Keithley electrometer Type 610B. No resonances were detected on initial attempts in a xenon discharge of approximately 1 mTorr pressure. It was assumed that the absence of the resonance was due to the fact that an additional electrode was required to complete the series circuit to ground as was so in the experiments of Mayer and of Levitskii and Shashurin. [80] Therefore, a cylindrical strip was placed inside the wall of the discharge tube and connected to ground, (through a large capacitance). The strip (2.5 mm wide) formed a ring with the probe at its center.

The resonance was still not detected after the ring was installed; however, it was discovered that the fault was in the use of the electrometer; the electrometer could not be completely isolated from rf currents and the meter was quite sensitive to this. Upon replacement with a conventional microammeter, resonances were clearly detected in the dc probe current. Furthermore, later experiments on another probe far from the probe inside the shell, showed that the shell was not necessary for

the occurrence of the resonance. The resonance occurred at the same frequency for these two probes, which were both of the same radius but of differing length (0.62 and 0.93 cm).

Figure B3 shows the incremental dc increase for the case of a xenon plasma at a pressure of 8.7 mTorr and discharge current of 20 ma. In this case the probe is about 15 v negative with respect to the space potential. The rf voltage is 1 volt peak to peak. The double peak shown here was found in several cases and has also been noted by others. The main resonance peak occurs at 710 MHz.

By use of Langmuir probe characteristics taken at the same conditions the plasma frequency was found to be 1.07 GHz and the Debye length 9.8 x 10^{-3} cm.

Experimentally the resonance is found to occur at $\omega/\omega_p = 0.78$ where ω_p has been determined from conventional Langmuir probe characteristics, whereas for a spherical probe of the same radius the simple theory of Harp predicts $\omega/\omega_p = 0.85$.

The half-width of the resonance is about 120 MHz which is large compared to the electron-neutral collision frequency of 35 MHz. This is consistent with Harp's prediction of a damping due to an rf phase mixing mechanism akin to Landau damping. However, in the present case, the broadening may be due to an entirely separate mechanism, viz. moving striations.

The scatter in resonant frequencies with changing densities is quite large as shown in Fig. B4 where the resonant frequency is plotted against plasma frequency. However, there is a definite trend toward higher resonant frequencies as the plasma frequency increases which shows that the resonance is indeed with the plasma and not the external circuit.

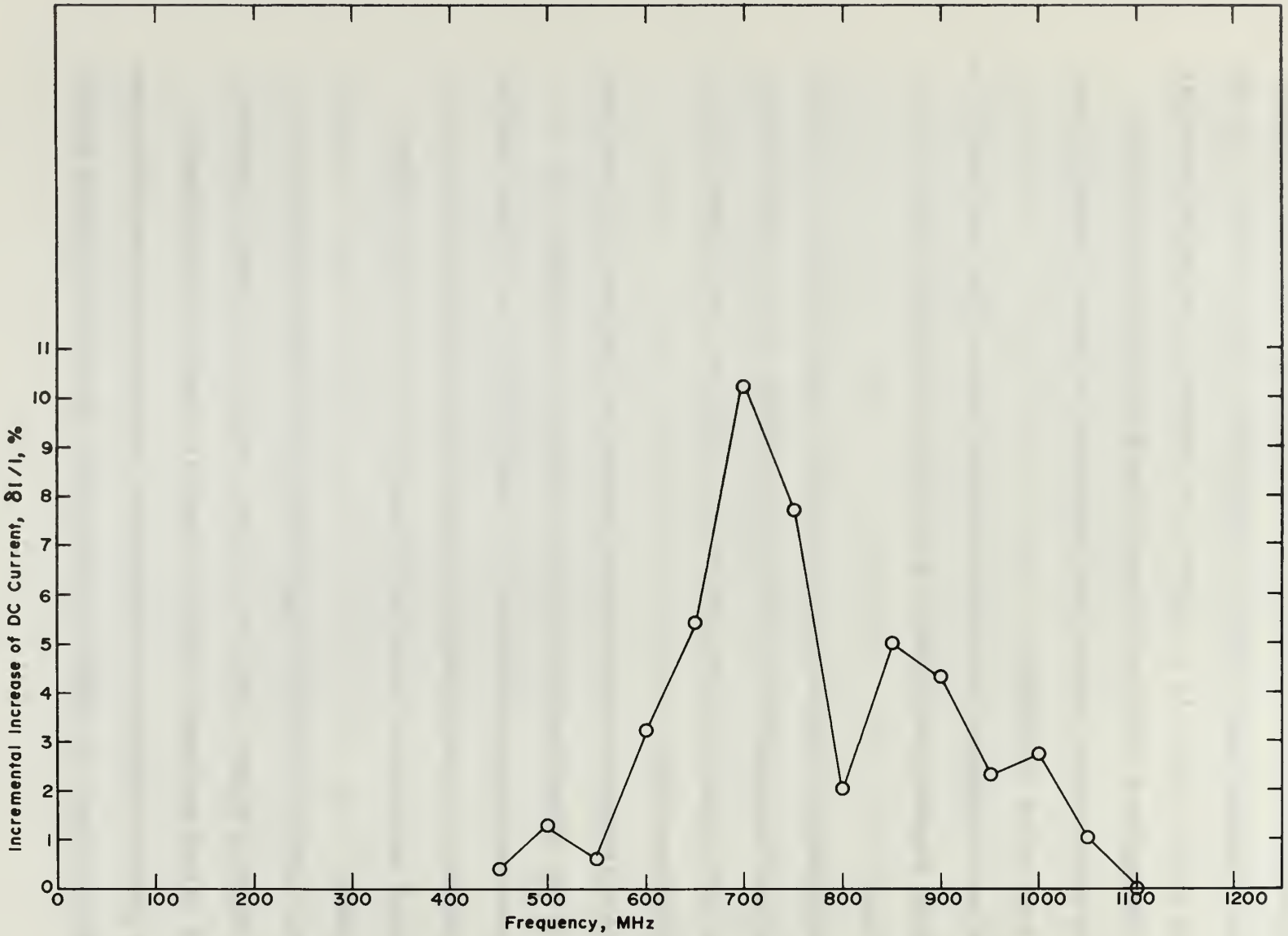

Figure B-3

Incremental dc increase of probe current for resonance probe in xenon, 8 mTorr, discharge current 20 ma, plasma frequency 1.07 gHz

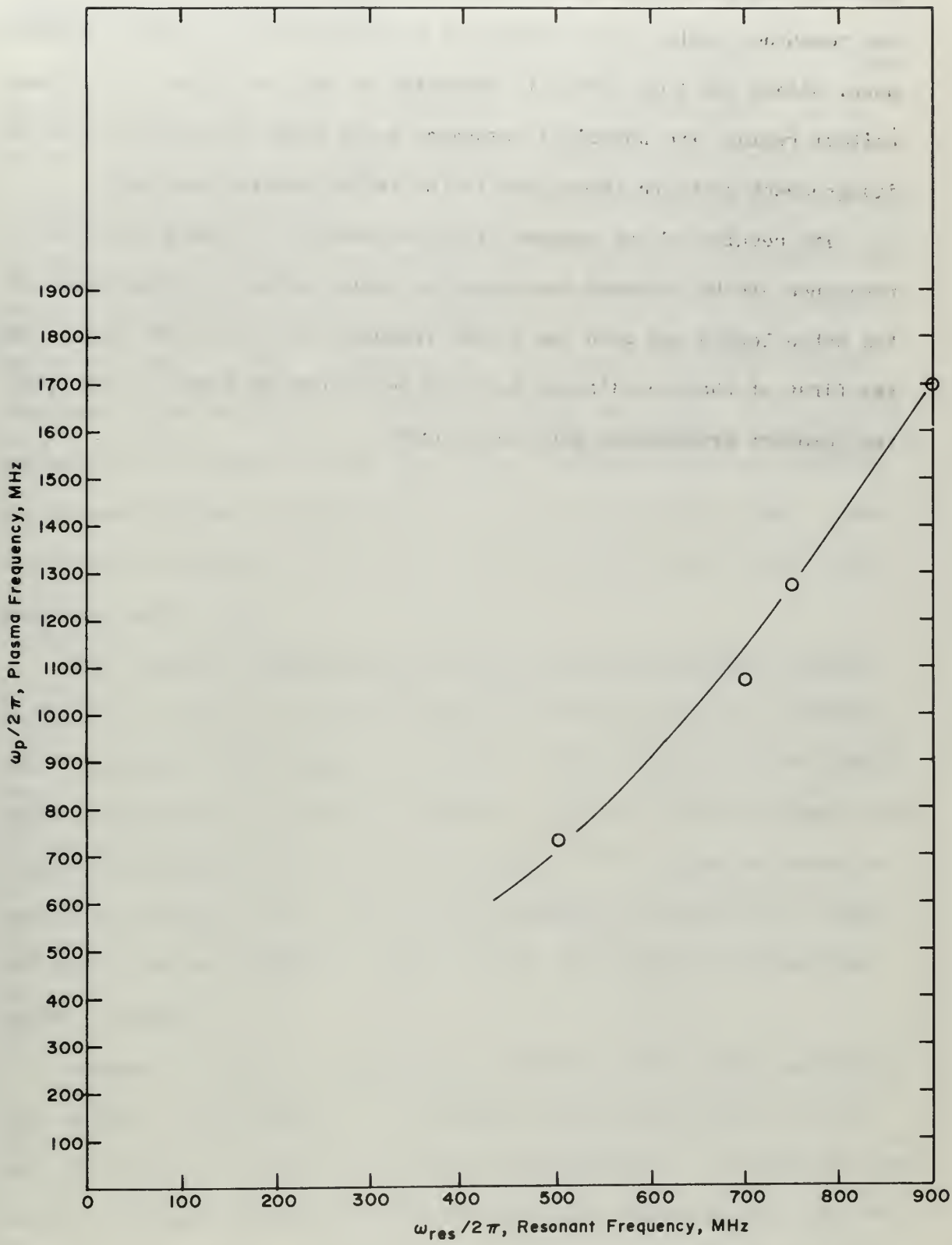

Figure B.4. Resonant frequency of cylindrical resonance probe versus plasma frequency for xenon plasma, 8 mTorr

Unfortunately, since the theory is not developed for the cylindrical geometry and the mathematics is quite complicated for its development, the resonance probe is not useful for diagnostics in this case. Furthermore, unless the tube radius is increased so that the probe is in a more uniform region, the spherical resonance probe might be expected to be in disagreement with the theory due to the radial density gradient.

The results of the present study are useful in showing that the resonance can be observed even when the probe radius is on the order of the Debye length and when the plasma frequency is in the UHF range. While the first of these conditions has also been noted by Baker, et.al. [81] the resonant frequencies were much lower.

APPENDIX C

ELECTRONEGATIVE PLASMA STUDIES

At the conslusion of the work reported on the rare gases, an attempt was made to produce an electronegative plasma in iodine vapor. By an electronegative plasma is meant a plasma in which the concentration of negative ions is comparable to or greater than the concentration of electrons. The objective of producing an electronegative plasma was to study resonances which might be observed in the spatial electron distribution of such a column. (there is also the possibility that a second resonance spectrum might exist due to the negative ions.) There is some evidence that in such a column the radial distribution of the electrons may be much different from the case of an electropositive column. Also, the electron densities are expected to be much lower and a lower plasma frequency would result.

Some extensive experiments have been recently performed on moving striations in iodine by Woolsey. [82] This work was done in a discharge tube containing iodine vapor at 0.2 Torr. Probe results in these experiments indicate that an electron density of about 10^7 cm^{-3} is present with negative and positive ion densities of about 10^{10}. Striations were observed in the high current form of the discharge at velocities of about 10^3 cm/sec and wavelengths of about 0.5 cm. The striations moved from anode to cathode.

Attempts to produce a steady state plasma in iodine were unsuccessful, however, some remarks of the attempts are presented here as it is felt they may be of some help to future experimenters. A column was constructed of Pyrex brand glass with the dimensions shown in Fig. C1. The tube was processed as follows: Iodine of 99.8% purity was placed in the

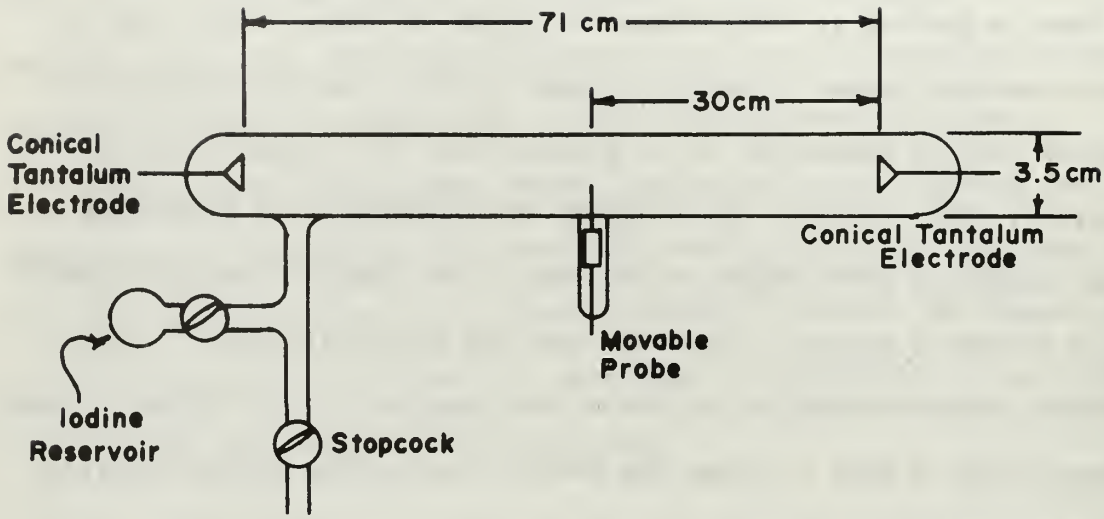

Figure C·1

Plasma discharge tube designed for use with iodine vapor

reservoir and the reservoir stopcock closed. The tube was connected to a vacuum system and a liquid nitrogen trap was inserted in series with the stopcock at A. The trap was filled with LN and the iodine reservoir was rough pumped to a few microns pressure. The reservoir was again closed and the main discharge tube was pumped to low pressure with a diffusion pump using DC 704 pumping fluid. The electrodes of the tube were outgassed with an induction heater to 2×10^{-5} Torr and the tube baked for four hours with heating tapes. The iodine reservoir was then immersed in an LN filled dewar and the stopcock opened. Then the entire system was pumped to 10^{-6} Torr and the main stopcock at A was closed. The tube was removed from the vacuum system at A and was remounted for experimental use.

First attempts to ignite the discharge where the reservoir was at room temperature of 23° C. yielded no observable current with voltages up to 2800 volts. As the voltage was raised above this value a small current was observed on the order of 0.01 ma. Further increase of the supply voltage caused the current to increase discontinuously to a few tenths of a milliampere, representing, it is believed, the high current form reported by Woolsey.

The discharge in all cases was unstable and was found upon observing the current on an oscilloscope to be made up of spikes of current with a repetition rate of several kHz. At the higher current form, the current did not drop entirely to zero between spikes, but the pulsed current represented a large fraction of the total. At the low current form, the discharge was pale violet in color and at higher currents it was whitish-violet, consisting of a constricted core which sometimes moved back and forth across the tube. The glass wall fluoresced green where the discharge contacted it.

When the temperature of the bulb was decreased from 23° C to 0° C, somewhat lower voltage was required to start the discharge, but the pulsed character of the discharge was still evident. For some currents (0.7 ma) at 0° C the discharge was pale yellow in color and was easily deflected when a grounded object was placed near the outside of the column. It seems apparent that the current form of the discharge in the cases observed is that of a relaxation oscillation. No steady state discharge could be obtained.

As time progressed, the discharge became more and more difficult to operate. Increasingly higher voltages were required to cause breakdown and operation became more unstable and intermittent. The difficulty seems to be associated with the condition of the electrode surfaces. From the very beginning, a black coating built up on the electrodes, particularly the cathode and the glass around the cathode also became covered with a black coating. Ultimately the discharge could not be ignited, even with a voltage in excess of 10 kv and further increases were considered hazardous.

Upon opening the tube to the atmosphere the black coating immediately reacted with the air producing a yellow-white powder on the wall of the tube. It was concluded that the black deposit was tantalum iodide which was formed under the influence of the discharge and low pressure. In spite of tantalum being unattacked by iodine at atmospheric conditions, the iodide formed on the surfaces of the electrodes and insulated them to the point that the discharge could not be operated.

From the experiments, it appears that in order to maintain a discharge in iodine vapor at low pressure fouling of the electrodes would have to be prevented. Woolsey, who used nickel electrodes, found it

necessary to open the tube and clean the electrodes often in order to maintain operation. Since the present system was not permanently connected to a vacuum system, such a process was not possible. It had been hoped that the tantalum electrode would make this unnecessary but, obviously, it did not.

For future attempts it is recommended that the tube be constructed with tungsten or platinum electrodes in the hope that these substances might prove to be less reactive with iodine. Also, it is suggested that the tube electrodes be placed closer together to allow lower voltage operation. This might also prevent relaxation oscillations and allow a steady current to be obtained. A permanent connection to a vacuum system would allow disassembly and alterations to be conducted more easily than in a tube which is closed off and removed from the vacuum system as in the present experiment.

BIBLIOGRAPHY

1. L. Tonks, Phys. Rev. 37, 1458 (1931)

2. L. Tonks, Phys. Rev. 38, 1219 (1931)

3. N. Herlofson, Arkiv for Fysik 3, 347 (1951)

4. D. Romell, Nature 167, 243 (1951)

5. A. Dattner, Ericsson Technics 2, 309 (1957)

6. F. I. Boley, Nature 182, 790 (1958)

7. B. Agdur, B. Kerzar, and F. Sellberg, Phys. Rev. 128, 1 (1962)

8. R. W. Gould, Paper given at VIIth Int. Conference on Ionization Phenomena, Belgrade, Yugoslavia, August 1965

9. A. M. Messiaen and P. E. Vandenplas, Physica 28, 537 (1962)

10. J. Willis and I. Petroff, IRE Trans PGMTT 10, 395 (September 1962)

11. F. W. Crawford, Microwave Laboratory Report 1045, Stanford University, California (June 1963)

12. T. R. Kaiser and R. L. Closs, Phil. Mag. 43, 1 (1952)

13. R. E. B. Makinson and D. M. Slade, Australian J. Phys. 7, 268 (1954)

14. G. H. Keitel, Proc. IRE 43, 1481 (1955)

15. R. W. Gould, California Institute of Technology Report No. 1, Contract DA36-039 SC-85317 (1960)

16. D. Bohm and E. P. Gross, Phys. Rev. 75, 1851 and 1864 (1949)

17. P. E. Vandenplas and R. W. Gould, Plasma Physics (J. Nucl. Energy Part C) 6, 449 (1964)

18. P. E. Vandenplas and A. M. Messiaen, P asma Physics (J. Nucl. Energy Part C) 6, 459 (1964)

19. F. C. Hoh, Phys. Rev. 133, A1016 (1964)

20. P. Weissglas, Plasma Physics (J. Nucl. Energy Part C) 6, 251 (1964)

21. J. V. Parker, J. C. Nickel, and R. W. Gould, Phys. Fluids 7, 1489 (1964)

22. J. V. Parker, California Institute of Technology Report No. 23, Contract Nonr 220(50)(1964)

23. J. C. Nickel, California Institute of Technology Report No. 22, Contract Nonr 220(50) (1964)

24. L. Tonks and I. Langmuir, Phys. Rev. 34, 876 (1929)

25. F. W. Crawford, G. S. Kino, S. A. Self, and J. Spalter, J. Appl. Phys. 34, 2186 (1963)

26. F. W. Crawford, J. Appl. Phys. 35, 1365 (1964)

27. W. M. Leavens, Radio Science, J. Res. Natl. Bur. Std. 69D, 1321 (1965)

28. G. H. Bryant and R. N. Franklin, Proc. Phys. Soc. (London) 83, 971 (1964)

29. R. L. Moore and J. R. Johnston, Douglas Aircraft Company Paper 2071, Prepared for Presentation at the American Physical Soc., Washington, D. C., 27 - 30 April (1964)

30. S. Wolschke, Akademie der Wissenschaften, Berlin. Monatsberichte, 7-8, 517 (1965)

31. R. N. Franklin, J. of Electronics and Control 17, 513 (1964)

32. K. J. Nygaard, Phys. Letters 20, 370 (1966)

33. H. J. Schmitt, Am. J. Phys. 34, 120 (Feb 1966)

34. R. A. Stern and N. Tzoar, Phys. Rev. Letters 15, 485 (1965)

35. A. M. Messiaen, Physica 29, 1117 (1963)

36. R. A. Stern, J. Appl. Phys. 34, 2562 (1963)

37. R. A. Stern, Appl. Phys. Letters 4, 80 (1964)

38. R. A. Stern, Phys. Rev. Letters 14, 538 (1965)

39. S. Kojima, S. Hagiwara, and H. Ogihara, J. Phys. Soc. (Japan) 20, 851 (1965)

40. G. F. Haggquist, Plasma Resonance in Argon and Neon, U.S. Naval Postgraduate School Thesis (1963)

41. R. H. Huddlestone and S. L. Leonard, Plasma Diagnostic Techniques, Academic Press, New York (1965) p. 198

42. G. A. Woolsey and E. W. Gray, J. Sci. Instr 43, (1966)

43. J. C. Hosea, J. Appl. Phys. 37, 2695 (1966)

44. D. M. Alderson and J. D. Leonard, Plasma Oscillations in a Low Pressure Neon Discharge, U.S. Naval Postgraduate School Thesis, (1961)

45. I. Langmuir, Gen. Elec. Rev. 27, 449 (1924)

46. M. Hoyaux, Direct Current 1, 22 (1953)

47. G. R. Nicoll and J. Basu, J. Electronics and Control 12, 23 (1962)

48. M. J. Druyvesteyn, Z. Physik 64, 781 (1930)

49. J. E. Allen, R. L. F. Boyd, and P. Reynolds, Proc. Phys. Soc. (London) 70B, 297 (1957)

50. I. B. Bernstein and I. Rabinowitz, Phys. Fluids 2, 112 (1959)

51. L. S. Hall and R. P. Freis, University of California, Lawrence Radiation Laboratory Report UCRL-12480 (1965)

52. J. G. Laframboise, University of Toronto, Institute for Aerospace Studies Report No. 100 (1966)

53. F. F. Chen, Plasma Physics (J. Nucl. Energy Part C) 7, 47 (1965)

54. A. M. Messiaen and P. E. Vandenplas, J. Appl. Phys. 37, 1718 (1966)

55. P. E. Vandenplas, private communication

56. A. von Engel, Ionized Gases, Oxford, 1955, p. 223

57. A. von Engel, Ionized Gases, Oxford, 1955, p. 215

58. S. J. Buchsbaum, L. Mower, and S. C Brown, Phys. Fluids 3, 806 (1960)

59. K. I. Thomassen, J. Appl. Phys. 36, 3642 (1965)

60. A. L. Gardner, University of California Institute of Engineering Research Report No. HE-150-129 (1955)

61. A. L. Gardner, private communication

62. C. D. Lustig, Physics Letters 9, 315 (1964)

63. L. Landau, J. Phys. (USSR) 10, 25 (1946)

64. R. W. Huggins and M. Raether, Phys. Rev. Letters 17, 745 (1966)

65. F. W. Crawford and J. D. Lauson, Plasma Physics (J. Nucl. Energy Part C) 3, 179 (1961)

66. K. G. Emeleus, W. T. Kennedy and J M. Jones, Phys. Letters 23, 74 (1966)

67. I. Alexeff and W. D. Jones, Thermonuclear Div. Semiann. Progr. Rept. Apr. 30, 1964, ORNL-3652, p. 56

68. W. Pupp, Physik. Z. 34, 756 (1933)

69. L. Pekarek and V. Krejci, Czech. J. Phys. B12, 450 (1962)

70. L. Pekarek and V. Krejci, Czech. J. Phys. B13, 881 (1963)

71. A. Hirose, M. Koganei, and H. Tanaca, J. Phys. Soc. (Japan) 21, 806 (1966)

72. V. Vesely, Beitr. Plasma Phys. 3, 149 (1964)

73. G. A. Swartz and L. S. Napoli, Phys. Fluids 8, 1517 (1965)

74. C. D. Lustig, Appl. Phys. Letters 4, 194 (1964)

75. J. M. Jones and K. G. Emeleus, Physics Letters 12, 187 (1964)

76. H. Ikegami and K. Takayama, Institute of Plasma Physics, Nagoya University, Nagoya, Japan, Report No. IPPJ-10 (1963)

77. H. M. Mayer, Proceedings of the VIth International Conference of Ionization Phenomena in Gases (Paris, July, 1963) (SERMA Publishing Co., Paris, 1964) Vol. 4, p. 129

78. H. Ikezi and K. Takayama, Institute of Plasma Physics, Nagoya University, Nagoya, Japan, Report No. IPPJ-48 (1966)

79. R. S. Harp and F. W. Crawford, J. Appl. Phys. 35, 3436 (1964)

80. S. M. Levitskii and I. P. Shashurin, Sov. Phys. - Tech. Phys. 8, 319 (1963)

81. K. D. Baker, A. M. Despain, and J. C. Ulwick, J. Geophys. Res. 71, 935 (1966)

82. G. A. Woolsey, Studies of Electronegative Plasmas, Queens University Belfast Ph.D. Thesis (1963)

INITIAL DISTRIBUTION LIST

		No. Copies
1.	Defense Documentation Center Cameron Station Alexandria, Virginia 22314	20
2.	Library Naval Postgraduate School Monterey, California 93940	2
3.	Office of Naval Research Department of the Navy Washington, D.C. 20360	1
4.	Prof. N. L. Oleson Naval Postgraduate School Monterey, California 93940	5
5.	LT D. A. Hart, USN SMC #1519 Naval Postgraduate School Monterey, California 93940	5

UNCLASSIFIED

Security Classification

DOCUMENT CONTROL DATA - R&D

(Security classification of title, body of abstract and indexing annotation must be entered when the overall report is classified)

1. ORIGINATING ACTIVITY *(Corporate author)* Naval Postgraduate School Monterey, California 93940	2a. REPORT SECURITY CLASSIFICATION UNCLASSIFIED 2b GROUP

3. REPORT TITLE

AN EXPERIMENTAL STUDY OF TONKS-DATTNER RESONANCES IN RARE GAS PLASMAS

4. DESCRIPTIVE NOTES *(Type of report and inclusive dates)*

Thesis, Doctor of Philosophy, December 1966

5. AUTHOR(S) *(Last name, first name, initial)*

HART, David Austin

6. REPORT DATE December 1966	7a. TOTAL NO. OF PAGES 192	7b. NO. OF REFS 82

8a. CONTRACT OR GRANT NO. b. PROJECT NO. c. d.	9a. ORIGINATOR'S REPORT NUMBER(S) 9b. OTHER REPORT NO(S) *(Any other numbers that may be assigned this report)*

CMK 11/6/69

10. AVAILABILITY/LIMITATION NOTICES

This document has been approved for public release and sale; its distribution is unlimited.

[redacted]

11. SUPPLEMENTARY NOTES	12. SPONSORING MILITARY ACTIVITY Office of Naval Research Department of the Navy Washington, D. C. 20360

13. ABSTRACT

A quantitative experimental study of the dipole Tonks-Dattner resonance oscillations of a cylindrical plasma column has been made for neon, argon and xenon plasma columns. Discharges were operated in the range of a few mTorr and resonances have been observed in the UHF and microwave frequency range. The resonances have been studied using strip-line and waveguide techniques and diagnostic studies have been employing Langmuir probes and microwave cavity methods. For xenon, good agreement has been found with the theory of Parker, Nickel and Gould but for neon and argon definite discrepancies exist. This departure has been attributed to ion mean free paths which are not long compared to the tube radius. The effect of ion collisions seems to be to raise the electron density near the wall of the tube causing the resonances to occur at higher frequencies than are predicted by theory for the case of long ion mean free paths. The appearance of fewer and broader resonances than are observed in mercury columns is attributed primarily to the occurrence of moving striations which produce variations of electron density of about $\pm$ 50% of the average.

DD FORM 1 JAN 64 1473

UNCLASSIFIED

Security Classification

14. KEY WORDS	LINK A ROLE	LINK A WT	LINK B ROLE	LINK B WT	LINK C ROLE	LINK C WT
Ne, Ar, Xe						
1 - 100 u Hg						
Resonances in UHF frequency range						
Moving striations present						
Ion collisions alter resonance conditions						

INSTRUCTIONS

1. ORIGINATING ACTIVITY: Enter the name and address of the contractor, subcontractor, grantee, Department of Defense activity or other organization *(corporate author)* issuing the report.

2a. REPORT SECURITY CLASSIFICATION: Enter the overall security classification of the report. Indicate whether "Restricted Data" is included. Marking is to be in accordance with appropriate security regulations.

2b. GROUP: Automatic downgrading is specified in DoD Directive 5200.10 and Armed Forces Industrial Manual. Enter the group number. Also, when applicable, show that optional markings have been used for Group 3 and Group 4 as authorized.

3. REPORT TITLE: Enter the complete report title in all capital letters. Titles in all cases should be unclassified. If a meaningful title cannot be selected without classification, show title classification in all capitals in parenthesis immediately following the title.

4. DESCRIPTIVE NOTES: If appropriate, enter the type of report, e.g., interim, progress, summary, annual, or final. Give the inclusive dates when a specific reporting period is covered.

5. AUTHOR(S): Enter the name(s) of author(s) as shown on or in the report. Enter last name, first name, middle initial. If military, show rank and branch of service. The name of the principal author is an absolute minimum requirement.

6. REPORT DATE: Enter the date of the report as day, month, year; or month, year. If more than one date appears on the report, use date of publication.

7a. TOTAL NUMBER OF PAGES: The total page count should follow normal pagination procedures, i.e., enter the number of pages containing information.

7b. NUMBER OF REFERENCES: Enter the total number of references cited in the report.

8a. CONTRACT OR GRANT NUMBER: If appropriate, enter the applicable number of the contract or grant under which the report was written.

8b, 8c, & 8d. PROJECT NUMBER: Enter the appropriate military department identification, such as project number, subproject number, system numbers, task number, etc.

9a. ORIGINATOR'S REPORT NUMBER(S): Enter the official report number by which the document will be identified and controlled by the originating activity. This number must be unique to this report.

9b. OTHER REPORT NUMBER(S): If the report has been assigned any other report numbers *(either by the originator or by the sponsor)*, also enter this number(s).

10. AVAILABILITY/LIMITATION NOTICES: Enter any limitations on further dissemination of the report, other than those imposed by security classification, using standard statements such as:

(1) "Qualified requesters may obtain copies of this report from DDC."

(2) "Foreign announcement and dissemination of this report by DDC is not authorized."

(3) "U. S. Government agencies may obtain copies of this report directly from DDC. Other qualified DDC users shall request through _____."

(4) "U. S. military agencies may obtain copies of this report directly from DDC. Other qualified users shall request through _____."

(5) "All distribution of this report is controlled. Qualified DDC users shall request through _____."

If the report has been furnished to the Office of Technical Services, Department of Commerce, for sale to the public, indicate this fact and enter the price, if known.

11. SUPPLEMENTARY NOTES: Use for additional explanatory notes.

12. SPONSORING MILITARY ACTIVITY: Enter the name of the departmental project office or laboratory sponsoring *(paying for)* the research and development. Include address.

13. ABSTRACT: Enter an abstract giving a brief and factual summary of the document indicative of the report, even though it may also appear elsewhere in the body of the technical report. If additional space is required, a continuation sheet shall be attached.

It is highly desirable that the abstract of classified reports be unclassified. Each paragraph of the abstract shall end with an indication of the military security classification of the information in the paragraph, represented as *(TS)*, *(S)*, *(C)*, or *(U)*.

There is no limitation on the length of the abstract. However, the suggested length is from 150 to 225 words.

14. KEY WORDS: Key words are technically meaningful terms or short phrases that characterize a report and may be used as index entries for cataloging the report. Key words must be selected so that no security classification is required. Identifiers, such as equipment model designation, trade name, military project code name, geographic location, may be used as key words but will be followed by an indication of technical context. The assignment of links, roles, and weights is optional.

DD FORM 1 JAN 64 1473 (BACK)

[redacted]

thesH2936
An experimental study of Tonks-Dattner r
3 2768 002 07745 5
DUDLEY KNOX LIBRARY